A NOVEL FINITE ELEMENT FOR MODELING A FASTENER IN A LAP JOINT ASSEMBLY

A Dissertation by

Brian D. Foster

Master of Science, Wichita State University, 2007

Bachelor of Science, Iowa State University, 1994

Submitted to the Department of Aerospace Engineering
and the faculty of the Graduate School of
Wichita State University
in partial fulfillment of
the requirements for the degree of
Doctor of Philosophy

December 2014

Copyright 2014 by Brian D. Foster
All Rights Reserved

A NOVEL FINITE ELEMENT FOR MODELING A FASTENER IN A LAP JOINT ASSEMBLY

The following members of the faculty have examined the final copy of this dissertation for form and content, and recommend that it be accepted in partial fulfillment of the requirement for the degree of Doctor of Philosophy with a major in Aerospace Engineering.

Charles Yang, Committee Chair

Walter Horn, Committee Member

Suresh Raju, Committee Member

Hamid Lankarani, Committee Member

Wilfredo Moscoso-Kingsley, Committee Member

Accepted for the College of Engineering

Royce Bowden, Dean

Accepted for the Graduate School

Abu Masud, Dean, Interim

ACKNOWLEDGEMENTS

Without the guidance, assistance, insight, and above all, patience, from my advisor, Dr. Charles Yang, this work would not have been possible. For that, I am grateful.

ABSTRACT

This work documents the development of a novel finite element. This element introduces parameters that allow more accurate modeling for the specific application of mechanically fastened lap joints. The research here bridges the gap between two traditional methods commonly used in industry today. The novel element is *more accurate* than the first traditional method, by using a single-beam element to join plate elements with a linear solution. It is also *more computationally compact* than the second traditional method, which consists of an assembly of solid, three-dimensional elements with a non-linear solution.

The case studies used are specifically limited to mechanically fastened lap joints pulled in tension, also referred to as "secondary bending." The plates joined together with these fasteners are loaded up to a fraction of a yielding load of the plate material in order to maintain linearity. Isotropic materials are used exclusively for both the plates and fasteners.

Ultimately, the fastening element created in this study is intended strictly for a linear calculation. The calculation contains a one-dimensional beam element with two nodes that connects two, two-dimensional plate elements together. To match the problem more accurately, this research introduces the principle of finite element Hertzian contact mechanics, which is specifically applied to mechanically fastened lap joints. This addition to the existing beam finite element allows for a more accurate simulation while holding to the simplicity of a linear solution of a single element with two nodes in a plate/beam/plate element modeling scheme. Transverse deflections resulting from the applied loading in this new finite element are first compared to the two baseline finite element models that the new element is intended to bridge. The new model is also compared to the deflections calculated from empirically formulated stiffness values generated for the neutral line model.

TABLE OF CONTENTS

Chapter		Page
1.	INTRODUCTION	17
	1.1 Overview	17
	1.2 Scope of Work	25
2.	LITERATURE AND THEORETICAL REVIEW	26
	2.1 Literature Review	26
	2.2 Common Configurations Currently Used in Industry	37
	2.3 Beam Theories and FEM Implementation	40
	2.4 Euler-Bernoulli Beam Theory and Finite Element Method	42
	2.5 Timoshenko Beam Theory	46
	2.6 Axial Deflection	53
	2.7 Combining Different Theories	53
	2.8 Hertzian Contact Mechanics	54
	2.9 Winkler Foundation	58
	2.10 Literature Review Conclusion	60
3.	FASTENER ELEMENT FORMULATION	61
	3.1 Problem Description	61
	3.2 Finite Element Development	63
	3.3 Typical Mid-Plane Processing	70
	3.4 Linearized Cylindrical Hertzian Contact	70
4.	TEST CASE STUDY 1	77
	4.1 Single-Bolt Test Case Layout	77
	4.2 Results and Analysis	83
5.	TEST CASE STUDY 2	90
	5.1 Three-Bolt Test Case Layout	90
	5.2 Results and Analysis	94
6.	TEST CASE STUDIES 3 AND 4	102
	6.1 Three-Bolt Test Case Layout	102
	6.2 Results and Analysis	104

TABLE OF CONTENTS (continued)

Chapter Page

7. CONCLUSIONS, RECOMMENDATIONS, AND FURTHER STUDY 116

7.1 Conclusions 116
7.2 Recommendations 117
7.3 Areas for Further Research 118

BIBLIOGRAPHY 121

APPENDICES 132

APPENDIX A AN ALTERNATIVE DERIVATION 133

APPENDIX B AVERAGING OF STIFFNESS TERMS 136

APPENDIX C METHODS USED FOR PRELOAD IN SOLID ELEMENTS 137

APPENDIX D HERTZIAN CONTACT OF PARALLEL CYLINDERS 139

APPENDIX E NEUTRAL LINE MODEL 141

APPENDIX F MODELS WITH AND WITHOUT RIGID BODY ELEMENTS 145

APPENDIX G PROGRAMS AND SUPPORTING DATA FILES 149

LIST OF FIGURES

Figure		Page
1.1	Break down an assembly into smaller parts.	18
1.2	Typical line elements.	19
1.3	Typical surface elements.	19
1.4	Typical solid elements.	20
1.5	Solid element calculation (CATIA/Elfini processor).	21
1.6	Bar/plate element calculation (NX NASTRAN processor).	21
1.7	Types of bending in a lap joint.	23
1.8	Finite element design field	24
2.1	Assembly of 1D elements (Rutman et al., 2000).	26
2.2	Multiple elements simulating fastener (Paroissien et al., 2006).	28
2.3	Compression cone (Shigley and Mischke, 1988; Wileman et al., 1991; Lee, 2010a).	31
2.4	Bolt/member contact regions.	36
2.5	Beam element (CBAR) with spider elements (RBE).	37
2.6	Beam element (CBAR) with spider elements (RBE) around holes.	37
2.7	Spider elements only (RBE) around holes.	38
2.8	Beam element with spider elements (RBE) forming washers.	38
2.9	Hexa (solid) element with spider elements only (RBE).	39
2.10	CFAST element.	40
2.11	NASTRAN Hi-Lok™ element.	40
2.12	Shear force-bending moment relations	42
2.13	Beam with applied loads and elastic foundation (Reddy, 2006).	43

LIST OF FIGURES (continued)

Figure		Page
2.14	Euler-Bernoulli beam (Astley, 1992).	43
2.15	Beam discretization (Reddy, 2006).	45
2.16	Timoshenko beam theory (Reddy, 2006).	47
2.17	Three-node beam element	50
2.18	Newton's rings.	55
2.19	Two cylinders in contact with parallel axes (Puttock et al., 1969).	56
2.20	Two cylinders in contact with parallel axes (Young, 2011)	57
2.21	Relative diameter (Young, 2011)	57
2.22	Bed of springs (Felippa, 1998)	59
3.1	Problem definition with single fastener.	61
3.2	Fastener free-body diagram shown within joint cross section	62
3.3	Free-body diagram (minus solid representation and rotated).	63
3.4	Primary and secondary variables.	67
3.5	Primary and secondary variables.	69
3.6	Plate and beam element idealization.	70
3.7	Contact stiffness vs. applied force.	72
3.8	Using linear regression model to determine contact stiffness.	73
3.9	Fastener element (rotated and aligned with z-axis).	75
4.1	Case Study 1 layout.	77
4.2	Cross section of Case Study 1 layout	78
4.3	Finite element model constraints.	79

LIST OF FIGURES (continued)

Figure		Page
4.4	Plate element model for Case Study 1.	79
4.5	Beam element detail for Case Study 1.	80
4.6	Solid element model for Case Study 1.	81
4.7	Solid element model detail (eight elements across thicknesses).	81
4.8	Solid element model detail (four elements across plate thicknesses).	82
4.9	Corrected transverse deflection (Uoutput vs. Ucorrected).	83
4.10	Transverse deflection vs. slenderness ratio.	84
4.11	Transverse deflection vs. slenderness ratio.	85
4.12	Deflection vs. slenderness ratio, Timoshenko (IIE) vs. solid elements.	86
4.13	Deflection vs. slenderness ratio, Timoshenko (IIE) vs. solid elements.	86
4.14	Timoshenko (IIE) vs. solid elements vs. novel finite element.	87
4.15	Solid elements vs. novel finite element with various c_c values.	88
5.1	Case Study 2 layout.	91
5.2	Cross section of Case Study 2 layout	91
5.3	Three-bolt finite element model constraints.	92
5.4	Three-bolt finite element plate model.	92
5.5	Three-bolt solid model problem	93
5.6	Three-bolt solid model deflection.	93
5.7	Front fastener loads vs. total loads, 0.25-inch thick plates, Al vs. St.	99
5.8	Front fastener loads vs. total loads, 0.1875-inch thick plates, Al vs. St.	99
5.9	Front fastener loads vs. total loads, 0.125-inch thick plates, Al vs. St.	100

LIST OF FIGURES (continued)

Figure		Page
5.10	Front fastener loads vs. total loads, 0.0625-inch thick plates, Al vs. St.	100
5.11	Load ratios vs. plate thickness, Al vs. St.	101
6.1	Case Studies 3 and 4 layout.	104
6.2	Three-bolt plate FE model, 0.1875-in x 0.25-in Al plates.	107
6.3	Three-bolt plate FE model, 0.125-in x 0.25-in Al plates.	107
6.4	Three-bolt plate FE model, 0.0625-in x 0.25-in Al plates.	108
6.5	Three-bolt plate FE model, 0.25-in x 0.25-in Al/St plates	108
6.6	Three-bolt solid FE model, 0.25-in x 0.25-in Al/St plates	109
6.7	Three-bolt solid model, side view.	109
6.8	Three-bolt solid FE model, 0.1875-in x 0.25-in Al plates.	110
6.9	Three-bolt solid FE model, 0.125-in x 0.25-in Al plates.	110
6.10	Three-bolt solid FE model, 0.0625 -in x 0.25-in Al plates.	111
6.11	Shear load across fasteners without RBE.	112
6.12	Shear load across fasteners with RBE.	113
6.13	Shear loads for Case Study 3.	115
6.14	Shear loads for Case Study 4.	115

LIST OF TABLES

Table		Page
3.1	Linearized Contact Stiffness Using Linear Regression	73
3.2	Goodness of Fit of Linear Regression Models	74
4.1	Case Study 1 Parameters	78
5.1	Case Study 2 Parameters	91
5.2	Fastener Load Reactions, Plate/Beam/Plate	95
5.3	Fastener Load Reactions, Solid Models	95
5.4	Fastener Load Reactions, Neutral Line Model with Huth Flexibilty	96
5.5	Fastener Load Reactions, Plate with Novel Element	96
5.6	Fastener Load Reactions, First/Middle Load Ratio, Aluminum vs. Steel	97
6.1	Case Study 3 Parameters	103
6.2	Case Study 4 Parameters	103
6.3	Case Study 3 Load Results Part 1	105
6.4	Case Study 3 Load Results Part 2	105
6.5	Case Study 4 Load Results, Part 1	106
6.6	Case Study 4 Load Results, Part 2	106
6.7	Case Studies 3 and 4 Shear (without RBE) (Plate Models)	112
6.8	Case Studies 3 and 4 Shear (with RBE) (Plate Models)	112
6.9	Case Study 2 Compared to Case Studies 3 and 4 Shear (with RBE) (Plate Models)	114

LIST OF ABBREVIATIONS

CAD	Computer-Aided Design
CATIA	Computer Aided Three-Dimensional Interactive Application
CBAR	Single-Beam Element
CBUSH	Spring Element
CFAST	Simplified Fastener Element
CIE	Consistent Interpolation Element
CPT	Classical Plate Theory
DOF	Degrees of Freedom
EBT	Euler-Bernoulli Theory
ED	Edge Distance
EI	Bending Stiffness
FEA	Finite Element Analysis
FEM	Finite Element Method
FSDT	First-Order Shear Deformation Theory (Reissner-Mindlin Plate Theory)
HEXA	Hexagonal Solid Element
IIE	Interdependent Interpolation Element
MITC	Mixed Interpolation of Tensorial Components
NASTRAN	NASA Structural Analysis
PE	Plane Elasticity
RBAR	Rigid-Bar Element
RBE	Rigid-Body Element
RIE	Reduced Integration Element

QUAD4	Quadrilateral Planar Element (or Plate Element)
TBT	Timoshenko Beam Theory

LIST OF SYMBOLS

A	Cross-sectional area of fastener
b_1, b_2	Full width of contact, in
C_e	Contact Modulus, psi
c_c	Contact stiffness via contact mechanics, lb/in
c_{c1}	Contact stiffness of contact of plate 1 with the fastener, lb/in
c_{c2}	Contact stiffness of contact of plate 2 with the fastener, lb/in
c_f	Foundational stiffness, lb/in
D_h, D_2	Fastener hole diameter, in
D_s, D_1	Fastener shank diameter, in
F_{cl}	Clamping force, lbs
E, E_f	Fastener material elastic modulus, lb/in^2
E_n	Sheet material elastic modulus of n^{th} member of the contact, lb/in^2
E_s	Sheet material elastic modulus, lb/in2
F	Force, axial, lbs
F_s	Shear strength, lbs
G	Shear modulus, lb/in^2
h	Distance between the nodes, in
I	Surface moment of inertia, in^4
J	Torsion moment of inertia, in^4
K	Stiffness matrix, lbs/in
K_d	Relative radius, in
K_s	Timoshenko shear correction coefficient

M	Bending moment, lbin
Q	Shear load, lbs
q_1, q_2	Distributed loads applied by member 1 and member 2, lbs/inch
P	Applied tensile load, or far-field load, lbs
T	Torsion, lbs
T_{bp}	Bypass load, lbs
T_{tr}	Transfer load, lbs
t_1, t_2	Selected sheet thickness of first and second members, i
U,u	Axial deflection
v, w	Transverse deflection, in
v, Δ	Weight functions
α	Fraction of element length, dimensionless
δ	Fastener deflection, in
θ	Axial twist, rad
μ	Friction coefficient, in
ν	Poisson's ratio, dimensionless
σ	Normal stress, lbs/in2
σ_b	Bending stress, lbs/in2
σ_y	Yield stress, lbs/in2
φ(x), Ψ(x)	Shape functions
Ψ	Beam rotation (Timoshenko theory)

CHAPTER 1.

INTRODUCTION

1.1 Overview

Finite element analysis (FEA) can be utilized in many ways to solve structural problems. With different methods come different advantages, disadvantages, and tradeoffs. One approach can be a relatively quick method that has a limited accuracy, while another can be very detailed but will take longer in preparation and calculation. This is a common tradeoff in engineering disciplines.

The research in this dissertation specifically identifies a modification of line (beam or bar) elements used in conjunction with surface (plate) elements in the modeling of mechanically fastened lap joints that experience tensile loading under a linear solution scheme. The new model is compared to non-linear three-dimensional models that use much more refined solid elements. The goal here is to capture additional mechanical phenomena that standard bar/plate elements do not include and, while maintaining a compactness associated with single bar elements, to approach a solid model response.

Finite elements can be viewed as the various "building blocks" of simple shapes that are easily understood from a physical standpoint. These elements are assembled together into a model, much like a child's building blocks might be assembled together to resemble something larger and more complex (Figure 1.1). For fans of childhood toys, Legos® provide the perfect metaphor for this idea. With the finite element method (FEM), it is also desirable that the assembly of these simple finite elements ultimately take a shape that is recognizable as the physical problem being modeled.

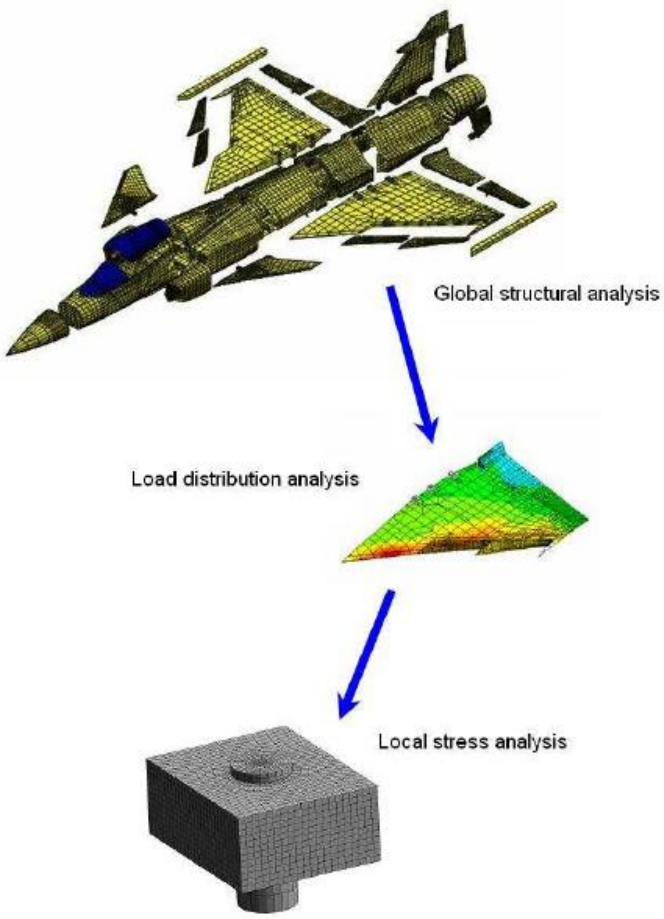

Figure 1.1: Break down of an assembly into smaller parts.

At this point, a brief description of the different types of finite elements commonly used is in order. Finite elements can be segregated into three different categories: line, surface, and solid. Finite elements are mainly segregated by spatial dimensions used in the application of differential equations, the solutions of which the finite element method is used to approximate.

Line elements are one-dimensional (1D) elements created to simulate axial loading and torsion (Figure 1.2). One-dimensional elements have also been created to capture transversely loaded beam structures using the Euler-Bernoulli beam theory (EBT) or Timoshenko beam theory (TBT). Commercial finite element codes define bar elements (sometimes referred to as beam elements) to solve all three of these phenomena simultaneously. Although these

phenomena are bound to the same two-node element, they are uncoupled, meaning that the solution of one of the differential equations has no impact on the solutions of the other two.

Figure 1.2: Typical line elements.

Plate, shell, and membrane elements are two-dimensional (2D) elements that have been idealized to capture what happens to a structure that tends to be thin (Figure 1.3). Aircraft structures that are usually fabricated from sheet materials are one such example. These elements utilize plane elasticity (PE), classical plate theory (CPT), or the more popular, Reissner-Mindlin plate theory, also known as the first-order shear deformation theory (FSDT). Two-dimensional elements are essentially the 2D expansion of 1D elements. Like line elements, plate elements solve both in-plane loading phenomena and transverse-loading phenomena simultaneously, yet are uncoupled.

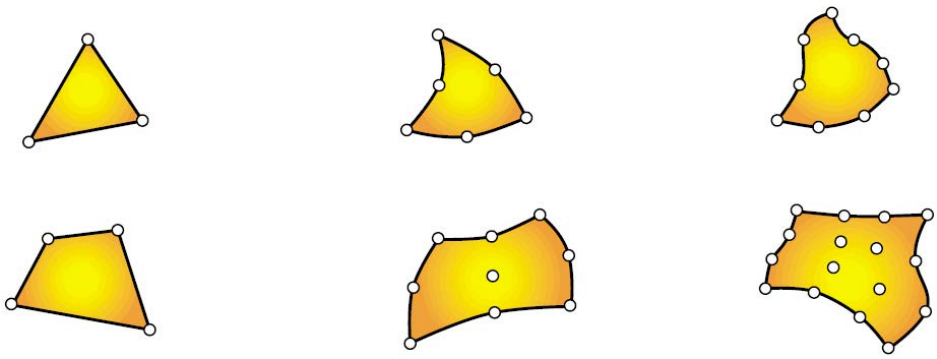

Figure 1.3: Typical surface elements.

Three-dimensional (3D) continuum (solid or volume) elements became very popular with the advancement of computer processing power and model storage (Figure 1.4). Three-dimensional elements utilize the concept of minimizing total potential energy of the system to solve the solid mechanics problem. Continuum elements have clear advantages. It is sensible to

use 3-D elements to model 3-D problems. Additionally, modern computer-aided design (CAD) packages usually have predefined solid geometry, which reduces some of the preprocessing, or setup time, of the FEA models.

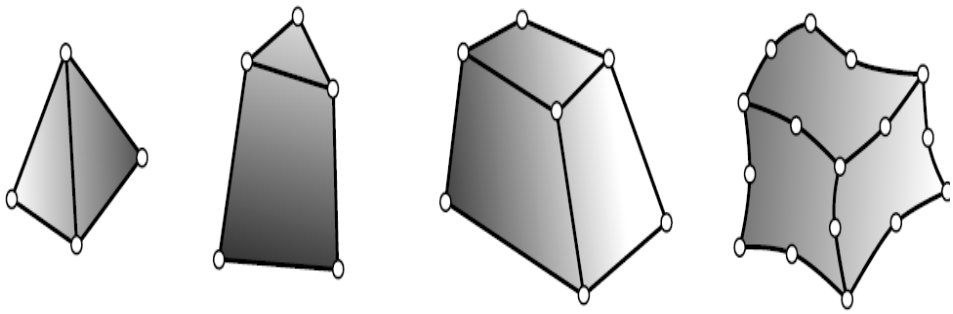

Figure 1.4: Typical solid elements.

Despite the obvious advantages that solid elements have in modeling, processing these elements unavoidably takes considerably more processing time and uses more memory storage than when using simpler 1D and 2D elements. More importantly, modern CAD models usually utilize assemblies, which contain multiple solids or parts interfacing with each other. Usually the purpose here is to identify unwanted interferences and to determine the ease of installation and/or removal of parts in the assembly. What this means to the structural analyst, is that s/he must also set up contact/connection schemes between mating surfaces of the solids in assemblies that have proper frictions, preloaded values, etc. If an assembly contains multiple parts, this can become a major, if not the major, cause of increased preprocessing time in setting up the analysis. This fact definitely complicates the setup time, and the analysis of contact in finite element analysis is inherently a "non-linear" phenomenon. Non-linear calculations involve an iterative process that updates solutions of the model, until the differences between the current level of solution and the previous solution are acceptably small. This is known as solution convergence. This method takes a considerable amount of time, compared to obtaining the linear solution.

As an illustrative example, Figure 1.5 shows a lap joint modeled exclusively with ten-node solid tetrahedron elements and full contact surfacing (containing approximately 74,000 nodes with three degrees of freedom [DOF] per node), which takes more than 15 minutes to generate a solution. However, as shown in Figure 1.6, modeling the same problem with bar and plate elements (66 nodes with six DOF per node) takes less than five seconds to calculate.

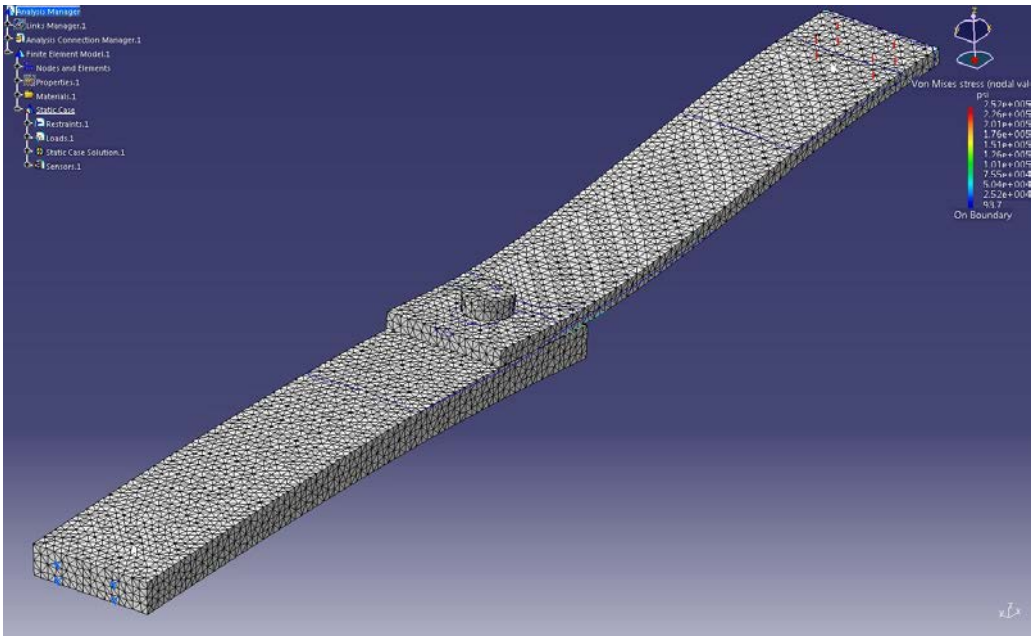

Figure 1.5: Solid element calculation (CATIA/Elfini processor).

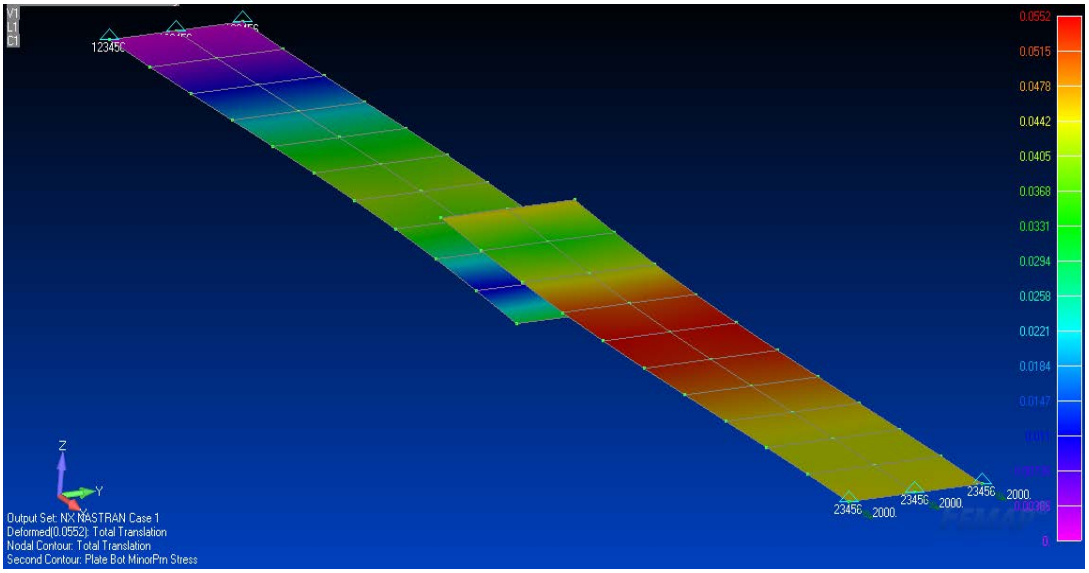

Figure 1.6: Bar/plate element calculation (NX NASTRAN processor).

Therefore, despite future advancements in computer memory and speed, it will always be advantageous to use methods that break down the setup process and reduce the requisite calculations, thereby reducing the time taken for both. Herein lies the basic premise of this research. Also, the work here is applied to a particular problem involving a fastened lap joint experiencing a tension load and modeled with traditional plate and line elements. The line elements are modified and designed to capture additional information in order to better simulate the joint than that currently provided by commercial codes for bar and beam elements.

The goal of this research is to develop a finite element that introduces additional information into a two-node line element connecting to plate elements that usually simulate the mid-planes of two joined members. This is a challenge, since a lap joint is inherently a non-linear problem, if only because of the contact mechanics that exist in the joint. Here, assumptions that still allow for a linear calculation are made.

This research also exposes a tradeoff that is inherent in structural analyses. Unquestionably, both preprocessing and processing times are considerably less when modeling a mechanically fastened lap joint with line and surface element combinations in a linear analysis. Also, unquestionably, a higher level of accuracy is expected when the same lap joint is modeled using solid elements exclusively in a non-linear analysis.

In some cases, a lap joint can be modeled simply with a small number of line and surface elements, which results in a processing time measured in mere seconds. The same problem can be modeled with a large number of solid elements with processing times that are easily measured in minutes. This fact makes research in enhancing simpler line and surface elements particularly useful. Given that assemblies typically involve multitudes of joints, FEM analysis using solid elements with contact calculations is particularly time consuming and, therefore, expensive. As

can be rightly inferred, the constraints of accuracy and compactness drive element design in opposite directions, whereby a higher consideration for one constraint necessarily sacrifices the other.

The lap joint is perhaps the most basic of any assembly. The problem at hand is the formulation of a novel finite element to model a removable mechanical fastener (i.e., bolt/nut) in a lap joint configuration that is as simple as possible yet captures the phenomena more accurately. The types of loading in a lap joint are illustrated in Figure 1.7. As shown, secondary bending of the lap joint is the focus of this research. According to one survey, secondary bending in lap joints existed in 86% of all joints in a given aerospace structure.

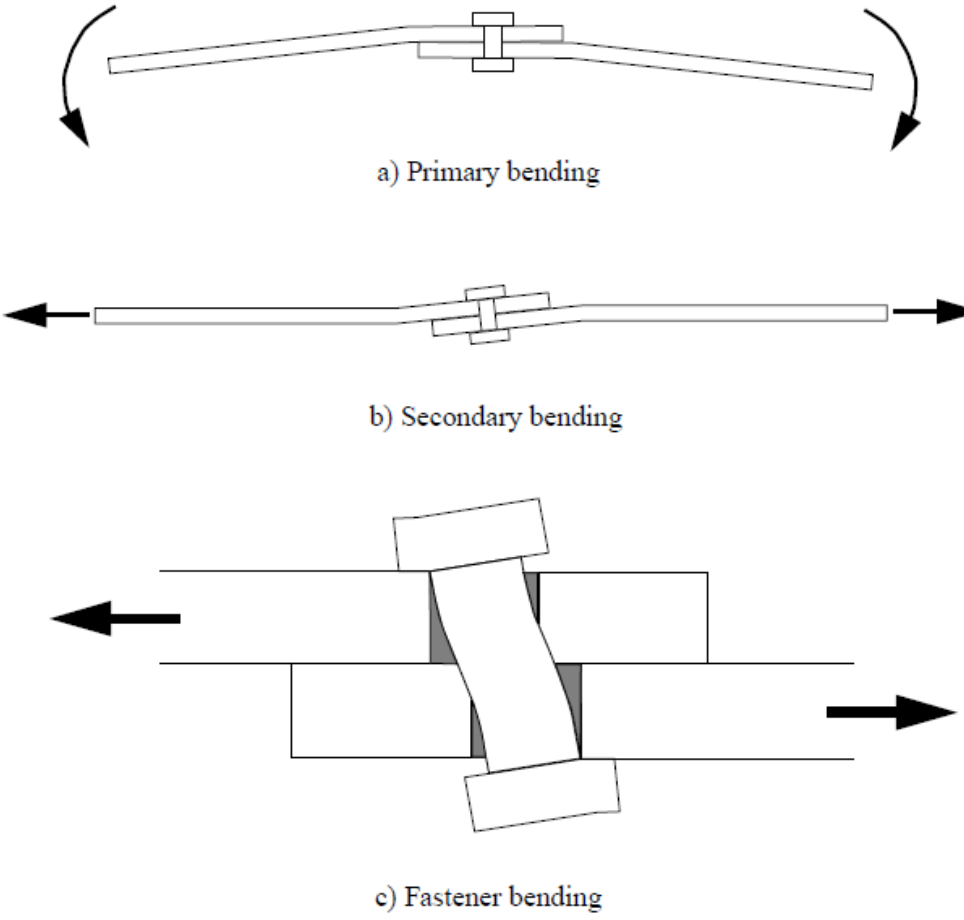

Figure 1.7: Types of bending in a lap joint.

Two methods capture the entire current design space of finite element modeling for mechanical fasteners in a lap joint. Two baselines that cover this wide swath are defined as follows: (1) a 3D model, as detailed as possible, that captures the physics of the problem, which also lends itself to the highest accuracy although being computationally expensive; and (2) a very simple model connecting two members, which results in the fastest calculation time and could be a 1D beam element that connects plate elements. The interaction between the fastener and the hole is not included in the basic model. These two baselines effectively subsume all conceivable possible solutions that solve the bolt/nut joint model. Between these two baselines lies a multitude of factors that can be included in the calculation. This element design space is illustrated in Figure 1.8.

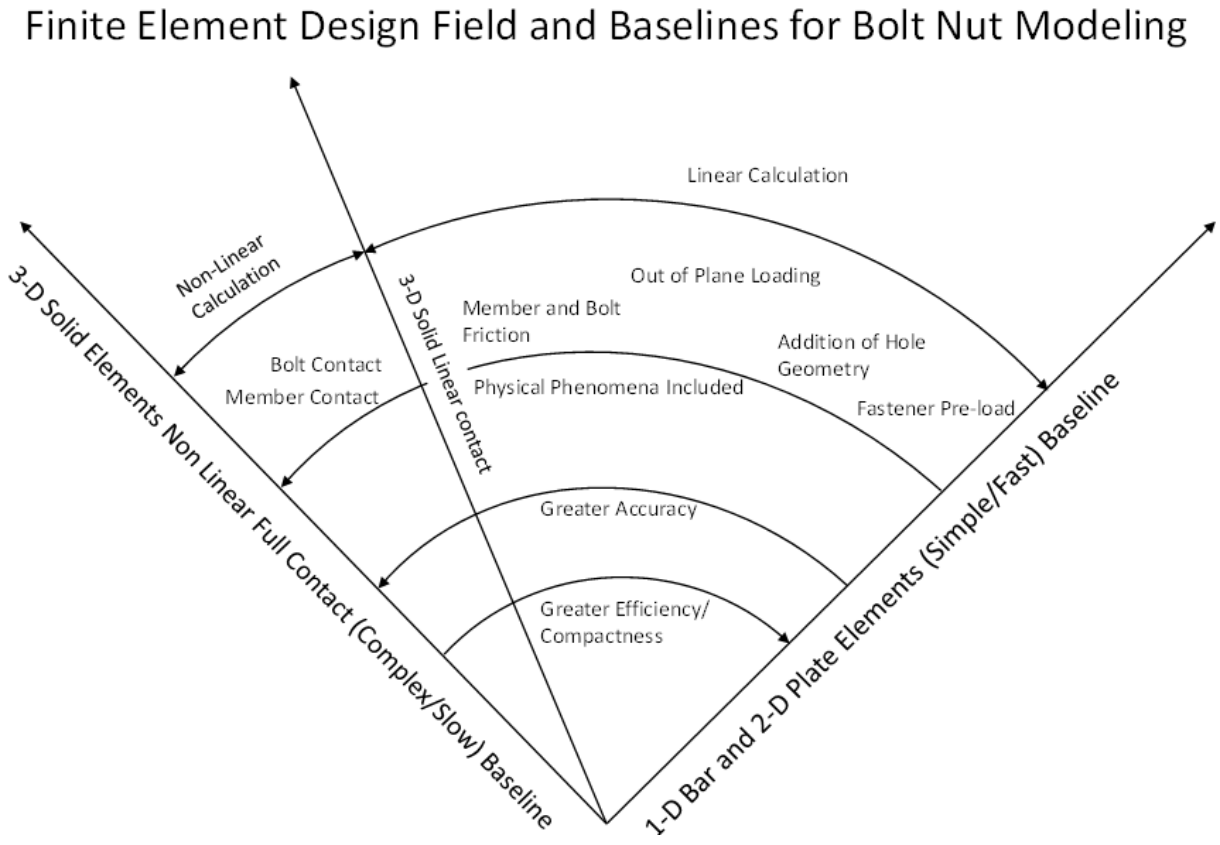

Figure 1.8: Finite element design field.

1.2 Scope of Work

The objective of this study is to develop a general formulation of joining two-dimensional plate elements that models the joined members in a lap joint configuration, and to model the bolt/nut combination by at least a one-dimensional beam element with two nodes. The ideal solution for this work is one that exclusively maintains linearity in the FEM calculation. The materials and properties used for the elements are assumed to be isotropic. The loads used are also limited in deforming the materials in their elastic ranges, and they are applied to the model statically. The calculation assumes small deflections in the solution. The small-deflection assumption is well suited since the differential equations governing the 2D plates and the 1D bar elements assume small deflections as well.

This dissertation is organized as follows: In Chapter 2, the Euler-Bernoulli beam theory and Timoshenko beam theory are reviewed briefly, providing context for the development at hand. Then a literature review of previous, relevant work done at the experimental, analytical, and theoretical levels is discussed. The general review of previous plate elements focuses on different types of Timoshenko beam elements.

Chapter 3 gives the proposed formulation of the new element, reviews its application and theory, and presents a derivation of the general formulation and its origins. The derivation of the novel fastening element, as shown in this chapter, involves a two-node, beam element meant to capture a contact stiffness due to the fastener/hole contact. Chapter 4 presents the application of the novel fastener element in the first case study, Chapter 5 presents the application of the novel fastener element in the second case study, and Chapter 6 introduces two additional case studies.

Finally, conclusions and recommendations are given in Chapter 7.

CHAPTER 2.

LITERATURE AND THEORETICAL REVIEW

2.1 Literature Review

The first place to review the preceding work is to the most poignant work done by Rutman et al. (2000) and Rutman and Bales-Kogan (2006). Their goal was, by far, the most similar to the goal of this research. In modeling fasteners located between plate shell elements (and in subsequent papers, solid elements as well), they modeled the joint problem in various ways with an assembly of existing elements that already exist in the NASA Structural Analysis (NASTRAN) element library. The main method of interest used to simulate the joints of plate and beam elements is with combinations of rigid-bar elements (RBARs), single-beam elements (CBARs), and spring elements (CBUSHs) (Figure 2.1).

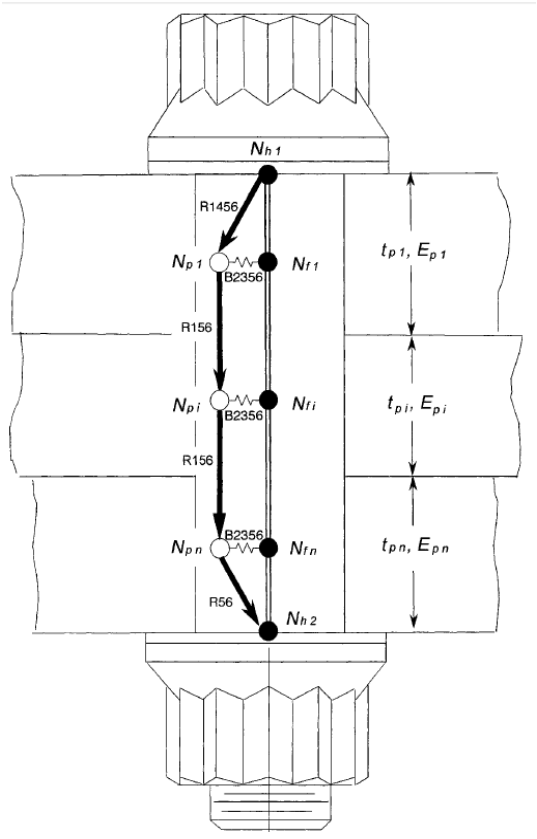

Figure 2.1: Assembly of 1D elements (Rutman et al., 2000).

The fastener was modeled with single-beam elements positioned between plate members and connected to the respective plates with spring elements. Additionally, rigid elements connected the "head" and "nut" to the plate elements and to the other plate elements as well. The research of Rutman et al. (2000) did not consider the effect of fastener pretension and fit, and did not take into account friction between the joined members. However, they maintain that the calculation of friction between the joints is not a common analysis practice in the aerospace industry. As a matter of generally accepted practice in industry, it is common to neglect this friction, since it is considered that the friction between the mating plates will allow some of the load to transfer from one plate to the other, instead of feeding shear load into the fastener itself. This negligence naturally drives conservatism into the joint design.

The treatment of the beam-element stiffness has traditionally contained only the stiffness properties of the fastening member of the joints. The most popular way of handling stiffness of the springs that connect the fastener to the plate elements, which has been defined as Huth contact stiffness, will be discussed later on in the discussion of the work of de Rijck (2005) and de Rijck and Fawaz (2000).

Paroissien et al. (2006, 2007) developed an analytical FEM 2D model for a bolted and bonded lap joint. They modeled joined elements consisting of 2D beams with a series of translational and rotational springs connecting the fastener, which is a rigid-body element. Their research included an adhesion parameter because they incorporated a set of "bonded beam elements" to simulate adhesive placed between the members. Their focus was more on the development of the bonded beam element than on the fastener itself. The bonded beam formulation lends accuracy to the present formulation for the physical problem of contacting

members with friction, although the present study does not take bonding or friction into account (Figure 2.2).

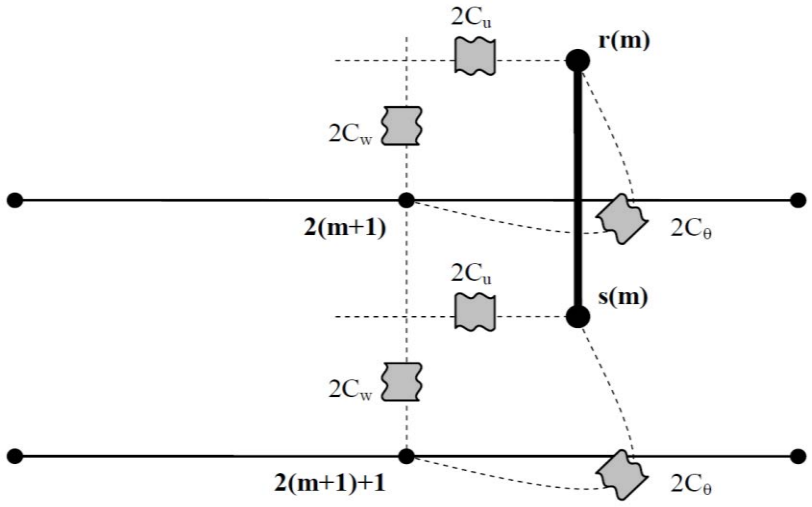

Figure 2.2: Multiple elements simulating a fastener (Paroissien et al., 2006).

At this point, it is convenient to mention, since Paroissien et al. (2006, 2007) reference this (as do many others), that Tate and Rosenfeld (1946) carried out an exhaustive study of lap joint stiffness calculations. They developed a recurrence formula, solving a statically indeterminate structural problem of a bolted linear array lap joint. Their solution to the problem resulted in the implementation of a system of second-order finite difference equations and provides for n-simultaneous linear equations involving n-unknown bolt loads. The application resulted in a very simple and direct determination of the bolt-load distribution in joints of uniform dimensions. This provides for a convenient and simple check with any new analytical method when modeling a lap joint, hence the reason for so many researchers referring to it.

Cope and Lacy (2004) modeled fasteners in single shear lap joints. Their main focus was on stress intensity factors for cracks in metallic joints in damage tolerance analysis. However, their aim was not necessarily a new formulation for the mechanical fastener as much as it was the use of a combination of existing elements. They provided an explicit code defining spring

elements for the fasteners. Stiffness was predetermined for both shear and bending, specifically adding in factors for the cross-sectional area and the shear and elastic moduli.

Both Paroissien et al. (2006, 2007) and Cope and Lacy (2004) cite Huth (1986), as do many other researchers. Huth (1986) attempted to improve the accuracy of fatigue life prediction methods for multiple-row riveted or bolted joints. He introduced an empirical equation for the compliance, C, or rather, its inverse of stiffness, K, which was derived from test results for riveted, bolted, metallic, and graphite/epoxy materials, as well as single and double lap joints (see equation [E.13] in Appendix E). Huth compared his equation to previous semi-empirical equations (also found in Appendix E) attributed to both the Boeing and Northrop Grumman corporations in unpublished papers and also Swift (1971), and showed that it is superior to other equations. The comparison he made was based on single shear lap joints. A compilation of these stiffness methods was incorporated into the neutral line method, which can be seen in the determination of load transfer shown by de Rijck (2005) and are conveniently compiled in Chapter 3 of this dissertation. deRijck cites the formulation of contact stiffnesses by various empirical formulae defined by Huth (1986) and Swift (1971), including stiffness formulae attributed to both the Northrop Grumman and Boeing corporations.

Barrios (1978) also determined stresses and displacements due to load transfer by fasteners in two volumes. The first volume focuses on clevis style joints in a double shear format, and the second volume focuses on lap joints in a single shear setting. His study centered on the determination of fatigue and failure behaviors of these mechanical joints and determining stress concentration factors. His initial formulation included a derivation of "foundational" stiffness produced earlier by Theocaris (1956). That foundational stiffness included a rudimentary value dependant on the elastic modulus of the fastener and the width of the plate

specimen and fastener diameter. The value of the joint stiffness was based simply on the relation E(1–d/w)/0.8, where E and d are the fastener's Young's modulus and diameter, respectively, and w is the width of the plate specimen.

Another paper that has been cited multiple times and becomes part of the foundation of lap joint analysis is the work of Wileman et al. (1991) who fitted a regression line of a non-dimensional stiffness ratio to conventional 3D finite element analysis. This regression analysis involved applying an exponential regression, and two non-dimensional coefficients were determined based on the types of material used. Wileman et al. (1991), as well as many other researchers, also cite Shigley and Mischke (1988), who, in developing an introductory textbook in the field of machine design, determined the stiffness of members in the clamped zone to be due to the pre-tightening of the nut/bolt assembly. They also treat joined members as an arrangement of springs in series. Wileman et al. (1991) refers to Ito et al. (1977) and their ultrasonic techniques used to determine pressure distribution at the member interface, as well as Rötscher's (1927) pressure-cone method used for stiffness calculations, which employs a variable cone approach with a fixed cone angle. Ito et al. (1977) assumed that the compression of the members was confined to the frustum of a hollow cone, of which the angle with the vertical axis was reported by Osgood (1979) to range from 25^{o} to 33^{o}. Shigley and Mischke (1988) split the difference between these limits and used 30^{o} outright (Figure 2.3). Their stiffness calculation follows a logarithmic/trigonometric function and works primarily for isotropic materials.

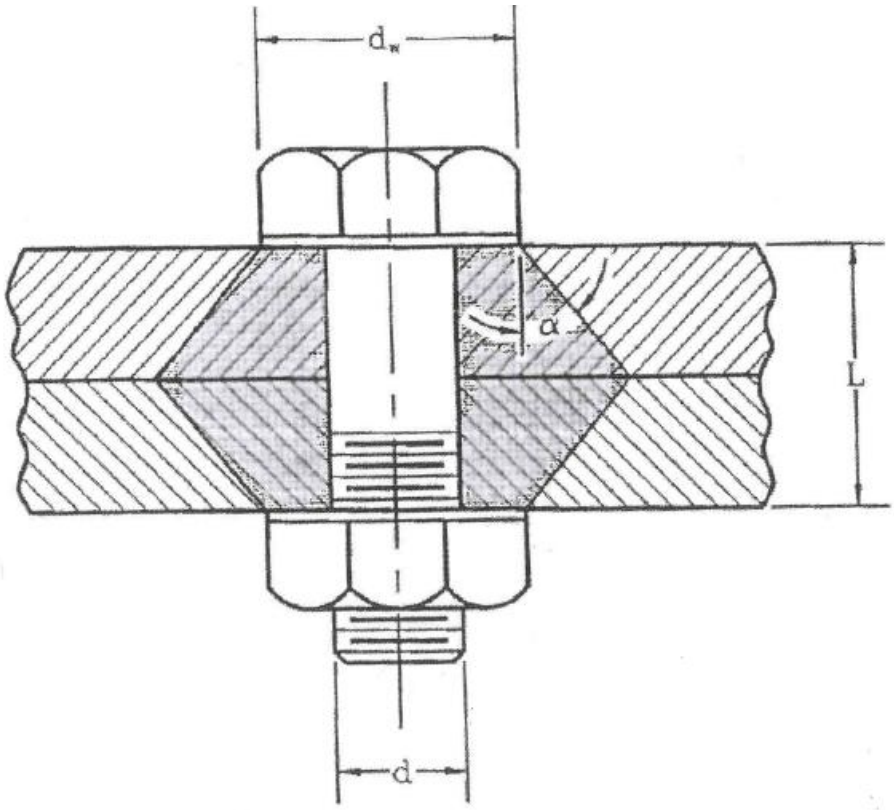

Figure 2.3: Compression cone (Shigley and Mischke, 1988; Wileman et al., 1991), Lee (2010a).

Shigley and Mischke (1988) are also quoted in a series of convenient articles written for *Machine Design* by Lee (2010a–e). Lee provides a series of equations taken from the work of Shigley and Mischke as well as the *Machinery's Handbook* by Green and McCauley (1996). Lee's articles present empirical and analytical equations that determine bolt stiffness, effective areas for clamped members, and flange stiffness. For clamped member stiffness, he uses three different methods: Shigley and Mishke's method, a clamped method assuming a spacer of known diameter, and double cone models with members of different thicknesses and materials. Again, the materials here are isotropic. Additionally, Lee notes how bolt preload affects the joined assembly as well as providing a simpler way to predict bolt preload. He also notes how bolted joints behave under internal loads. Of particular interest is the additional stiffness that is added to the stiffness calculation provided by the head of the bolt and the nut itself. The bolt

head and nut stiffness used are roughly approximated in terms of the stiffness of the bolt shank, at one-third of the shank stiffness added on for the bolt head and one-half of the shank stiffness added on for the nut. Lee compiles this convenient information into a series of fastening articles meant mainly for industry. Additionally, the stiffness of the joint appears to be only the stiffness in the axial direction of the fastener. No comment is made about the effect of preload on lateral stiffness of the joint.

The value of the papers mentioned so far are largely empirical in nature, using fairly rudimentary spring-like stiffness to simulate joined member stiffness and simple enough to be calculated by hand. A number of finite element analyses make comparisons, including comparisons to the general "spring" stiffness models. For instance, Musto and Konkle (2006) performed a finite element analysis in contrast to stiffness determined non-dimensionally by using a p-adaptive FEA method to calculate the out-of-plane deflection. They concluded that the stiffness-combining procedure of the individual members in joint-like springs in series can be inaccurate, due to the high dependence of joint stiffness on its geometry. This holds true especially when the thicknesses of the two members are nearly equal. Their proposed procedure, although not introducing new elements, shows a better performance in determining stiffness than traditional methods shown by Lee (2010a), Wileman (1991), and Shigley and Mischke (1988).

As suggested in the introduction, several researchers have analyzed bolt/nut lap joints. One example from and McCarthy et al. (2005) and McCarthy and McCarthy (2005), in a two part paper, provided three-dimensional finite element models for composite members in lap joint configurations. In the first paper, McCarthy et al. (2005) found a number of factors that were found to affect the accuracy and efficiency of the solution. Efficiency was improved by defining contact bodies as "sub-parts" of the joint components and using a contact table to define which

bodies could come into contact. Extra care was taken for the types of contact used. In the second paper, McCarthy and McCarthy (2005) identified an analysis and the importance on bolt-hole clearances. Both papers focused on the analytical processes and validations with test results and very little on simplified procedures. The contact issues in the first paper did touch on efficiency, but the analyses were solely based on 3D continuum elements.

Another example of bolt/nut lap joints is from the work of Iancu et al. (2004). Their investigation involved 3D modeling of thick, single-lap, bolted joints. They learned that the most difficult problem when dealing with finite element modeling of a joint resides in the necessity of creating contact surfaces, the parameters of which will greatly affect the final result. Interestingly, they showed that higher torque applied on the bolt during preload resulted in a lower maximum stress in the plate member. But if a certain value of the torque was exceeded, then the joint failed. For example, with a small value of torque, equivalent to finger tightening the bolt, the maximum shear stress in the plate decreased by 50%. This lends to the generally accepted notion that shear load transfer of the fastener is traded off for increased pre-loading tension.

Pedersen and Pedersen (2008a, 2008b, and 2009) had two goals: establishing a simplified formula for obtaining member stiffness when the width of the member is larger, and establishing a simplified formula for the member stiffness when the width becomes finite. They assumed contact without friction, they used the finite element method to verify stiffness, and they incorporated a direct formulation of the contact between the bolt and the joined members. Several useful observations resulted from this research. One observation was that bolt designs should be primarily controlled by loading conditions. They provided an FE model of an axis-symmetric part of a bolt and integrated washer with different assumed pressure distributions of

the head on the top member. They determined that their bolt stiffness calculation was straightforward and concluded that their method agrees with that of other researchers. It is interesting to note that the bolt-head load distribution has little influence on bolt stiffness; however, determining the combined stiffness of the clamped members becomes more complicated. They used FE with contact analysis to calculate the elastic energy in both the bolt and the plate members, and from those energies, they directly calculated the stiffness. The advantage here is that the displacement does not need to be defined and provides a clearer definition of the stiffness relative to what is found in most of the literature. When contact is determined, a "superelement technique" that removes the iterative nature of calculating the contact forces is applied. This removal considerably simplifies the computations.

At this point, it is helpful to provide a cursory definition of superelement, which, in simplest terms, is a superelement is a grouping of finite elements that, upon assembly, may be regarded as an *individual element* for computational purposes. These purposes may be driven by modeling or processing needs (Felippa, 1998). This is not to say that a random assortment of elements does not necessarily make up a superelement. To be considered a superelement, it must form a structural component on its own. This condition imposes certain mathematical conditions. One such requirement is "rank sufficiency." In general terms, an element is said to be rank-sufficient if its only zero-energy modes are rigid-body modes. Equivalently stated, the superelement does not possess spurious kinematic mechanisms.

Several authors (Ekh, 2006; Ekh and Schon, 2005, 2008a, 2008b; and Schon et al., 2005) have modeled multi-fastener single-lap joints in composite structures. These studies focused on a simplified finite element design but did not determine spring stiffness for bolts, and some conclusions of the lap joint problem are pertinent. They concluded that common analysis

approaches are based on the complex function method, or 2D FEM method. They did make particular note of "knife edging" of bolts with hole clearances and mentioned initial stress concentrations. These authors challenged the spring-based methods, claiming that they were restricted to joints with fasteners arranged in a single column. Furthermore, important mechanisms such as fastener clamp-up, friction, and out-of-plane deformation were not taken into consideration. The models they used were based on an in-line multi-bolt arrangement, which diminished the importance of the stress field in member plates. Additionally, they stressed the importance of bolt/hole contact and tolerance errors that could increase the load of one bolt over another. They also applied frictional forces between the members via connector elements based on compressive forces acting in the connector and on the coefficient of friction. They also noted that bolt-hole clearance is the most important factor, but fastener clamp-up and friction should also be accounted for in order to make accurate predictions. They also noted that caution should be exercised in using linear kinematics, which may yield unconservative results.

Hyer and Klang (1985), Madenci et al. (1998), Kradinov et al. (2000, 2004), and Ekh and Schon (2005) have spent considerable effort in determining the effects of bolt/hole contacts in composite members within a row of fasteners. The contact profile of the member on the bolt shaft is identified as having three regions, as shown in Figure 2.4. The first and second regions are contact regions, while the third region is a non-contact region. The difference between the first and second regions is that the first is a no-slip region that straddles the load.

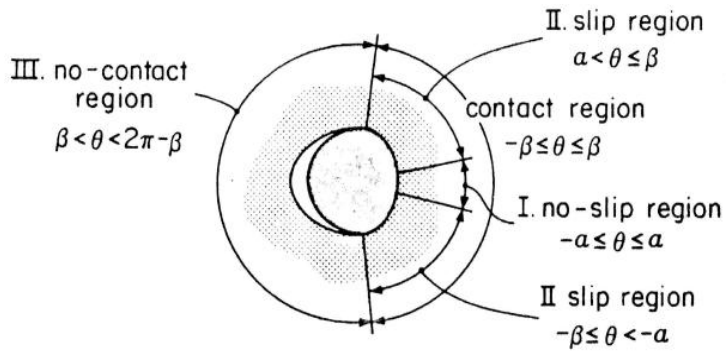

Figure 2.4: Bolt/member contact regions. (Hyer and Klang, 1985)

Hyer and Klang (1985) determined that the elasticity of the pin is not as important a variable as clearance and friction, but noted that incorporating pin elasticity reduces peak stresses. They also noted that a rigid pin analysis, including the effects of clearance and friction, would be quite satisfactory, at least for steel pins. They also found that the angle in the no-slip region was in the 10–15 degree range for higher coefficients of friction, say 0.4, and the no-slip region dropped down to less than 4.5 degrees for lower coefficients of friction, say 0.2. Radial load profiles against the bolt shaft showed good agreement to a sinusoidal function. They employed the complex function method used for both the pin and plate, accounting for deformation in both. This suggested that the loading transfer between the hole and fastener is largely a normal force, and in the simplification of the problem, shear stresses can be ignored.

De Jong (1977) also used the complex function method, assuming a stress distribution for the applied load on the pin (bolt), which transforms the contact problem into a boundary-value problem. A full description of the complex potential method is beyond the scope of this research, but can be found in the work of Lekhnitski (1981).

2.2 Common Configurations Currently Used in Industry

This section presents several figures illustrating some of the many ways that current elements are joined to simulate lap joints. In all examples, there are no "new" finite elements but rather an assembly of elements to make the connections and simulate the behavior.

The first configuration is the simplest, involving a singular beam element with a length between both plate elements and two nodes. If there is no direct connection between the single-beam element (CBAR) and the plate elements, it is usually connected to the corresponding plate elements by two rigid body elements (RBEs), also known colloquially as spider elements. One RBE exists for the top plate and one for the bottom plate (Figure 2.5).

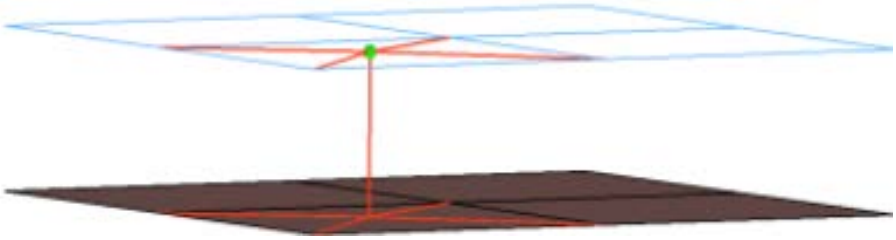

Figure 2.5: Beam element (CBAR) with spider elements (RBE).

Figure 2.6 illustrates the connection of the RBE elements around pre-existing holes in the plate elements. This occurs in the event that solid model geometry used to create the mid-plane already contains holes.

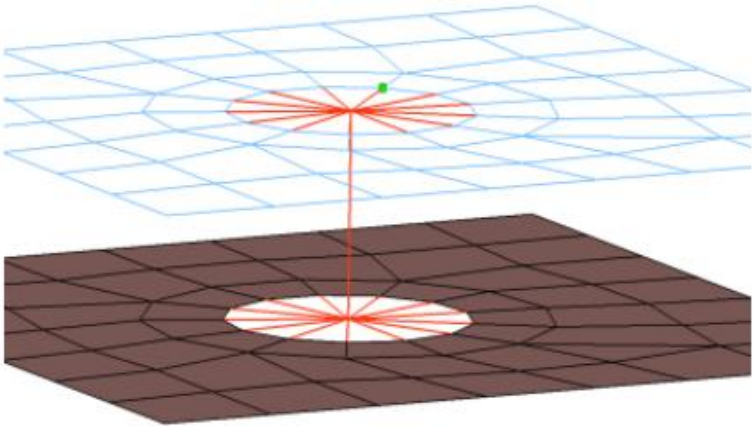

Figure 2.6: Beam element (CBAR) with spider elements (RBE) around holes.

Figure 2.7 illustrates the use of rigid body elements only. The connector location can be either on the edges, in the center, or at the midpoint between holes.

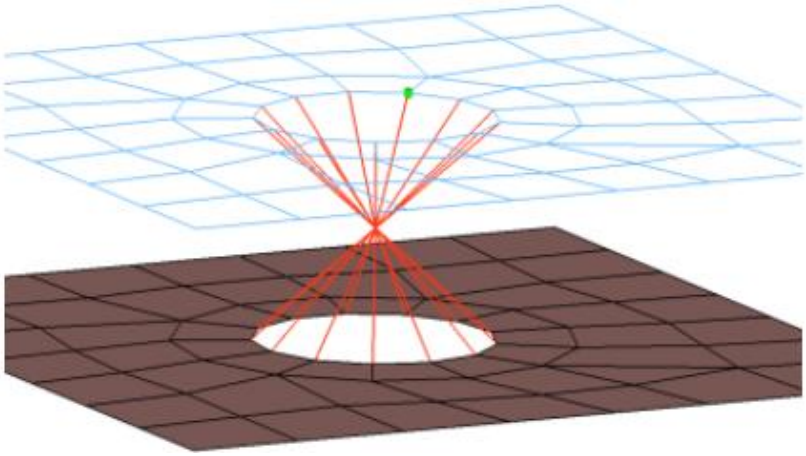

Figure 2.7: Spider elements only (RBE) around holes.

Figure 2.8 shows a CBAR element simulating the fastener body and RBE elements. It differs from previous examples because the spider elements do not connect to the edges of the holes but rather one element row further into the plate, in order to capture the footprints that washers will have on the plate members.

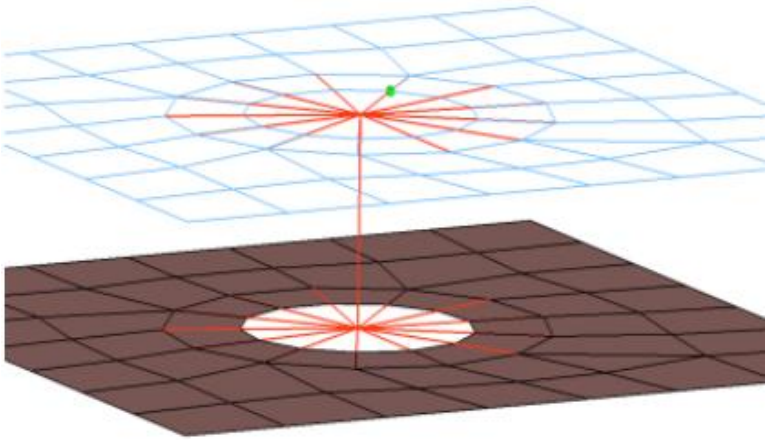

Figure 2.8: Beam element with spider elements (RBE) forming washers.

Figure 2.9 shows a single, hexagonal, solid element (HEXA8) connected to plate elements using two RBE elements. This particular configuration uses plate thicknesses to

calculate the offset from the plate elements themselves. The length of the hexahedron element in the axial direction of the fastener is "equivalenced" to half the sum of the plate thicknesses (t1 + t2)/2. Here, the upper and lower surfaces of the solid elements of the plate members shown are connected to the hexagonal solid element via four separate rigid body elements. The difference in this element is that the mid-planes are not constructed; instead, the surfaces of the element are connected.

The simplified fastener element (CFAST), shown in Figure 2.10, is an element defined for NASTRAN (supported largely by MSC NASTRAN) users that allows for the selection of two plate surfaces and ensures the orthogonality of the element with the two plate surfaces, regardless of nodal locations of the plate element. Finally, Figure 2.11 shows an element assembly designed specifically for Hi-Lok™ fasteners, which illustrates the combination of existing elements. The research in this dissertation is specifically intended to replace the compilation of elements like this and utilize Hertzian contact theory to address the contact stiffness of the joints.

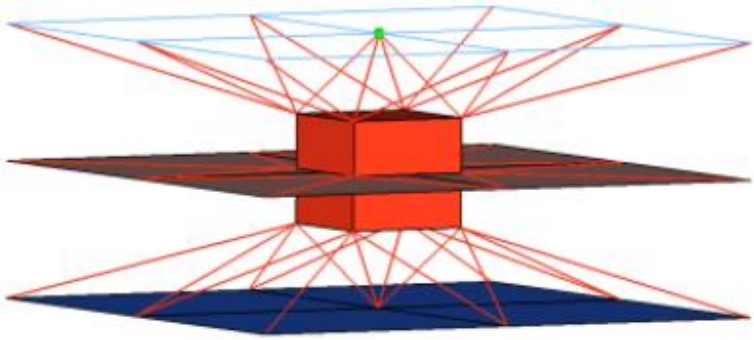

Figure 2.9: Hexa (solid) element with spider elements only (RBE).

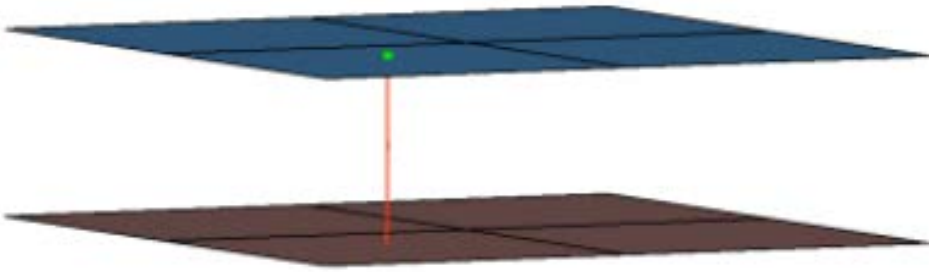

Figure 2.10: CFAST element.

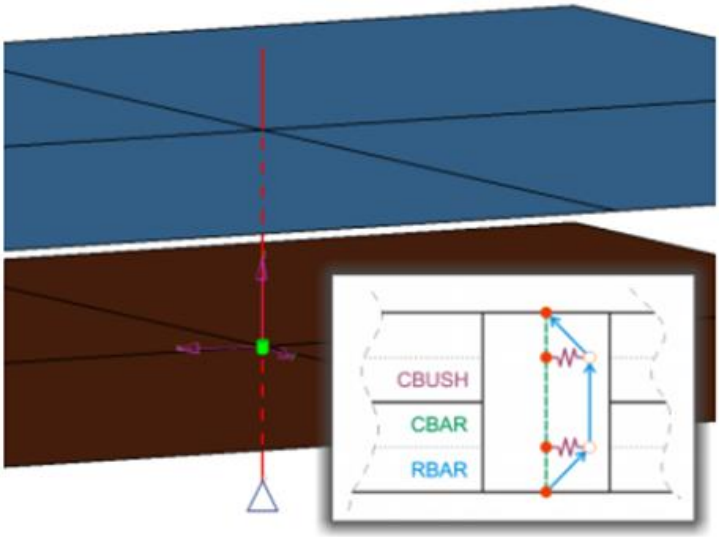

Figure 2.11: NASTRAN Hi-Lok™ element.

This concludes a short list of different methods using 1D and 2D elements to create mechanically fastened joints in industry. All but one of them (CFAST element) are simply an assembly of preexisting elements.

2.3 Beam Theories and FEM Implementation

Regarding the theory of elasticity, Timoshenko (1921) showed that if a beam is bent in one of its principal planes by two equal and opposite couples applied at the ends, and the deflection occurs in the same plane of the six stress components, then only the normal stress relative to the axis of the bar is non-zero. This stress is proportional to the distance from the neutral axis. Additionally, Timoshenko and Goodier (1970) showed that during bending of a

cantilevered beam by a force applied transversely at its end, in addition to normal stresses that are proportional in each cross section to the bending moment, shearing stresses are present and proportional to the shearing force acting on the beam as well. They also assumed that normal stresses over a cross section at a distance from the fixed end are distributed in the same manner as in the case of pure bending. Shearing stresses do not depend on the distance along the axis and are the same in all cross sections of the beam. From here, 1D beam theories began. One-dimensional beam theories result from a simplification of the theory of elasticity in three dimensions. Based on Timoshenko's added shear stress in beam cross sections, the transverse deflection of the beam is not only caused by beam curvature, which results from normal strain, but is also the direct transverse shear strain. This added deformation is especially important for beams with a relatively large thickness (or depth) or beams with relatively higher in-plane normal stiffness compared to transverse shear stiffness.

Two theories dominate beam elements. The first, and simplest, is the Euler-Bernoulli theory, named after Daniel Bernoulli and Leonhard Euler, and developed circa 1750. A successive theory developed in 1921 is the Timoshenko beam theory, which expanded the utility of the Euler-Bernoulli Theory, and is named after Stephen Timoshenko. The most popular developments of both theories lay out the beam along the x-axis with the positive transverse deflection pointing downward (Timoshenko and Goodier, 1970; Reismann and Pawlik, 1980; Reddy, 2006; and others). Other developments orient positive transverse deflection in the opposite direction (Bathe and Dvorkin, 1985; Astley, 1992; Hughes, 2000). Results for both methods are similar, and the outputs are the same in magnitude, if not the sign. Where possible, equations defining the finite element in this thesis will be made for both cases.

2.4 Euler-Bernoulli Beam Theory and Finite Element Method

The Euler-Bernoulli theory is based fundamentally on the notion that a straight beam in the presence of a constant moment deforms into a curvature, which is a simplification of the linear theory of elasticity. For a beam with its centroidal axis along the x-axis, with a cross-sectional area (A), second moment of inertia (I), and Young's modulus (E), bending moment (M), shear force (V), and axial force (P), the resulting displacements are v(x) and w(x) in the y and z directions, respectively (Astley, 1992).

$$-EI\frac{d^2w}{dx^2} = M \tag{2.1}$$

The main assumption about displacements under this theory is that plane sections perpendicular to the centroidal axis remain planar and perpendicular to the axis after deformation.

Traditional moment and shear relationships apply as well, where q is the distributed load, and c_f is the stiffness of the elastic foundation, as shown in Figure 2.12. The governing equations are as follows:

$$-\frac{dV}{dx} + c_f w = q(x) \tag{2.2}$$

$$-\frac{dM}{dx} + V = 0 \tag{2.3}$$

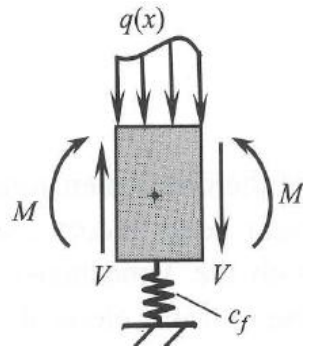

Figure 2.12: Shear force-bending moment relations.

Using the convention that Astley (1992) uses, in order to drive the constraint that the cross sections remain planar, the rotation of the end planes, θ_1 and θ_2, are equal to the slopes of the axis at those locations, μ_1 and μ_2, respectively (Reddy [2006] uses dw/dx for the deflection angle of the x axis, and γ_{xz} for shear strain). The addition of the "c_c" term noted in equation (2.2) comes from describing "contact stiffness." This term usually is not found in traditional formulations of beam elements but is useful in applications that involve typical civil engineering problems, such as a beam resting on a continuum like soil or rails resting on railroad ties. The term used in civil engineering applications is known as "foundational stiffness," which assumes a rigid base. Figure 2.13 illustrates the foundation as a "bed of springs," which is traditionally referred to as the "Winkler foundation." The assumptions that make the Winkler foundation possible will be discussed later in this chapter, in section 2.9. Both Figures 2.13 and 2.14 show the degrees of freedom of the nodes and the choice of orientation of the axes.

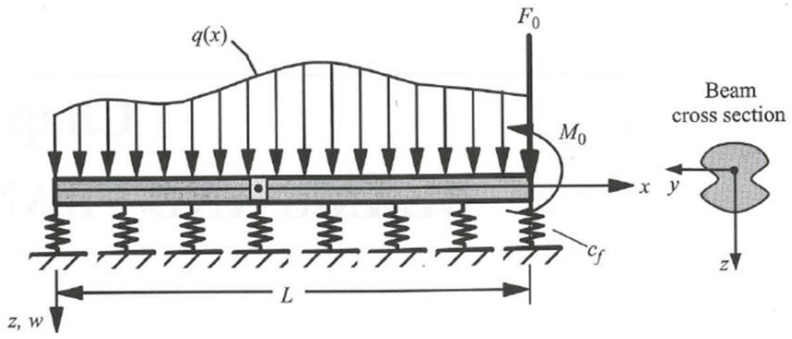

Figure 2.13: Beam with applied loads and an elastic foundation (Reddy, 2006).

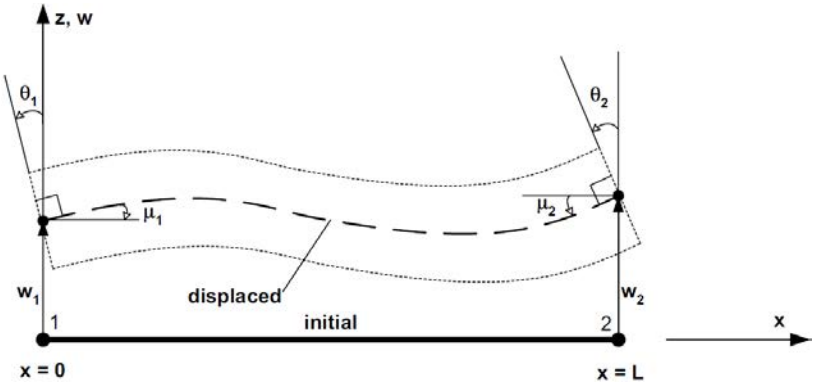

Figure 2.14: Euler-Bernoulli beam (Astley, 1992).

By substituting equations (2.1), (2.2), and (2.3), it is clear that the transverse deflection, w(x), of the beam is governed by a fourth-order differential equation:

$$\frac{d^2}{dx^2}\left(EI\frac{d^2w}{dx^2}\right) + c_f w = q(x) \tag{2.4}$$

Applying the weak form of this yields

$$\int_{x_e}^{x_{e+1}} \frac{d^2}{dx^2}\left(EI\frac{d^2w}{dx^2}\right) + c_f w - q(x)dx = 0 \tag{2.5}$$

$$\int_{x_e}^{x_{e+1}} EI\frac{d^2v}{dx^2}\frac{d^2w}{dx^2} + c_f vw - vq(x)dx + \left[v\frac{d}{dx}\left(EI\frac{d^2w}{dx^2}\right) - \frac{dv}{dx}\left(EI\frac{d^2w}{dx^2}\right)\right]_{x_e}^{x_{e+1}} = 0 \tag{2.6}$$

After identifying the bilinear and linear forms of the equation, a quadratic functional is formed and becomes known as the total potential energy and is represented by

$$\pi_e(w) = \int_{x_e}^{x_{e+1}} \left(\frac{EI}{2}\left(\frac{d^2w}{dx^2}\right)^2 + \frac{1}{2}c_f w^2 - wq(x)\right)dx - w(x_e)Q_1 - w(x_{e+1})Q_3 - \left(-\frac{dw}{dx}\right)\Big|_{x_e} Q_2 - \left(-\frac{dw}{dx}\right)\Big|_{x_{e+1}} Q_4 \tag{2.7}$$

where the source terms Q_i are the shear and moments, w(x) are the deflections, and dw/dx are the slopes. Figure 2.15 illustrates the discretization of the beam into elements. Figure 2.15(a) identifies the loads on the beam, where Figure 2.15(b) identifies the "eth" element after discretization, and Figure 2.15(c) identifies the primary and secondary variables in the beam.

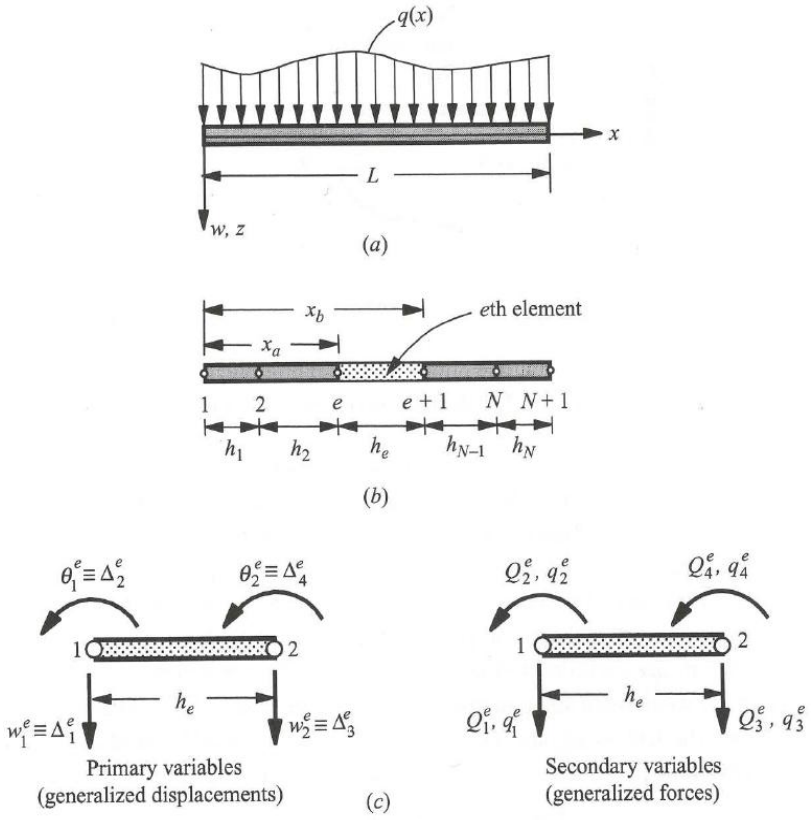

Figure 2.15: Beam discretization (Reddy, 2006).

The Euler-Bernoulli theory requires that the interpolation functions used across the elements be continuous with nonzero derivatives up to the second order. This satisfies the essential boundary conditions of the element, and by satisfying these boundary conditions, the approximation automatically satisfies the continuity conditions. Since there are four conditions for any element, a four parameter polynomial is selected for w(x) (refer to equation [2.8]) and dw/dx. Therefore, the interpolation functions, φ, need to be third-order functions, and they are known as Hermite cubic interpolation functions (refer to equation [2.9]). Simpler Lagrange interpolation functions for the same could be derived to interpolate the transverse deflections but not their derivatives. Slopes of the dependent variables are required to be continuous at the nodes of the EBT. Lagrange interpolation functions cannot do this, and are therefore insufficient for use of the shape functions (Reddy 2006).

$$w(x) \approx w_h^e = c_h^e + c_h^e x + c_h^e x^2 + c_h^e x^3 \tag{2.8}$$

$$w_h^e = \Delta_1^e \varphi_1^e + \Delta_2^e \varphi_2^e + \Delta_3^e \varphi_3^e + \Delta_4^e \varphi_4^e = \sum_{i=1}^4 \Delta_i^e \varphi_i^e \tag{2.9}$$

The beam finite element model that models the EBT is obtained by substituting the finite element interpolation for w and φ for the weight functions into the weak form. Since there are four degrees of freedom in one particular plane, this results in a system of four equations and four unknowns. Equation (2.10) runs for both "i" and "j" going from 1 to 4.

$$0 = \sum_{i=1}^4 \int_{x_e}^{x_{e+1}} \left(EI \left(\frac{d^2 \varphi_i^e}{dx^2} \right) \left(\frac{d^2 \varphi_j^e}{dx^2} \right) + c_f \varphi_i^e \varphi_j^e \right) dx \, u_j^e - \int_{x_e}^{x_{e+1}} \varphi_j^e q(x) dx \, u_j^e - Q_j \tag{2.10}$$

The EBT element leads to the exact nodal values for any distribution of the transverse load q(x), provided that the bending stiffness (EI) is an element-wise constant and that $c_f = 0$. This fact makes the element a "superconvergent element." In expanded form,

$$\frac{2EI}{L^3} \begin{bmatrix} 6 & -3L & -6 & -3L \\ -3L & 2L^2 & 3L & L^2 \\ -6 & 3L & 6 & 3L \\ -3L & L^2 & 3L & 2L^2 \end{bmatrix} \begin{Bmatrix} U_1 \\ U_2 \\ U_3 \\ U_4 \end{Bmatrix} = \frac{q_0 L}{12} \begin{Bmatrix} 6 \\ -L \\ 6 \\ -L \end{Bmatrix} + \begin{Bmatrix} Q_1 \\ Q_2 \\ Q_3 \\ Q_4 \end{Bmatrix} \tag{2.11}$$

2.5 Timoshenko Beam Theory

Timoshenko beam theory is a modification of the Euler-Bernoulli theory. This theory makes the same assumptions as the EBT, with one addition. It does not assume that the planar cross sections of the beam axis necessarily remain normal to the longitudinal axis of the beam after bending. This results in a non-zero transverse shear strain, $\gamma_{xz} = 2\varepsilon_{xz} \neq 0$. The rotation of the transverse normal plane about the y-axis is not necessarily equal to the slope of the axis itself, –dw/dx. The rotation about the y-axis is denoted by an independent function, Ψ(x), which actually becomes the sum of the slope and the transverse shear strain (Figure 2.16):

$$\Psi(\mathrm{x}) = \gamma_{\mathrm{xz}} - \frac{\mathrm{dw}}{\mathrm{dx}} \tag{2.12}$$

In this application, the assumption is that although the transverse plane's normal vector is no longer tangential to the longitudinal axis, the cross section is still "planar," or rather, the change in transverse shear along the thickness of the beam is linear.

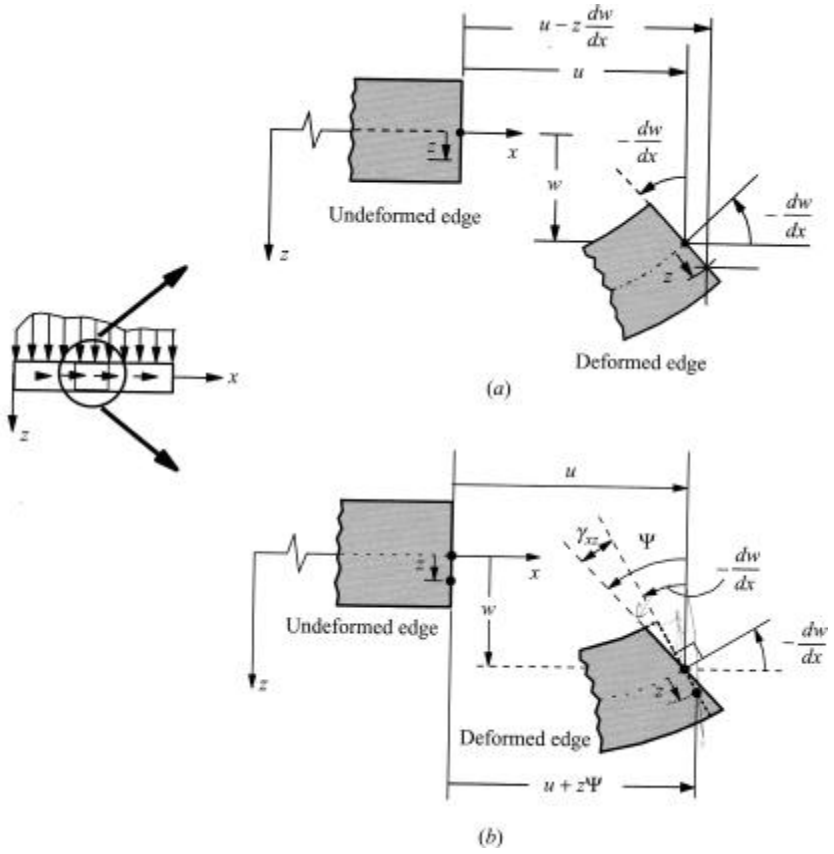

Figure 2.16: Timoshenko beam theory (Reddy 2006).

The primary advantage of Timoshenko over Euler-Bernoulli is that the EBT is generally limited to thin beams (with length-to-depth ratios [L/D], also called slenderness ratios, of 20 or larger), where the TBT allows for a relaxation to this limitation. The TBT is tailor-made for applications involving composites in which stiffness changes across the thickness of plates as well as across the small length-to-thickness ratios. The equilibrium equations of the TBT are the same as those of the EBT, but there is one additional relationship:

$$-\frac{dV}{dx} + c_c = q,\ -\frac{dM}{dx} + V = 0,\ M = EI\frac{d\Psi}{dx},\ V = GAK_s(\frac{dw}{dx} + \Psi) \tag{2.13}$$

The governing differential equations in terms of the transverse deflection, w, and rotation function, Ψ, become

$$-\frac{d}{dx}\left[GAK_s\left(\frac{dw}{dx}+\Psi\right)\right]+c_c w=q \tag{2.14a}$$

$$-\frac{d}{dx}\left(EI\frac{d\Psi}{dx}\right)+GAK_s\left(\frac{dw}{dx}+\Psi\right)=0 \tag{2.14b}$$

where G is the shear modulus, and K_s represents a shear correction coefficient. The variable K_s is introduced to factor in an average constant shear stress across the cross section of the beam in the TBT. It also simplifies the parabolic variation of the shear stress predicted by the theory of elasticity through the beam thickness. The typical value given by Timoshenko for K_s is approximately 5/6 for maximum shear in circular cross sections. Different figures have been determined by Rosinger and Ritchie (1977) and by Gruttman and Wagner (2001). In both cases, they have shown that the shear correction factor is sensitive to Poisson's ratio. Rosinger and Ritchie (1977) found that for circular cross sections

$$K_s=\frac{6(1+\nu)}{7+6\nu} \tag{2.15}$$

The weak form of the TBT is expressed by two equations:

$$\int_{x_e}^{x_{e+1}}\left(\frac{dv_1}{dx}\left[GAK_s\left(\frac{dw}{dx}+\Psi\right)\right]+c_f v_1 w-v_1 q\right)dx-\left[v_1 GAK_s\left(\frac{dw}{dx}+\Psi\right)\right]_{x_e}^{x_{e+1}}=0 \tag{2.16a}$$

$$\int_{x_e}^{x_{e+1}}\left[\frac{dv_2}{dx}\left(EI\frac{d\Psi}{dx}\right)+v_2 GAK_s\left(\frac{dw}{dx}+\Psi\right)\right]dx-\left[v_2 EI\frac{d\Psi}{dx}\right]_{x_e}^{x_{e+1}}=0 \tag{2.16b}$$

The first equation governs the transverse shear in the beam, whereas the second equation governs the moment:

$$GAK_s\left(\frac{dw}{dx}+\Psi\right)\equiv V \tag{2.17}$$

$$EI\frac{d\Psi}{dx}\equiv M \tag{2.18}$$

This also means that the weight functions v_1 and v_2 in equations (2.16a) and (2.16b) both have physical meanings: that v_1 is equivalent to the transverse deflection, w, and v_2 represents the rotation function, Ψ. In this case, Ψ contains both the rotation of the beam and the transverse shear terms. Similar to the FEM formulation for the EBT, the quadratic functional for the TBT in the principle of virtual displacement equation becomes

$$\Pi_e(w,\Psi) = \int_{x_e}^{x_{e+1}} \left(\frac{EI}{2}\left(\frac{d\Psi}{dx}\right)^2 + \frac{GAK_s}{2}\left(\frac{dw}{dx}+\Psi\right)^2 + \frac{1}{2}c_f v w^2 - wq(x) \right) dx - w(x_a)Q_1 - \Psi(x_a)Q_2 - w(x_b)Q_3 - \Psi(x_b)Q_4 \tag{2.19}$$

Both equations comprising the TBT involve only first derivatives with respect to the length of the beam in the x-direction. Since the primary variables become the dependent unknowns (and their derivatives do not factor in), Lagrange shape functions are appropriate here. The minimum admissible degree of interpolation is linear. Variables w and Ψ do not have the same physical units, and they can be interpolated with different degrees of interpolation, although interpolating with identical degrees is the most common. This poses a problem, since rotation is linear, which is not consistent with what w(x) would predict, since it also would be linear. The implication from this order is that the rotation function, Ψ, is constant, but a constant Ψ would drive the bending energy of the element, represented by the following integral, to be zero:

$$\int_{x_a}^{x_b} \frac{EI}{2}\left(\frac{d\Psi}{dx}\right)^2 dx \tag{2.20}$$

This phenomenon is commonly known as *shear locking*. To address this problem, two procedures are most commonly used today: consistent interpolation and reduced integration. Since the new finite element in this research follows the consistent interpolation element (CIE), it is covered in this review.

Consistent interpolation uses an approximation of w, which has a quadratic interpolation, and Ψ, such that dw/dx and Ψ have a linear interpolation. This consistency sidesteps the shear locking problem altogether. However, in order to establish a higher-order shape function to capture the deflection, w(x) of the beam, and the lower-order shape function to capture the rotation, ψ(x) of the beam, this requires three nodes for the beam element to capture deflection, but only two of those nodes are necessary to capture rotation. The additional node that must be introduced is used for the deflection equation, and its effect is then split evenly into the two end nodes for determining that deflection (Figure 2.17). This reduces the problem from a five-equation system to a four-equation system, which are illustrated in equations (2.21) to (2.25) (in matrix form, Ψ(x) is represented by the variable S to eliminate confusion between the variables representing the shape functions and the rotation variable).

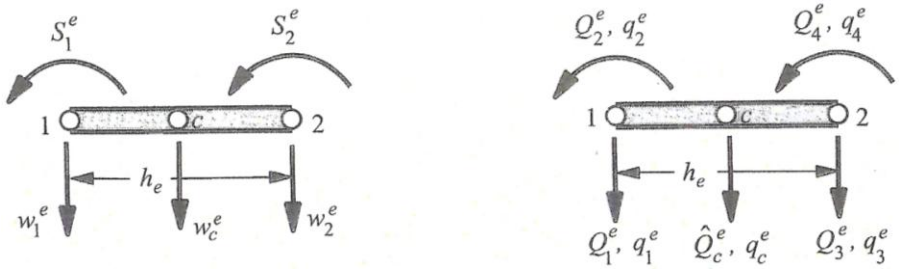

Figure 2.17: Three-node beam element.

$$K_{ij}^{11} = \int_0^h GAKs \frac{d\Psi i}{dx}\frac{d\Psi j}{dx}dx + \int_0^h c_f \Psi i \Psi j \, dx \tag{2.21}$$

$$K_{ij}^{12} = K_{ij}^{21} = \int_0^h GAKs \frac{d\Psi i}{dx}\Psi j dx \tag{2.22}$$

$$K_{ij}^{22} = \int_0^h EI \frac{d\Psi i}{dx}\frac{d\Psi j}{dx} + GAKs\Psi i\Psi j dx \tag{2.23}$$

$$F_i^1 = \int_0^h q\Psi \, dx \tag{2.24}$$

$$\begin{bmatrix}[K^{11}] & [K^{12}] \\ [K^{21}] & [K^{22}]\end{bmatrix}\begin{Bmatrix}\{w\} \\ \{S\}\end{Bmatrix} = \begin{Bmatrix}\{F^1\} \\ \{F^2\}\end{Bmatrix} \tag{2.25}$$

In the matrix shown in equation (2.25), it is assumed that the contact coefficient, c_c, is zero. Adding c_c into this matrix is part of the new finite element formulation covered in Chapter 3.

$$K11 = \frac{GAKs}{3h}\begin{bmatrix} 7 & -8 & 1 \\ -8 & 16 & -8 \\ 1 & -8 & 7 \end{bmatrix} + \frac{c_f h}{30}\begin{bmatrix} 4 & 2 & -1 \\ 2 & 16 & 2 \\ -1 & 2 & 4 \end{bmatrix} \tag{2.26}$$

$$K12 = K21^T = \frac{GAKs}{6}\begin{bmatrix} -5 & -1 \\ 4 & -4 \\ 1 & 5 \end{bmatrix} \tag{2.27}$$

$$K22 = \frac{EI}{h}\begin{bmatrix} 1 & -1 \\ -1 & 1 \end{bmatrix} + \frac{GAKsh}{6}\begin{bmatrix} 1 & -1 \\ -1 & 1 \end{bmatrix} \tag{2.28}$$

$$\frac{GAKs}{6h}\begin{bmatrix} 14 & -16 & 2 & -5h & -h \\ -16 & 32 & -16 & 4h & -4h \\ 2 & -16 & 14 & h & 5h \\ -5h & 4h & h & 2h^2 & h^2 \\ -h & -4h & 5h & h^2 & 2h^2 \end{bmatrix}\begin{Bmatrix} w1 \\ wc \\ w2 \\ S1 \\ S2 \end{Bmatrix} = \begin{Bmatrix} q1 \\ qc \\ q2 \\ 0 \\ 0 \end{Bmatrix} + \begin{Bmatrix} Q1 \\ Qc \\ Q3 \\ Q2 \\ Q4 \end{Bmatrix} \tag{2.29}$$

where

$$= 1 - 6 \quad , \quad = 1 + 3 \quad , \; \mu_0 = 12 \quad , \quad = \frac{\mathrm{EI}}{\mathrm{GAKsh}^2} \tag{2.30}$$

Condensing out the second equation in the matrix and rearranging yields

$$\frac{2EI}{\mu_0 h^3}\begin{bmatrix} 6 & -3h & -6 & -3h \\ -3h & h^2(1.5+6\Lambda) & 3h & h^2(1.5-6\Lambda) \\ -6 & 3h & 6 & 3h \\ -3h & h^2(1.5-6\Lambda) & 3h & h^2(1.5+6\Lambda) \end{bmatrix}\begin{Bmatrix} w1 \\ S1 \\ w2 \\ S2 \end{Bmatrix} = \begin{Bmatrix} q1 + 0.5qc \\ -qc \times h/8 \\ q2 + 0.5qc \\ qc \times h/8 \end{Bmatrix} + \begin{Bmatrix} V1 \\ M1 \\ V2 \\ M2 \end{Bmatrix} \tag{2.31}$$

For a two node element undergoing deflection and rotation, there are four DOF in each plane of action.

A modification can be done to the CIE-1 element, which is called CIE-2 or interdependent interpolation element (IIE). Consistent interpolation is also used on the same differential equations, but instead of having a single internal node to capture an additional point defining displacement only, the shape functions used are based on cubic Lagrange functions for

displacement and quadratic functions for the rotation, requiring seven total degrees of freedom, and three internal nodes (w_1, w_2, w_3, w_4, S_1, S_2, S_3). Condensation of the internal nodes to the outer nodes again reduces the element to a two-node, four DOF element. This element is a superconvergent element, and when the terms responsible for transverse shear approach zero, the element identically becomes the EBT element (note: μe = 1+12):

$$\frac{2EI}{\mu e \times h^3}\begin{bmatrix} 6 & -3h & -6 & -3h \\ -3h & 2h^2\Sigma & 3h & h^2\Theta \\ -6 & 3h & 6 & 3h \\ -3h & h^2\Theta & 3h & 2h^2\Sigma \end{bmatrix}\begin{Bmatrix} w1 \\ S1 \\ w2 \\ S2 \end{Bmatrix} = \begin{Bmatrix} q1 + 0.5qc \\ -qc \times h/8 \\ q2 + 0.5qc \\ qc \times h/8 \end{Bmatrix} + \begin{Bmatrix} V1 \\ M1 \\ V2 \\ M2 \end{Bmatrix} \tag{2.32}$$

The last element discussed, and the most commonly used commercial code, is known as the reduced integration element (RIE). This element utilizes only first-order Lagrange shape functions. It is also able to use the properties of Gaussian quadrature, a numerical integration scheme in which particular points (or integration points) of interest across the length are multiplied by factors that result in an approximation across a specific interval [–1,1]. The K11, K12, K21, and bending portion of K22 (in equations (2.26 to 2.28) are integrated with a two-point quadrature scheme, and the shear term inside the K22 term is integrated with a one-point quadrature scheme (or reduced integration).

The stiffness matrix for the RIE is the same as the stiffness matrix for the CIE-1. The only difference is the residual force vector load representation. In the CIE-1, the load vector is the same as the EBT theory, whereas in the RIE, the distributed load only contributes to the force degrees of freedom and not the moment degrees of freedom.

$$K11 = \frac{GAKs}{h}\begin{bmatrix} 1 & -1 \\ -1 & 1 \end{bmatrix} \tag{2.33}$$

$$K12 = K21^T = \frac{GAKs}{2}\begin{bmatrix} 1 & -1 \\ -1 & 1 \end{bmatrix} \tag{2.34}$$

$$K22 = \frac{EI}{h}\begin{bmatrix} 1 & -1 \\ -1 & 1 \end{bmatrix} + \frac{GAKsh}{4}\begin{bmatrix} 1 & -1 \\ -1 & 1 \end{bmatrix} \tag{2.35}$$

$$\frac{2EI}{\mu_0 h^3}\begin{bmatrix} 6 & -3h & -6 & -3h \\ -3h & h^2(1.5+6\ ) & 3h & h^2(1.5-6\ ) \\ -6 & 3h & 6 & 3h \\ -3h & h^2(1.5-6\ ) & 3h & h^2(1.5+6\ ) \end{bmatrix}\begin{Bmatrix} w1 \\ S1 \\ w2 \\ S2 \end{Bmatrix} = \begin{Bmatrix} q1 \\ 0 \\ q2 \\ 0 \end{Bmatrix} + \begin{Bmatrix} V1 \\ M1 \\ V2 \\ M2 \end{Bmatrix} \tag{2.36}$$

2.6 Axial Deflection

The axial deflection, u(x), of the beam is governed by the following second-order differential equations:

$$\frac{d}{dx}\left(EA\frac{du}{dx}\right) = f(x) \tag{2.37}$$

$$\frac{EA}{h}\begin{bmatrix} 1 & -1 \\ -1 & 1 \end{bmatrix}\begin{Bmatrix} U1 \\ U2 \end{Bmatrix} = \begin{Bmatrix} F1 \\ F2 \end{Bmatrix} \tag{2.38}$$

The shape functions used for the approximation are linear Lagrange formulas, and there are only two degrees of freedom for this equation with a two node element. With a constant E*A, this element also provides exact nodal values for the deflection and is also considered a super convergent element.

Torsion along the shaft can be directly formulated from the basic torsion formulation:

$$\frac{GJ\theta}{h} = T \tag{2.39}$$

Using the same formulation procedure as with axial translation, the finite element that results is

$$\frac{GJ}{h}\begin{bmatrix} 1 & -1 \\ -1 & 1 \end{bmatrix}\begin{Bmatrix} \theta 1 \\ \theta 2 \end{Bmatrix} = \begin{Bmatrix} T1 \\ T2 \end{Bmatrix} \tag{2.40}$$

2.7 Combining Different Theories

In current commercial codes, beam (or bar) elements are actually a compilation of previously discussed theories that are applied simultaneously, but uncoupled. The beam finite element uses a combination that covers axial deflection of the two nodes, transverse deflection and rotation of the nodes in the two orthogonal planes, and torsion along the x-axis. This means that the beam element could be bent, stretched, or twisted, but bending in one plane will not have

any effect on stretching or torsion, or bending in the other orthogonal plane, etc. Typical two-node beam finite elements have a total of twelve DOF, six DOF per node.

Axial tension and torsion incorporates two degrees of freedom in the longitudinal direction each, which adds four equations to the system. By also adding four more degrees of freedom in bending for the y-axis and z-axis separately, the finite element for the traditional beam results in a system of 12 equations and 12 unknowns. Although deflection in the most general terms in Cartesian coordinates determines 12 unknowns, if transverse loads in the y and z directions could be combined, and if the moment of inertia about the neutral axis remains unchanged (as would be the case for circular geometry with material that is assumed to be isotropic), then the transverse loading and deflection could be reduced from a system of 12 equations to a system of eight equations.

$$\begin{bmatrix} [Kaxial] & 0 & 0 & 0 \\ 0 & [Ktorsion] & 0 & 0 \\ 0 & 0 & [Kbending1] & 0 \\ 0 & 0 & 0 & [Kbending2] \end{bmatrix} \begin{Bmatrix} \{U\} \\ \{\theta\} \\ \{W\} \\ \{V\} \end{Bmatrix} = \begin{Bmatrix} \{Q1\} \\ \{Q2\} \\ \{Q3\} \\ \{Q4\} \end{Bmatrix} \quad (2.41)$$

Equation (2.41) is a 12 x 12 matrix defined as the stiffness matrix, where the first two sub-matrices (two DOF each) represents the stiffness of the beam in the longitudinal direction in axial deflection and twist, and the two remaining sub-matrix groupings of 4 by 4 elements represent the bending stiffness in the y and z directions.

2.8 Hertzian Contact Mechanics

Hertzian contact theory is used to simulate the interaction between the fastener and the hole. Contact mechanics is largely associated with the work of Heinrich Hertz (1882), who solved the contact problem of two elastic bodies with curved surfaces. His classical solution provides the foundation for contact mechanics. It applies to normal contact between two elastic solids that are smooth and can be described locally with orthogonal radii of curvature.

Anecdotally, Hertz observed elliptical rings (called Newton's rings, Figure 2.18), which formed on glass spheres, which applied pressure on lenses and were largely used in the field of astronomy. He used the formation of these rings to validate his theory with experiments in calculating the displacement caused by the sphere on the lens. Several combinations of shapes have been developed, including contact of spheres, spheres on flat plates, and cylinders in contact with axes of various angles.

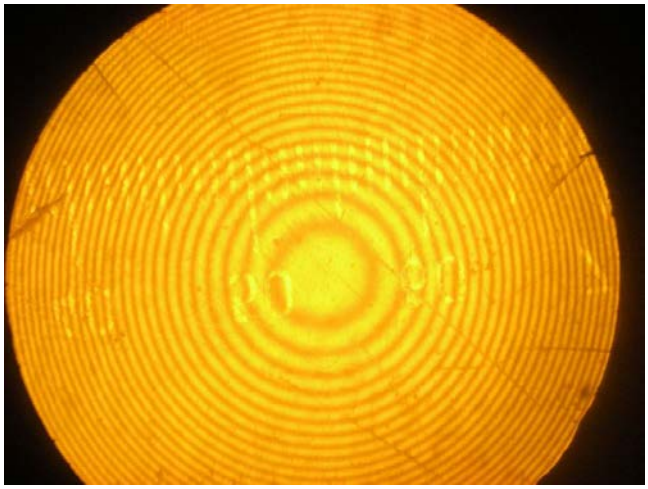

Figure 2.18: Newton's rings.

Extensive literature covers the contact problem and a review of Hertzian theory, which includes both stress and strain analysis, as well as a comprehensive bibliography published by Lubkin (1962). Among the works of particular interest are those of Love (1892), Prescott (1924), Landau and Lifshitz (1959), and Shtaerman (1949). The work of Shtaerman is considered a complete treatise on the contact problem (Puttock and Thwaite, 1969).

Several fundamental assumptions have been used to develop contact stress theory, most of which are ideally based on simple geometry, behavior of elastic bodies, and static equilibrium:

- Both surfaces in contact are smooth.

- Contact stresses and deformations satisfy differential equations for stress and strain of homogeneous, isotropic, and elastic bodies in static equilibrium.
- Far from the contact area, stress due to the contact disappears.
- Tangential stress components are zero on both surfaces, both in and outside of the contact zone. Additionally, there are no frictional forces in the contact action.
- Normal stress components are zero on both surfaces outside of the contact zone.
- The stress integrated over the contact zone is equal to the force that pushes the two bodies together.
- The distance between the bodies is zero in the contact zone but finite outside of the contact zone.
- Absent the external force, the contact between the two bodies becomes a point.

Although several shape combinations exist in contact theory, here we limit this brief introduction to contact of cylinders that have parallel axes (Figure 2.19).

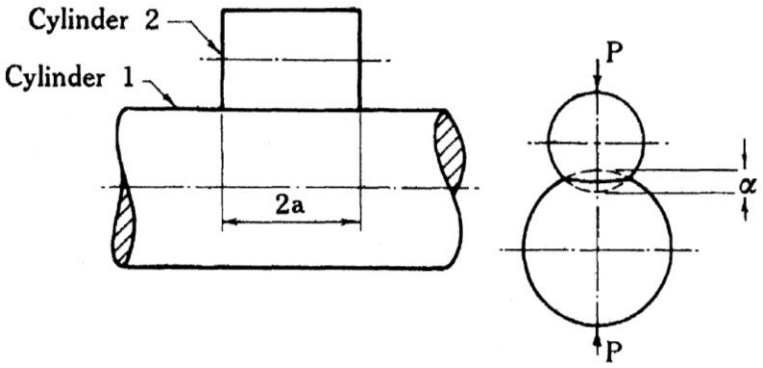

Figure 2.19: Two cylinders in contact with parallel axes (Puttock and Thwaite 1969).

The general formulation for parallel axes/cylinder contact is derived for both diameters having a positive radius. The formulation presented here is based on the information provided by Young (2011) and Shigley and Mishke (1988). Young's formulation makes the assumption that both contacting materials are made from the same material, but here, the terms are parsed to

generate a more general case that may include differing materials. The formulation is essentially a plane strain problem throughout the length of the fastener, which assumes that it is infinitely long and that the deflection and stress profiles are constant along the fastener axis. Shigley and Mischke (1988) (and others) have neglected this and simply apply the concept regardless of the thinness of the plate elements that the fastener is joining.

When two cylinders are in contact with a force, P, the contact area takes the shape of a rectangle of width, b, and length, t. A relationship of load to width of the contact, b, is established by (Figure 2.20):

$$b = \sqrt{\frac{8PK_DC_E}{\pi t}} \tag{2.42}$$

where K_D is known as the relative diameter and defined by (Figure 2.21)

$$K_D = \frac{D_1D_2}{D_1 - D_2} \tag{2.43}$$

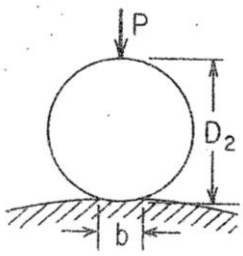

Figure 2.20: Two cylinders in contact with parallel axes (Young, 2011)

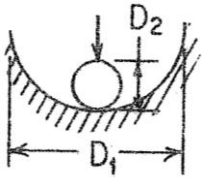

Figure 2.21: Relative diameter (Young, 2011)

The parameter C_E is defined as the contact modulus as

$$C_E = \frac{1-\upsilon_1^2}{\pi E_1} + \frac{1-\upsilon_2^2}{\pi E_2} \tag{2.44}$$

The distance from the cylinder centers, as shown in Young (2011) formulas for stress and strain, is

$$\delta = \frac{2P(1-\nu^2)}{\pi E t}\left(\frac{2}{3} + \ln\frac{2D_1}{b} + \ln\frac{2D_2}{b}\right) \tag{2.45}$$

Again, the formula assumes that both contacting materials are identical, as evidenced by the term $\frac{2(1-\nu^2)}{E}$. This term can be easily replaced by the more general contact modulus, C_E, thus yielding the following equation while combining the logarithmic terms:

$$\delta = \frac{PC_E}{t}\left(\frac{2}{3} + \ln\frac{4D_1D_2}{b^2}\right) \tag{2.46}$$

A transverse stiffness can be easily determined from this. It is clear from this equation, and similar, subsequent variants and modifications of it, that contact mechanics is inherently a nonlinear phenomenon. While the P term at the front of the deflection equation can be easily parsed in, thus determining the stiffness, K (K = P/δ), the "b" term has the load "P" inextricably imbedded in it.

2.9 Winkler Foundation

When a beam is supported elastically along the span, it may be idealized by a bed of springs. This is known as the Winkler foundation and is a simplification in providing continuous support. The simplification ignores multidimensional elasticity effects as well as friction, and the discrete nature of the "bed of springs" (Figure 2.22) smears out the actual physics of the phenomenon. The Winkler foundation can be seen as a continuation of the "bed of springs" treatment. In this case, the transverse direction is defined along the y-axis. Also, the beam/foundation separation is neglected in order to maintain a linear solution.

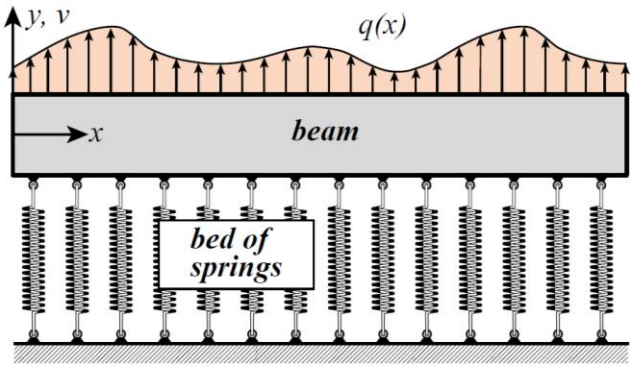

Figure 2.22: Bed of springs (Felippa, 1998).

Taking a differential slice of the beam between x and $x + dx$, the spring reaction force acting on the beam is taken to be $df = -c_f v(x)\, dx$. Here $v(x)$ is the transverse deflection, and c_f is the foundational stiffness. The internal energy stored in the slice of the contact stiffness is $\frac{1}{2} c_f v^2$. The effect of elastic supports is to modify the internal energy of the beam element so that it becomes

$$U_{total} = U_{beam} + U_{contact} \tag{2.47}$$

where the energy stored in the elastic contact is defined by

$$U_{contact} = \frac{1}{2}\int_0^h c_f v^2\, dx \tag{2.48}$$

When incorporating this into the beam element, the element stiffness is determined by adding the contact stiffness to the beam stiffness (assuming transverse direction downward for consistency with the beam element).

$$Kf = \frac{Cfh}{420}\begin{bmatrix} 156 & -22h & 54 & 13h \\ -22h & 4h^2 & -13h & -3h^2 \\ 54 & -13h & 156 & 22h \\ 13h & -3h^2 & 22h & 4h^2 \end{bmatrix} \tag{2.49}$$

With the stiffness matrix arranged in nodal order ($w1$, $S1$, $w2$, $S2$), it is clear that the formulation of the contact stiffness does not lend to equal and opposite forces and moments at the nodes, as is expected with a traditional beam element. The elastic foundation formulation tends to bleed off load away from the element, and the load that will be seen is not the usual F_1 =

$-F_2$ but rather $F_1 = -F_2 - F_{contact}$. In the research in this dissertation, this concept is adapted to the application and renamed from "foundational" stiffness, c_f, to "contact" stiffness, c_c.

2.10 Literature Review Conclusion

No theoretical or analytical models have been found that provide a foundation that is readily implemented to develop a *single beam element* modeling a fastener to connect plate elements in a finite element model. The goal of this research is to develop a *single fastener element* to connect plate elements in a finite element model to determine the load transfer of each fastener for a multi-row fastener configuration that incorporates contact mechanics. Determination of fastener loads is important in predicting proper load distribution in joints.

CHAPTER 3.

FASTENER ELEMENT FORMULATION

3.1 Problem Description

Lap joints consist of two plate members having plate thicknesses t_1 and t_2, a shared hole size with diameter D_h, and elastic moduli E_1 and E_2. The lap joint that experiences a tension force experiences secondary bending, as shown previously in Figure 1.7(b). The fastener, of length $2h$ (where $2h = t_1 + t_2$) and diameter D_s (where $D_s < D_h$), joins the plate members together, and experiences a non-constant, distributed bearing load along its shaft due to the load transmission from the plate members to the fastener (Figures 3.1 and 3.2). Additionally, the head (and nut) introduces a non-constant distributed load, causing both a tension along the shaft of the fastener and a moment that must be balanced by transverse loading along the shaft. This holds true particularly for the heads of the leading and trailing bolts in a multi-fastener arrangement. For purposes of element modeling of the fastener, the effect of the head and the nut on the joint is treated in the same way, effectively making a fastener that has "two heads."

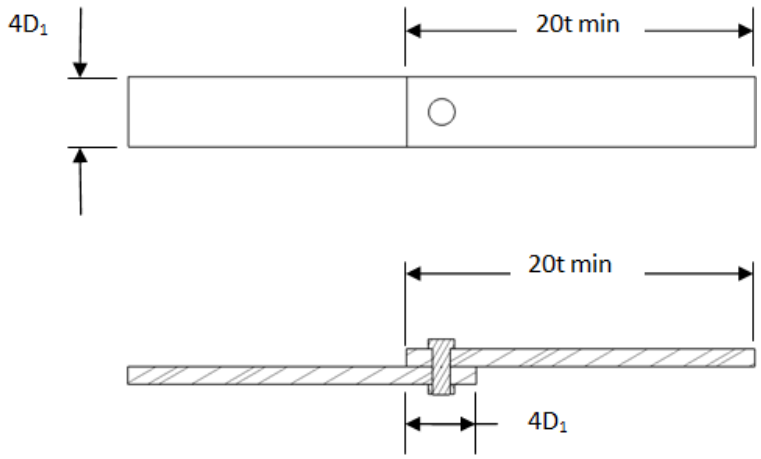

Figure 3.1: Problem definition with single fastener.

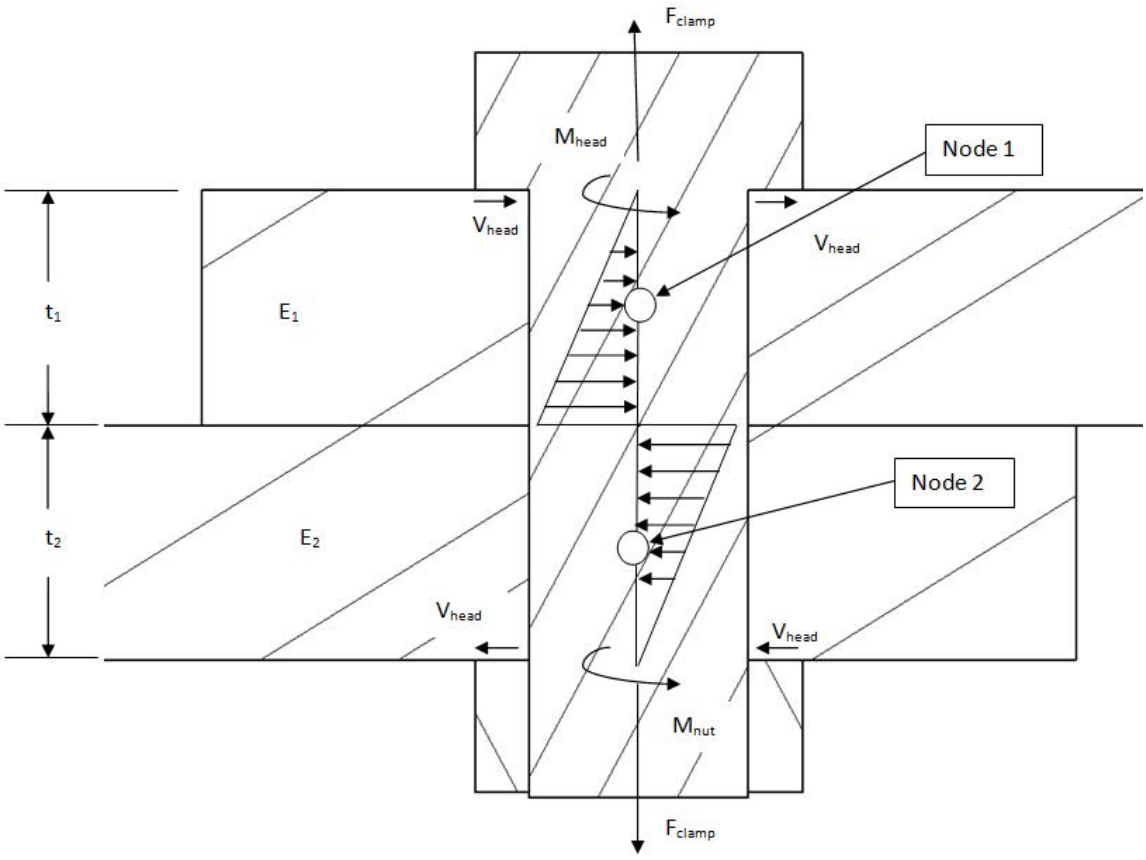

Figure 3.2: Fastener free-body diagram shown within joint cross section.

A typical design layout for a fastener requires a minimum edge distance (ED) and a minimum distance between fasteners. When the fastener is a rivet, the distance between fasteners is commonly referred to as pitch distance. Typically, the minimum ED is equal to twice the diameter of the fastener shaft (or 2D), measured from the center of the installation hole to the nearest edge. Typical minimum fastener spacing, or pitch, is usually four diameters of the larger installation hole diameter (or 4D). Given these sizing and spacing minimums, the fastener element is designed with this configuration in mind. For purposes of this analysis, the length of the plate member is at least five times longer than the width of the plate, and 20 times longer than the width of the plate, in order to minimize the effect of "far field" constraints.

3.2 Finite Element Development

For purposes of developing a finite element that models this fastener, the load distribution along the shaft is assumed to be non-constant, to the extent and limit that the plate elements mate with the fastener. The head and nut apply a pre-load, which is "off-centered" in the presence of the distributed shaft load, and also a shear load due to the head being in contact with the plate members. This off-center load introduces a moment that is sympathetic and ultimately must be balanced by moments that are induced by shaft loads if static equilibrium is to occur. The free-body diagram for the fastener experiencing secondary bending is shown previously in Figure 3.2. The final product of the novel finite element is defined by a single, two-node element, but to reach this point, a mesh refinement of the fastener by a four-element, five-node system is introduced, and the four-element system is condensed down to a single element, as shown in Figure 3.3.

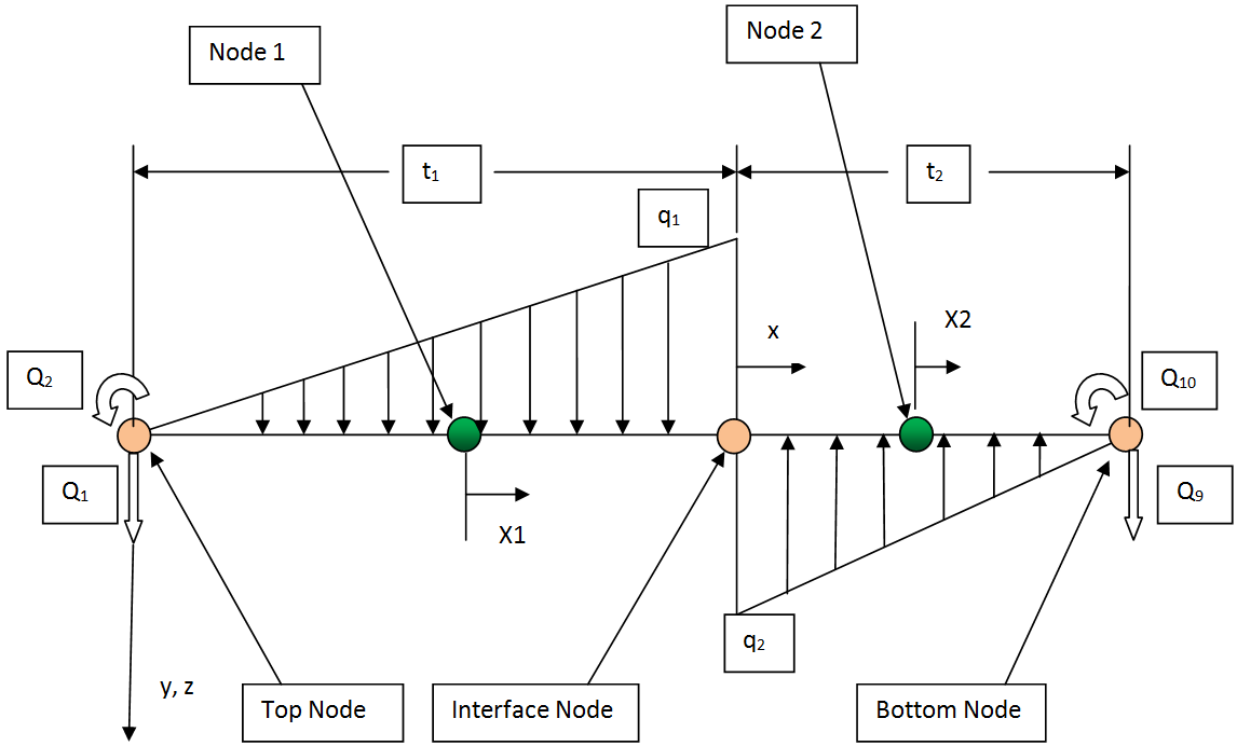

Figure 3.3: Free-body diagram (minus solid representation and rotated).

Note that in Figure 3.2, the load distributions along the fastener are shown as a linear distribution and reduce to zero at the intersections of the head and nut versus the shaft. In fact, it is not known whether this is precisely accurate for a given joint.

The difference in governing equations of these four elements and the Timoshenko beam element on the elastic foundation is the addition of the c_c term. The elastic foundation of Timoshenko beam derivation is stationary, while the distributed load due to contact of the current elements is based on the relative displacement of the fastener and the hole while the hole moves with the plate to which it is associated. It is assumed that the hole remains straight and has the same linear and rotational displacements as the center of the plate. For example, with node 1, the hole in the first plate has a displacement function of "$w_1 + x_1S_1$," where w_1 and S_1 are the displacement and rotation of the center of the hole, respectively, which is also node 1 of the novel element, as shown in Figures 3.2 and 3.3.

Equations for the first and second elements that are embedded in the thickness of the first plate ($-t1 < x < 0$) are

$$-\frac{d}{dx}\left[GAK_s\left(\frac{dw}{dx}+\Psi\right)\right]+c_{c1}(w-w_1-x_1S_1)=0 \tag{3.1}$$

$$-\frac{d}{dx}\left(EI\frac{d\Psi}{dx}\right)+GAK_s\left(\frac{dw}{dx}+\Psi\right)=0 \tag{3.2}$$

Equations for the third and fourth elements that are embedded in the thickness of the first plate ($0 < x < t2$) are

$$-\frac{d}{dx}\left[GAK_s\left(\frac{dw}{dx}+\Psi\right)\right]+c_{c2}(w-w_2-x_2S_2)=0 \tag{3.3}$$

$$-\frac{d}{dx}\left(EI\frac{d\Psi}{dx}\right)+GAK_s\left(\frac{dw}{dx}+\Psi\right)=0 \tag{3.4}$$

For equations (3.1) to (3.4), w is the horizontal (transverse) deflection of the fastener, based on Figure 3.2. The values of w_1 and w_2 are deflections of the fastener and the plates at

nodes 1 and 2, respectively. The values S_1, S_2 are values of the rotation at nodes 1 and 2, respectively. Values c_{c1} and c_{c2} are values of the contact stiffness of the fastener over the first plate and the second plate, respectively. Coordinates x_1 and x_2 are coordinates for the two plates and the origins located at the mid-plane of the two plates, respectively, as shown in Figure 3.3. The contact stiffnesses in this application are those between the fastener and the holes to which it is mounted, and they are discussed and derived in section 3.4 on linearized cylindrical Hertzian contact. Finally, the distributed loads that normally show on the right-hand side of the shear equations are already accounted for in the c_{c1} and c_{c2} terms.

In the process of developing a finite element model, the weak forms of differential equations (3.1) to (3.4) are employed. For the first plate, where c_{f1} is used, there are two elements. For each of the four elements, similar derivations as shown in section 2.5 are applied to derive the element stiffness matrix and the forcing terms. For example, for the first element,

$$\int_{-t_1}^{-\frac{t_1}{2}}[GAKs\frac{dv_1}{dx}\left(\Psi+\frac{dw}{dx}\right)+c_{c1}v_1(w-w_1-x_1S_1)\,]dx=v_1(-t_1)Q_1-v_1(-t_1/2)Q_3 \tag{3.5}$$

$$\int_{-t_1}^{-\frac{t_1}{2}}[EI\frac{dv_2}{dx}\frac{d\Psi}{dx}+(GAKs)v_2\left(\Psi+\frac{dw}{dx}\right)]dx=v_2(-t_1)Q_2-v_2(-t_1/2)Q_4 \tag{3.6}$$

where v_1 and v_2 are the two sets of interpolation functions, $\varphi_i{}^1$ and $\varphi_i{}^2$, used for w and Ψ, respectively.

After use of the approximation functions for each w and Ψ,

$$w=\sum_{i=1}^{3}w_i\varphi_i{}^{(1)} \tag{3.7}$$

$$S=\sum_{i=1}^{2}S_i\varphi_i{}^{(2)} \tag{3.8}$$

The terms inside the integrals make up the values of the stiffness terms of each of the corresponding elements. For example, the first finite element is

$$K_{ij}^{11}=\int_{-t_1}^{-\frac{t_1}{2}}[GAKs\frac{d\varphi_i{}^{(1)}}{dx}\frac{d\varphi_j{}^{(1)}}{dx}+c_{c1}\varphi_i{}^{(1)}\varphi_j{}^{(1)}\,]dx \tag{3.9}$$

$$K_{ij}^{12} = K_{ji}^{21} = \int_{-t_1}^{-\frac{t_1}{2}} [GAKs \frac{d\varphi_i^{(1)}}{dx} \varphi_j^{(2)}] \, dx \tag{3.10}$$

$$K_{ij}^{22} = \int_{-t_1}^{-\frac{t_1}{2}} [EI \frac{d\varphi_i^{(2)}}{dx} \frac{d\varphi_j^{(2)}}{dx} + GAKs \varphi_i^{(2)} \varphi_j^{(2)}] dx \tag{3.11}$$

The right-hand side of the stiffness equation is the remainder of the above equations:

$$F_i^1 = \int_{-t_1}^{-\frac{t_1}{2}} c_{c1} \varphi_i^{(1)} (w_1 + x_1 S_1) \, dx + \varphi_i^{(1)} (-t_1/2) Q_i \tag{3.12}$$

Since the first term in F_i^1 is related to w_1 and S_1, it is moved to the left-hand side and combined with the stiffness, K_{ij}. The center node is eliminated as the procedure used in deriving the Timoshenko CIE-1 element, and the remaining four-by-four stiffness matrix with forcing terms on the right-hand side will be used for further derivation of the new element. At this point, further detailing of the stiffness equations becomes cumbersome to present in the prose of a dissertation, and the remainder of this solution is continued in a Maple computer output, provided in Appendix G, and an alternative solution is described in Appendix A and another Maple computer output, also provided in Appendix G.

The fastener model shown in Figure 3.3 contains four elements connected by five nodes, which drives ten total degrees of freedom and can be seen in Figure 3.4. Since there are ten equations, the problem that leaves ten knowns and ten unknowns between the primary and secondary variables must be defined. In order to solve this problem, it should first be noted that there are only four externally applied nodal loads onto the fastener: Q_1, Q_2, Q_9, and Q_{10}. In order to determine the stiffness matrix of the new element, four stages of calculations of the four-element system are executed. Logan (2011) gives us the precedence for this calculation by "stages."

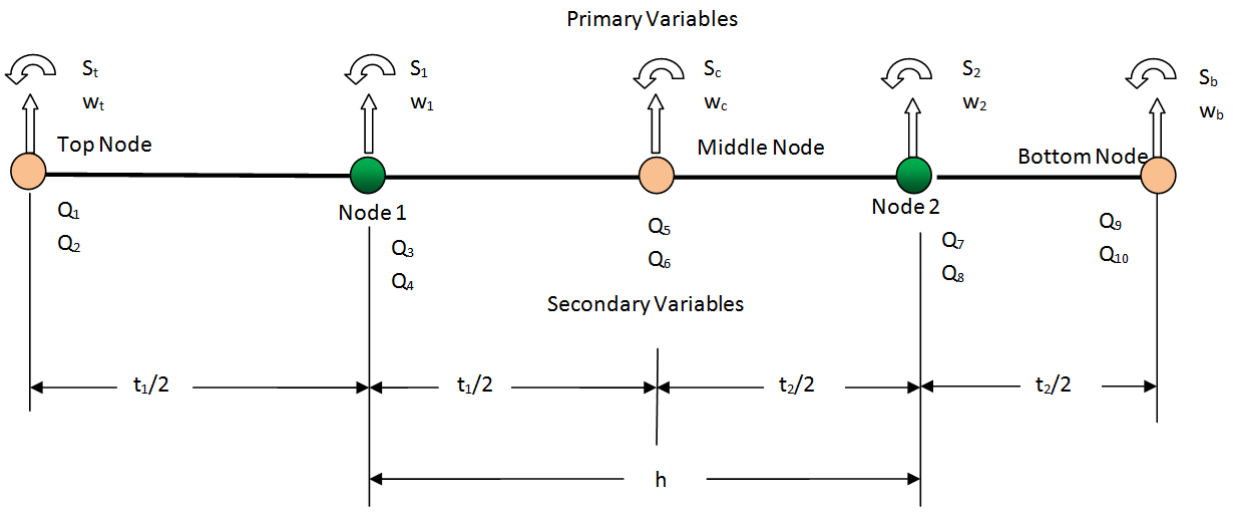

Figure 3.4: Primary and secondary variables.

In order to determine the stiffness matrix of the new element, four stages of calculations of the four-element system are executed. The rationale here is based on the understanding that the elements of the stiffness matrix, K_{ij}, can be determined from

$$\{QQ\} = [K]\{u\} \tag{3.13}$$

For a system of "n" equations,

$$\begin{Bmatrix} F_1 \\ \vdots \\ F_n \end{Bmatrix} = \left[\begin{pmatrix} K_{11} & \cdots & K_{1n} \\ \vdots & \ddots & \vdots \\ K_{n1} & \cdots & K_{nn} \end{pmatrix} \right] \begin{Bmatrix} u_1 \\ \vdots \\ u_n \end{Bmatrix} \tag{3.14}$$

Here we assume a structure to be forced into a displaced configuration defined by $u_1 = 1, u_2 = 0, \ldots u_n = 0$. Doing this drives the first column, $F_1 = K_{11}, F_2 = K_{21}, F_3 = K_{31}, \ldots\ldots, F_n = K_{n1}$. This process must be repeated for as many equations as exist in the system.

For the particular problem here, it is necessary to step through this process to determine the stiffness matrix by driving the values for w_1, S_1, w_2, and S_2 in four different stages:

Stage 1: $w_1 = 1$, $S_1 = 0$, $w_2 = 0$, $S_2 = 0$, and Q_3 to Q_8 are equal to zero.

Stage 2: $w_1 = 0$, $S_1 = 1$, $w_2 = 0$, $S_2 = 0$, and Q_3 to Q_8 are equal to zero.

Stage 3: $w_1 = 0$, $S_1 = 0$, $w_2 = 1$, $S_2 = 0$, and Q_3 to Q_8 are equal to zero.

Stage 4: $w_1 = 0$, $S_1 = 0$, $w_2 = 0$, $S_2 = 1$, and Q_3 to Q_8 are equal to zero.

While formulating the new two-node element, the distributed load due to contact needs to be considered as part of the nodal force. The contact force is now represented in the form of q, and values of q(x) are written in terms of the fastener displacements multiplied by the corresponding c_c:

$$q_1(x) = -c_{c1}(w - w_1 - x_1 S_1) \tag{3.15}$$

$$q_2(x) = -c_{c2}(w - w_2 - x_2 S_2) \tag{3.16}$$

The original stiffness matrix, K, is a ten-by-ten matrix:

$$\begin{bmatrix} K_{11}^e & K_{12}^e & K_{13}^e & K_{14}^e & 0 & 0 & 0 & 0 & 0 & 0 \\ K_{21}^e & K_{22}^e & K_{23}^e & K_{24}^e & 0 & 0 & 0 & 0 & 0 & 0 \\ K_{31}^e & K_{32}^e & K_{33}^e & K_{34}^e & K_{35}^e & K_{36}^e & 0 & 0 & 0 & 0 \\ K_{41}^e & K_{42}^e & K_{43}^e & K_{44}^e & K_{45}^e & K_{46}^e & 0 & 0 & 0 & 0 \\ 0 & 0 & K_{53}^e & K_{54}^e & K_{55}^e & K_{56}^e & K_{57}^e & K_{58}^e & 0 & 0 \\ 0 & 0 & K_{63}^e & K_{64}^e & K_{65}^e & K_{66}^e & K_{67}^e & K_{68}^e & 0 & 0 \\ 0 & 0 & 0 & 0 & K_{75}^e & K_{76}^e & K_{77}^e & K_{78}^e & K_{79}^e & K_{710}^e \\ 0 & 0 & 0 & 0 & K_{85}^e & K_{86}^e & K_{87}^e & K_{88}^e & K_{89}^e & K_{810}^e \\ 0 & 0 & 0 & 0 & 0 & 0 & K_{97}^e & K_{98}^e & K_{99}^e & K_{910}^e \\ 0 & 0 & 0 & 0 & 0 & 0 & K_{107}^e & K_{108}^e & K_{109}^e & K_{1010}^e \end{bmatrix} \begin{Bmatrix} w_t \\ S_t \\ w_1 \\ S_1 \\ w_c \\ S_C \\ w_2 \\ S_2 \\ w_b \\ S_b \end{Bmatrix} = \begin{Bmatrix} Q_1 \\ Q_2 \\ Q_3 \\ Q_4 \\ Q_5 \\ Q_6 \\ Q_7 \\ Q_8 \\ Q_9 \\ Q_{10} \end{Bmatrix} \tag{3.17}$$

In deriving the values of the new stiffness matrix, or K_{new}, each stage provides values that the right-hand side of the equation knows will populate a column of the matrix. In the four stages,

$$\begin{bmatrix} Knew_{11}^e & Knew_{12}^e & Knew_{13}^e & Knew_{14}^e \\ Knew_{21}^e & Knew_{22}^e & Knew_{23}^e & Knew_{24}^e \\ Knew_{31}^e & Knew_{32}^e & Knew_{33}^e & Knew_{34}^e \\ Knew_{41}^e & Knew_{42}^e & Knew_{43}^e & Knew_{44}^e \end{bmatrix} \begin{Bmatrix} 1 \\ 0 \\ 0 \\ 0 \end{Bmatrix} = \begin{Bmatrix} QQ_1 \\ QQ_2 \\ QQ_3 \\ QQ_4 \end{Bmatrix} \tag{3.18}$$

$$\begin{bmatrix} Knew_{11}^e & Knew_{12}^e & Knew_{13}^e & Knew_{14}^e \\ Knew_{21}^e & Knew_{22}^e & Knew_{23}^e & Knew_{24}^e \\ Knew_{31}^e & Knew_{32}^e & Knew_{33}^e & Knew_{34}^e \\ Knew_{41}^e & Knew_{42}^e & Knew_{43}^e & Knew_{44}^e \end{bmatrix} \begin{Bmatrix} 0 \\ 1 \\ 0 \\ 0 \end{Bmatrix} = \begin{Bmatrix} QQ_1 \\ QQ_2 \\ QQ_3 \\ QQ_4 \end{Bmatrix} \tag{3.19}$$

$$\begin{bmatrix} Knew_{11}^{e} & Knew_{12}^{e} & Knew_{13}^{e} & Knew_{14}^{e} \\ Knew_{21}^{e} & Knew_{22}^{e} & Knew_{23}^{e} & Knew_{24}^{e} \\ Knew_{31}^{e} & Knew_{32}^{e} & Knew_{33}^{e} & Knew_{34}^{e} \\ Knew_{41}^{e} & Knew_{42}^{e} & Knew_{43}^{e} & Knew_{44}^{e} \end{bmatrix} \begin{Bmatrix} 0 \\ 0 \\ 1 \\ 0 \end{Bmatrix} = \begin{Bmatrix} QQ_1 \\ QQ_2 \\ QQ_3 \\ QQ_4 \end{Bmatrix} \tag{3.20}$$

$$\begin{bmatrix} Knew_{11}^{e} & Knew_{12}^{e} & Knew_{13}^{e} & Knew_{14}^{e} \\ Knew_{21}^{e} & Knew_{22}^{e} & Knew_{23}^{e} & Knew_{24}^{e} \\ Knew_{31}^{e} & Knew_{32}^{e} & Knew_{33}^{e} & Knew_{34}^{e} \\ Knew_{41}^{e} & Knew_{42}^{e} & Knew_{43}^{e} & Knew_{44}^{e} \end{bmatrix} \begin{Bmatrix} 0 \\ 0 \\ 0 \\ 1 \end{Bmatrix} = \begin{Bmatrix} QQ_1 \\ QQ_2 \\ QQ_3 \\ QQ_4 \end{Bmatrix} \tag{3.21}$$

The right-hand side values for $Knew_{11}^{e}$ are determined by summing the shears and moments around the two remaining nodes. For example, in the first stage of the solution,

$$Knew_{11}^{e} = Q_1 + \int_{-\frac{t_1}{2}}^{\frac{t_1}{2}} q_1 dx_1 \tag{3.22}$$

$$Knew_{21}^{e} = Q_1 \frac{t_1}{2} + Q_2 + \int_{-\frac{t_1}{2}}^{\frac{t_1}{2}} q_1 (-x_1) dx_1 \tag{3.23}$$

$$Knew_{31}^{e} = Q_9 + \int_{-\frac{t_2}{2}}^{\frac{t_2}{2}} q_2 dx_2 \tag{3.24}$$

$$Knew_{41}^{e} = -Q_9 \frac{t_2}{2} + Q_{10} + \int_{-\frac{t_2}{2}}^{\frac{t_2}{2}} q_2 \, x_2 dx_2 \tag{3.25}$$

This process is repeated three more times to fill out the three other columns of the novel finite element. What results from the former finite element model utilizing four elements and five nodes reduces (or "condenses") down to a single two-node element, as shown in Figure 3.5.

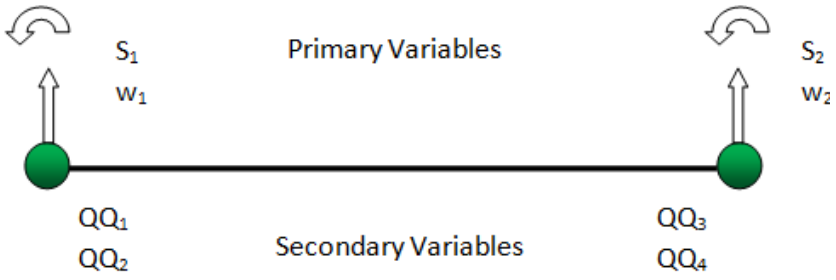

Figure 3.5: Primary and secondary variables.

The symbolically evaluated individual terms in this new finite element are not succinct enough to be presented within the prose of this text, but are instead shown in its entirety in Appendix G.

3.3 Typical Mid-Plane Processing

Typically, element preprocessing uses solid geometry that is already defined by computer design packages (CATIA, Pro Engineer, Solid Works, etc). If the structural engineer decides to perform element modeling on the geometry using plate elements, then traditionally, they must be defined on the solid parts' mid-planes, shown by the location of the plate elements, depicted in red in Figure 3.6 The resulting actual length of the beam element joining the plate elements together is half the sum of the plate thicknesses. The definition of the individual solid parts defined by plate elements is usually defined prior to any connection being defined between them. This fact will be used later on in helping to define the additional parameters defining the fastening element.

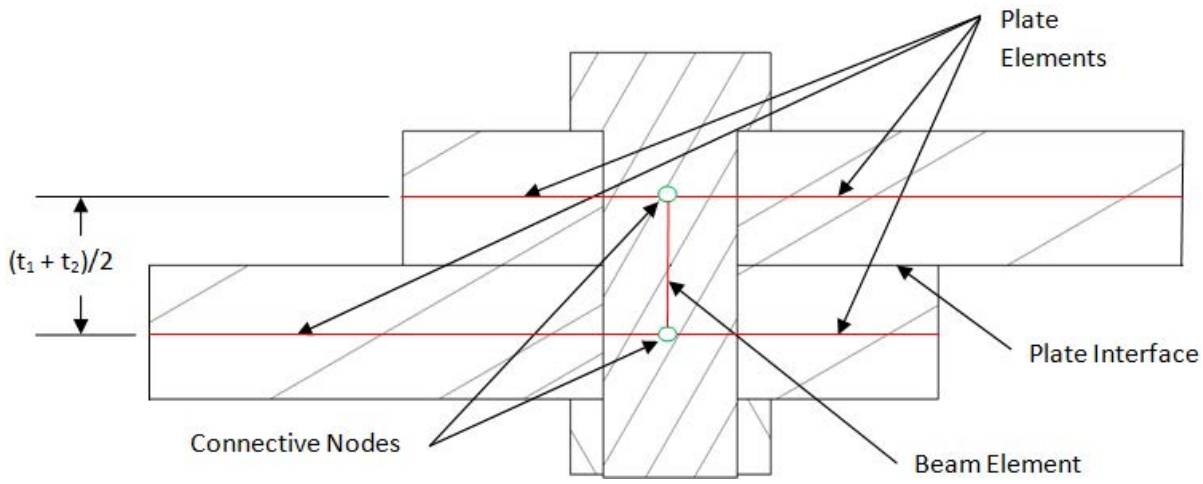

Figure 3.6: Plate and beam element idealization.

3.4 Linearized Cylindrical Hertzian Contact

The final question that remains in the beam element formulation regards the matter of the treatment of contact stiffness. Since the mating surfaces are parallel cylinders, one inside the

other, contact mechanics is introduced into the value of c_c, thus utilizing Hertzian theory. A challenge arises in the fact that the Hertzian contact stiffness formulation is non-linear, as was mentioned in Chapter 2. In order to apply this stiffness to a linear solution scheme, an assumption must be made. First, the following formulas are used:

$$b_i = 1.60\left(\frac{FK_D C_e}{t_i}\right)^{1/2} \tag{3.26}$$

$$K_D = \frac{D_1 D_2}{D_1 - D_2} \tag{3.27}$$

$$C_e = \frac{1-\nu_1^2}{E_1} + \frac{1-\nu_2^2}{E_2} \tag{3.28}$$

$$\delta = \left(\frac{F}{\pi t}\right) C_e \left(\frac{2}{3} + ln\left(\frac{4D_1 D_2}{b_1 b_2}\right)\right) \tag{3.29}$$

where b represents the full width of the contact, K_D represents the relative diameter (written in terms of the diameters of the hole and the fastener shaft, D_1 and D_2), and C_e is the contact modulus written in terms of the contact members' Poisson's ratio, ν_1 and ν_2, and the elastic moduli, E_1, and E_2. The reduction of the distance between the centers of the radii of the cylinders during contact is denoted by δ, where F is the force that passes through the contact, and t is the length of the contact. In the application here, this represents the thickness of the individual plate member. Using the traditional notion of stiffness,

$$c_c = F/\delta \tag{3.30}$$

$$c_c = \frac{\pi t}{C_e\left(\frac{2}{3} + ln\left(\frac{4D_1 D_2}{b_1 b_2}\right)\right)} \tag{3.31}$$

It should be made clear here that P is the far-field load applied to the plates, and load, F, is denoted as the maximum load that the contact area will transmit. Normally, these two values are taken to be equal. The relationship between the contact stiffness between the two cylinders

can be seen in Figure 3.7, assuming (D_1 = 0.25 in, D_2 = 0.257 in), with aluminum plate ($E_1 = 10.7 \times 10^6$psi) and steel fastener ($E_1 = 29.0 \times 10^6$ psi) across a plate thickness of 0.25 in.

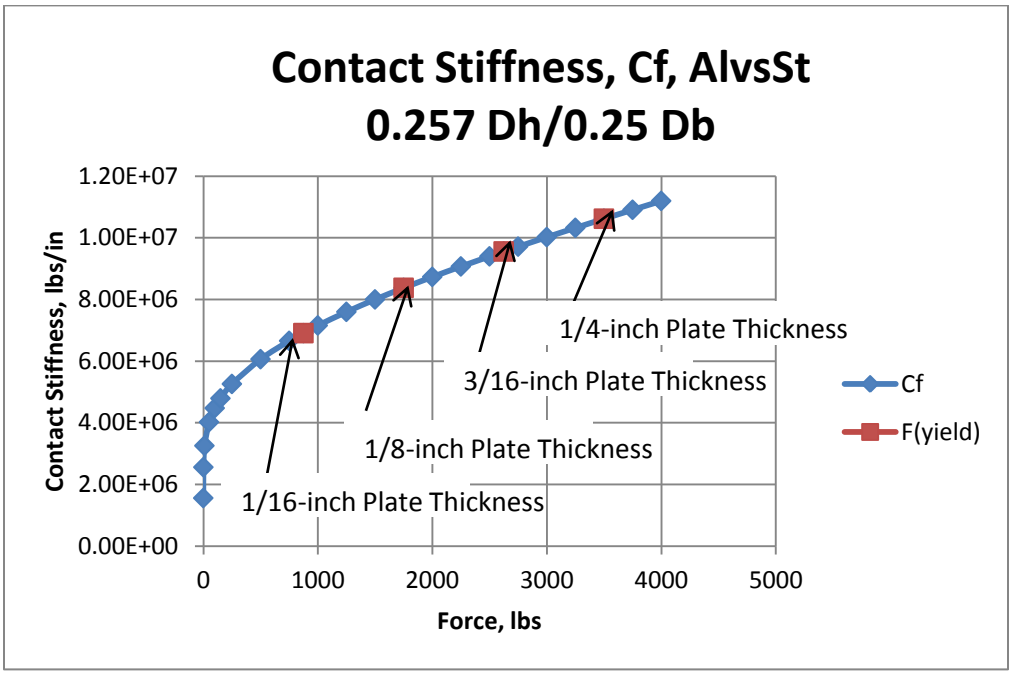

Figure 3.7: Contact stiffness vs. applied force.

One method used to establish a given c_c and force linearity of the problem, is by making a simple assumption that the load passing through the contact area can be *no larger* than that which would induce a yield stress in the plate under normal loading, and utilizing that value to establish stiffness. This is consistent with the Hertzian contact assumption that materials are loaded in the linear elastic range. For the plate strip modeled in this problem, where the width of the part is four bolt diameters and the thickness of the *i*th plate is t_i, F can be rewritten as

$$F_i = \frac{4}{3}\sigma_y D_s t_i \tag{3.32}$$

The first test case shows that the level of sensitivity that the adjustment of F has on the deflection of the fastener is largely negligible regarding displacement of the fastener.

Alternatively, and more favorably for this research, in order to determine the linearized contact stiffness and simultaneously detach the dependency of the contact stiffness to load, a

linear regression model can be used to simulate a constant stiffness across the varying loads experienced in the joint. The relationship, while certainly not linear, can be approximated in this fashion. For the example of aluminum plates joined by a steel bolt with varying load with 0.25-inch thick plates, the linear regression model yields a stiffness of 1.253 x 10^7 lbs/in (Figure 3.8).

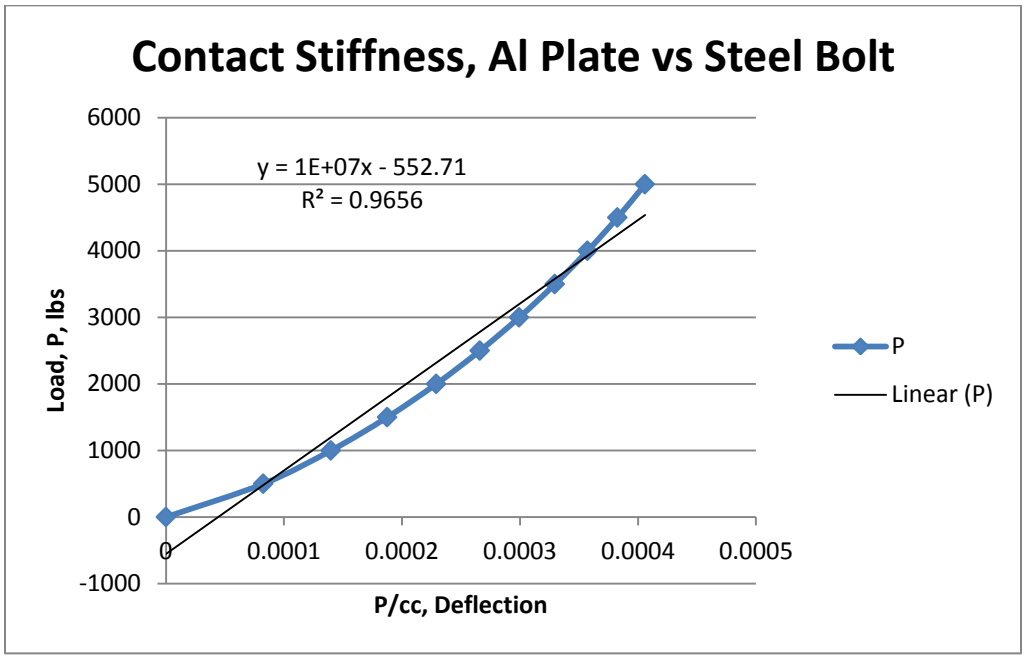

Figure 3.8: Using linear regression model to determine contact stiffness.

Table 3.1 presents the linear regression model-generated values of contact stiffness for various thicknesses and plate member/fastener combinations used in the case studies. Table 3.2 presents the coefficients of determination of all regression models.

TABLE 3.1: LINEARIZED CONTACT STIFFNESS USING LINEAR REGRESSION

Contact Stiffness, lb/in				
	Materials			
Thickness	Al vs St	St vs St	St vs Ti	Al vs Ti
0.0625	8.707E+06	1.357E+07	9.914E+06	7.326E+06
0.125	1.008E+07	1.533E+07	1.138E+07	8.593E+06
0.1875	1.134E+07	1.687E+07	1.271E+07	9.779E+06
0.25	1.253E+07	1.828E+07	1.395E+07	1.093E+07

TABLE 3.2: GOODNESS OF FIT OF LINEAR REGRESSION MODELS

Coefficients of Determination, R^2				
	Materials			
Thickness	Al vs St	St vs St	St vs Ti	Al vs Ti
0.0625	0.9804	0.9863	0.9825	0.9768
0.125	0.9751	0.9835	0.9782	0.9697
0.1875	0.9704	0.9812	0.9745	0.9630
0.25	0.9656	0.9791	0.9708	0.9560

Here, it is necessary to mention how to treat the other degrees of freedom in the finite element. With a fully functional traditional beam element, there are six degrees of freedom per node, resulting in twelve DOF that need to be addressed in this element. The novel element formulation addresses eight degrees of freedom, four DOF each for both orthogonal planes. Axial deflection for this novel element is not modified from the way commercial codes currently operate, and need not be covered here, which takes care of two more DOF. This means that two DOF have not been addressed. Commercial codes include torsional stiffness in the general beam element. However, since we are specifically modeling cylindrical fasteners, this novel finite element drops the stiffness that determines torsion. This results in a finite element that has two nodes, with five DOF each, resulting in a total ten DOF.

Equation (3.33) illustrates the final assembled stiffness matrix. The first two terms govern the axial loading, terms three to six concern the transverse displacement in the yz plane, and the last four terms concern the transverse displacement in the xz plane. All are based on the element orientation shown in Figure 3.9.

An alternative approach in formulating the novel finite element is documented in Appendix A. That formulation lends itself to a more succinct symbolic solution than the current condensation form described here.

$$\begin{bmatrix} K_{11}^e & K_{12}^e & 0 & 0 & 0 & 0 & 0 & 0 & 0 & 0 \\ K_{21}^e & K_{22}^e & 0 & 0 & 0 & 0 & 0 & 0 & 0 & 0 \\ 0 & 0 & K_{33}^e & K_{34}^e & K_{35}^e & K_{36}^e & 0 & 0 & 0 & 0 \\ 0 & 0 & K_{43}^e & K_{44}^e & K_{45}^e & K_{46}^e & 0 & 0 & 0 & 0 \\ 0 & 0 & K_{53}^e & K_{54}^e & K_{55}^e & K_{56}^e & 0 & 0 & 0 & 0 \\ 0 & 0 & K_{63}^e & K_{64}^e & K_{65}^e & K_{66}^e & 0 & 0 & 0 & 0 \\ 0 & 0 & 0 & 0 & 0 & 0 & K_{77}^e & K_{78}^e & K_{79}^e & K_{710}^e \\ 0 & 0 & 0 & 0 & 0 & 0 & K_{87}^e & K_{88}^e & K_{89}^e & K_{810}^e \\ 0 & 0 & 0 & 0 & 0 & 0 & K_{97}^e & K_{98}^e & K_{99}^e & K_{910}^e \\ 0 & 0 & 0 & 0 & 0 & 0 & K_{107}^e & K_{108}^e & K_{109}^e & K_{1010}^e \end{bmatrix} \begin{Bmatrix} u_{z1} \\ u_{z2} \\ v_{x1} \\ \theta_{x1} \\ v_{x2} \\ \theta_{x2} \\ w_{y1} \\ \theta_{y1} \\ w_{y2} \\ \theta_{y2} \end{Bmatrix} = \begin{Bmatrix} F_{z1} \\ F_{z2} \\ F_{x1} \\ M_{x1} \\ F_{x2} \\ M_{x2} \\ F_{y1} \\ M_{y1} \\ F_{y2} \\ M_{y2} \end{Bmatrix} \quad (3.33)$$

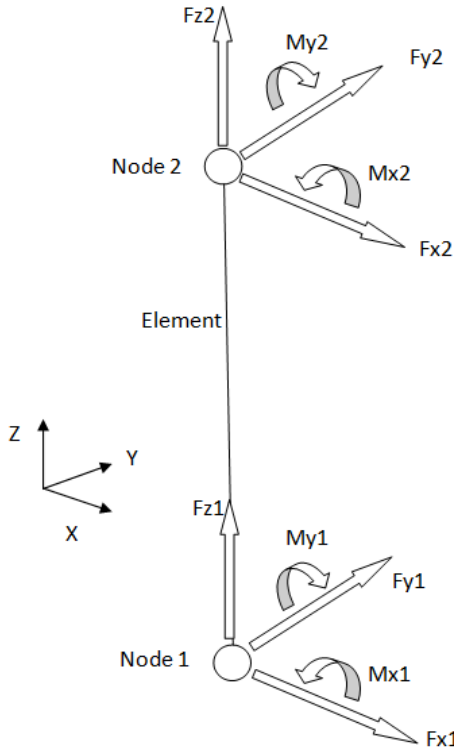

Figure 3.9: Fastener element (rotated and aligned with z-axis).

3.5 New Features/Limitations of Novel Element

The novel finite element has advantages and disadvantages. To ensure this element works properly, several assumptions are made:

- This fastener element must "know" the plate element's properties that connect to the shared nodes, in order to properly parameterize c_{c1} and c_{c2}. The elastic moduli, Poisson's ratios, and hole diameters must be known beforehand to successfully create the fastener element. This conforms to the typical preprocessing methods of meshing the plate members prior to fastening them together with this fastener element.
- The diameter of the shaft of the fastener cannot equal the diameter of the hole. Hertzian contact theory fails since the relative diameter value results in a divide-by-zero in this case.
- The connecting nodes of the plate elements that are used to define the ends of the fastener must be orthogonal relative to the joined plates, requiring that the plates are parallel to each other.
- The out-of-plane rotation is not a degree of freedom incorporated in this fastener element. As a result, a single fastener element will generally require additional constraints on the joined plates or additional fastener elements, in order to produce results for a static equilibrium. One way this can specifically be circumvented is by applying a predetermined load to balance forces on the fastener, but this exception is not generally useful. Plate materials that are mechanically fastened together with this novel element generally should not be singularly fastened, and this element follows the design principle. The distance between nodes of the fastening element is not used in the stiffness calculation; instead, that distance is set by pulling the values of the thicknesses of the plates. Therefore, the actual distance between the plate elements is not taken into account, which reduces preprocessing time of the mid-plane generation and consequent conditioning.

CHAPTER 4.

TEST CASE STUDY 1

4.1 Single-Bolt Test Case Layout

As mentioned previously, this research is an attempt to bridge the gap between two commonly used FE modeling techniques: plate and beam element modeling, and solid element modeling. In all of the case studies, the design of the lap joint is laid out based on assumptions that are used in the joint formulation discussed in Chapter 3. The lap joint consists of two identical plate elements that are four bolt diameters ($4D_1$) wide and 20 bolt diameters long. The fastener head has a diameter that is 1.5 times the shaft diameter. The head/nut height is at least one-half the shaft diameter. Again, as stated in Chapter 3, the location of the fastener is at least two shaft diameters ($2D_1$) from any edge (Figures 4.1 and 4.2).

This case study illustrates the deflection response of the new element and overlays that output over the output generated from the two baseline modeling techniques. For completeness, a variety of parameters are chosen and adjusted throughout the study.

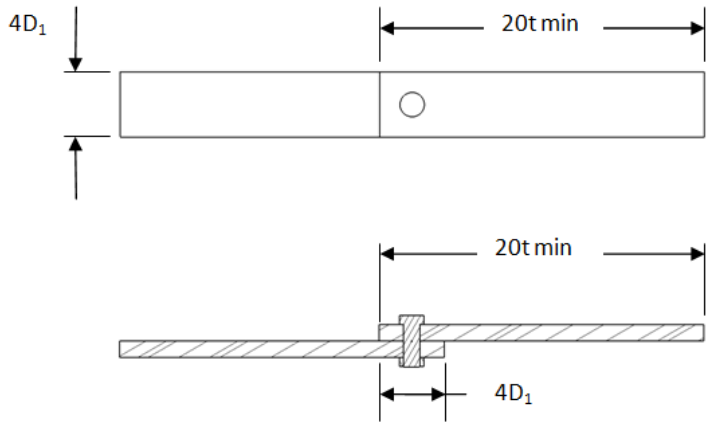

Figure 4.1: Case Study 1 layout.

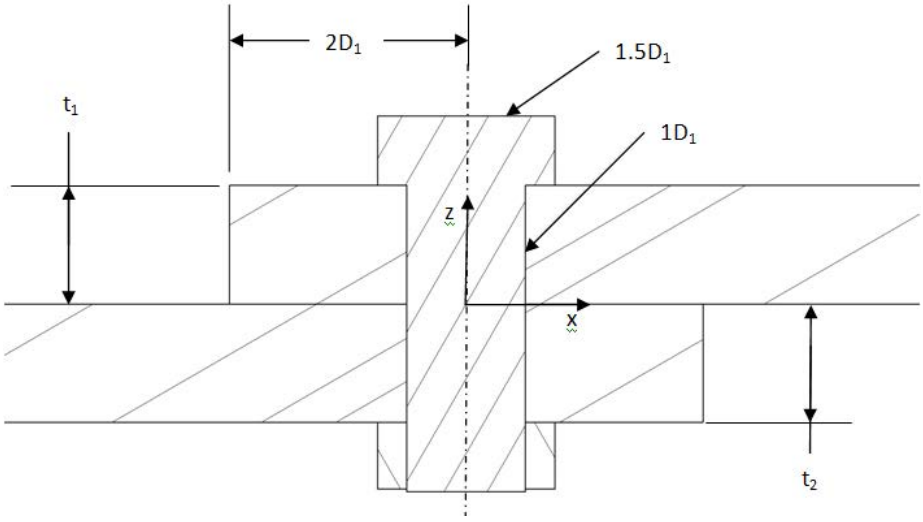

Figure 4.2: Cross section of Case Study 1 layout.

To provide a useful database from which to draw, four parameters are varied to four values, which results in 256 different combinations (4^4). The varied parameters are the external tensile loading, fastener preload, plate thickness, and fastener material/plate material ratio. Table 4.1 illustrates the size of this database. Considering the two baselines of plate/beam/plate and solids, 512 data sets define the baselines for this case study.

TABLE 4.1: CASE STUDY 1 PARAMETERS

	Parameter							
	Plate Load	Pre Load	Plate Thickness	Fastener Material	Plate Material	Elastic Modulus Fastener (10^6psi)	Elastic Modulus Plate (10^6psi)	Ef/Ep ratio
Parameter	500 lbs	500 lbs	1/4D	Steel	Aluminum	29	10.7	2.71
	1000lbs	1000 lbs	1/2D	Steel	Titanium	29	16	1.81
	1500 lbs	1500 lbs	3/4D	Titanium	Aluminum	16	10.7	1.49
	2000 lbs	2000 lbs	1D	Steel	Steel	29	29	1

In both baselines, the finite element models are constrained such that the middle of the fasteners are constrained in the middle of the bolt, and the ends of the plates are only free to slide longitudinally. Figure 4.3 illustrates how the models are constrained.

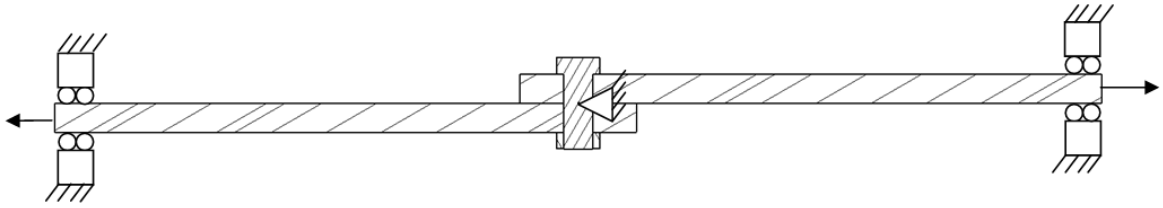

Figure 4.3: Finite element model constraints.

The first baseline method involves modeling two-dimensional plates that have uniform quad plate elements, 2D in size on each side. Therefore, the finite element model contains 40 quad elements and a beam element (66 nodes, 396 DOF) (Figure 4.4).

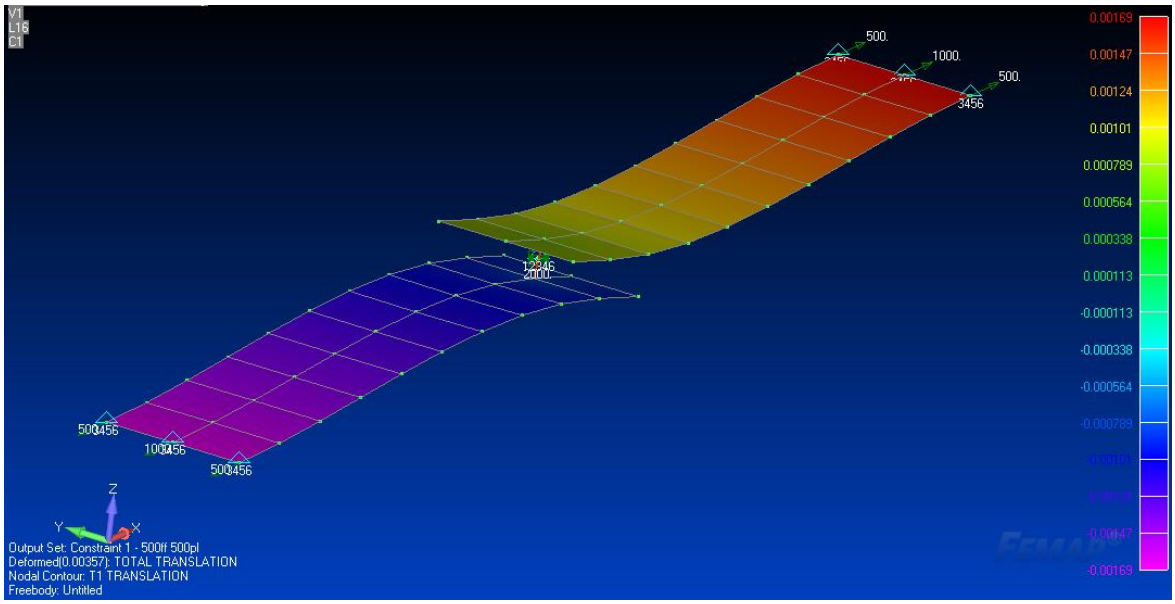

Figure 4.4: Plate element model for Case Study 1.

In order to assure symmetry of the problem, an additional node is placed in the middle of the beam element, and that element is split into two separate beam elements. The central node is constrained from translation but is free to rotate. The end nodes of the plate elements are constrained in all degrees of freedom, with the exception of translation in the same direction as the externally applied loads, which are located at the ends of the plate elements and equally pull the lap joint apart. Applying constraints in this manner ensures that the upper and lower plates deform exactly in the same way, which makes trends easier to isolate and see (Figure 4.5).

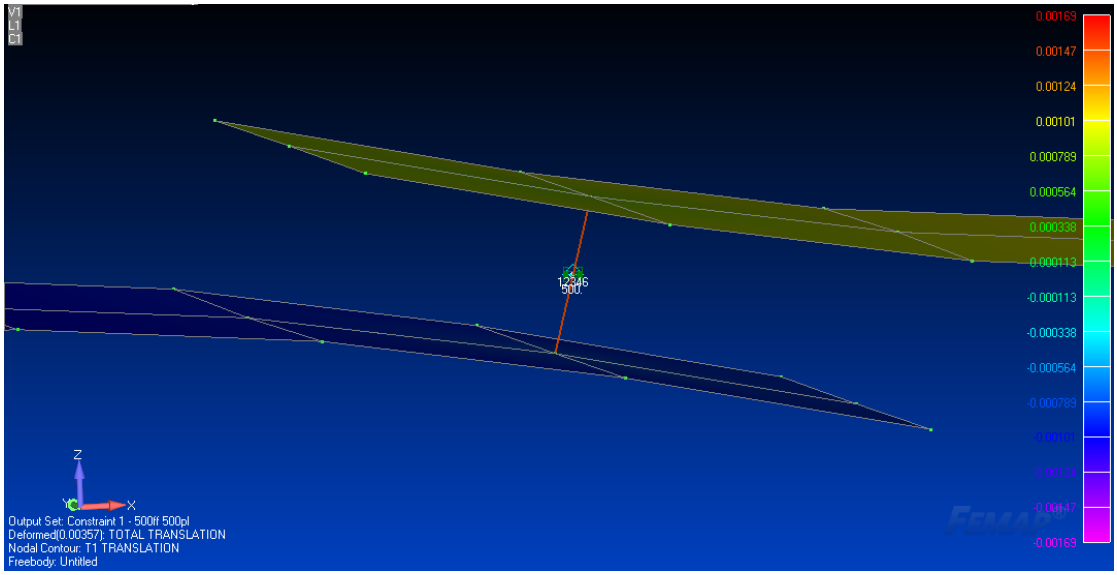

Figure 4.5: Beam element detail for Case Study 1

The solid model is constrained similarly to the plate model. The two thicker models (thickness, t, = 1 bolt diameter and ¾ bolt diameter) have eight elements running across the thickness of the plate members. The two thinner models have four elements running across the thickness of the plate members. The solid models use eight node hexahedrons exclusively. To reduce the size of the calculation, the model is split in half down the length of the problem. For the two larger thicknesses, the models have 10,752, eight-node hexahedron elements (13,395 nodes, 40,185 DOF). For the two thinner thicknesses, the models have 6,656, eight-node hexahedron elements (8,739 nodes, 26,217 DOF). As shown in Figures4.6, 4.7, and 4.8, half of the problem is modeled.

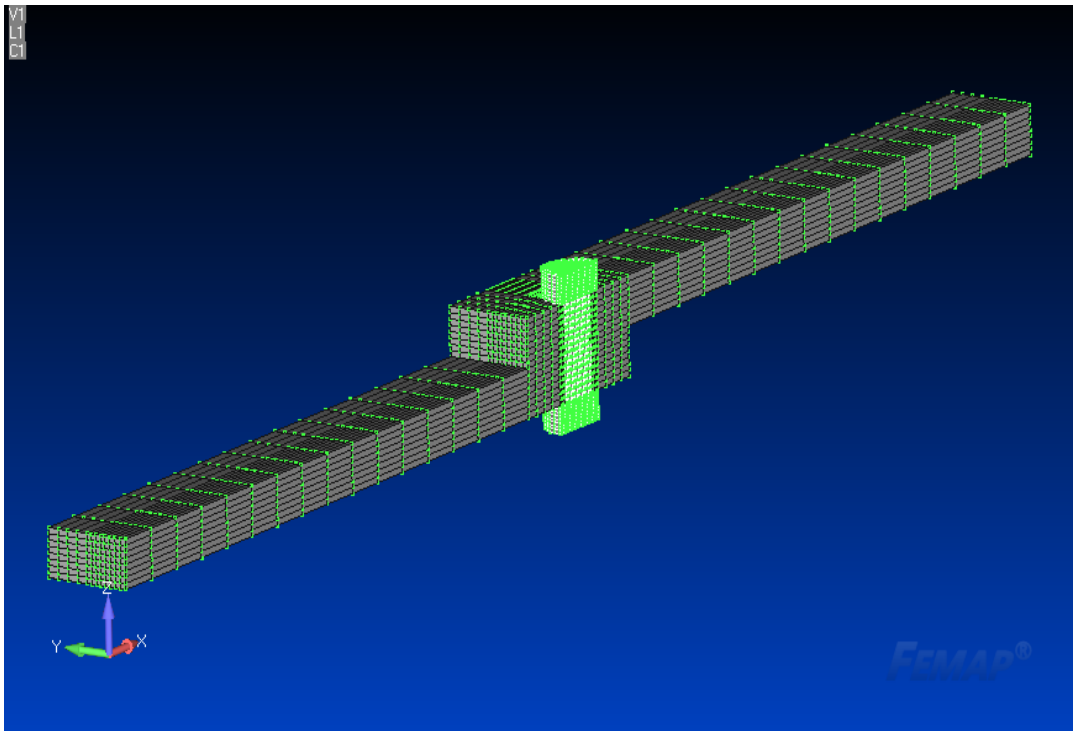

Figure 4.6: Solid element model for Case Study 1.

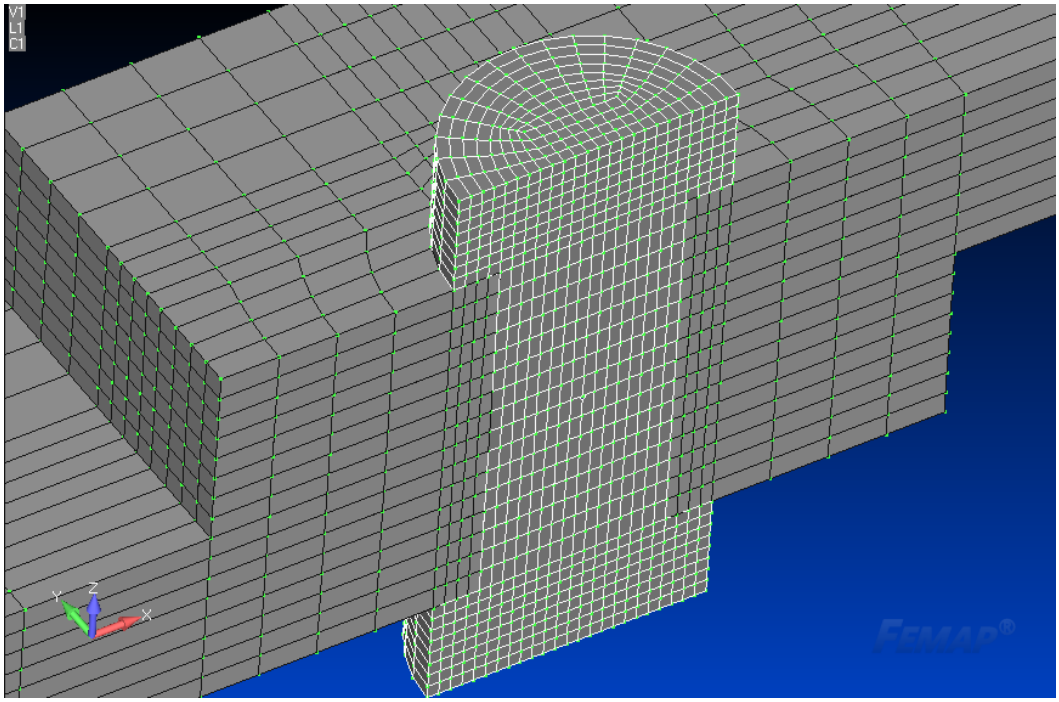

Figure 4.7: Solid element model detail (eight elements across thicknesses).

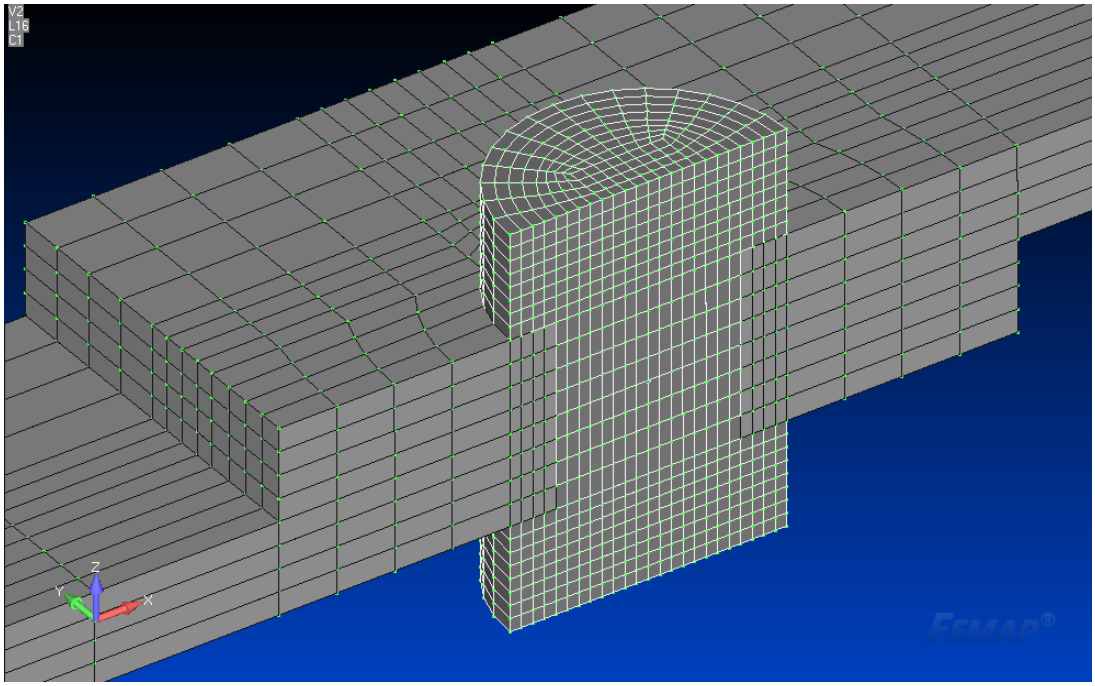

Figure 4.8: Solid element model detail (four elements across plate thicknesses).

For the single-fastener problem, the output of paramount interest becomes the deflection of the fastener. For the solid element baseline portion of this case study, the nodal deflections of fastener centerlines are of specific primary interest. After conditioning the output data to eliminate transverse deflection due to the product of the rotation of the joint and the distance of the points of interest and the plate interface, this data was compared against elements using the Euler-Bernoulli theory, Timoshenko beam theory, and the novel application. To determine the deflection of the fastener, the output needs conditioning to remove deflection caused by bending of the plate elements (Figure 4.9).

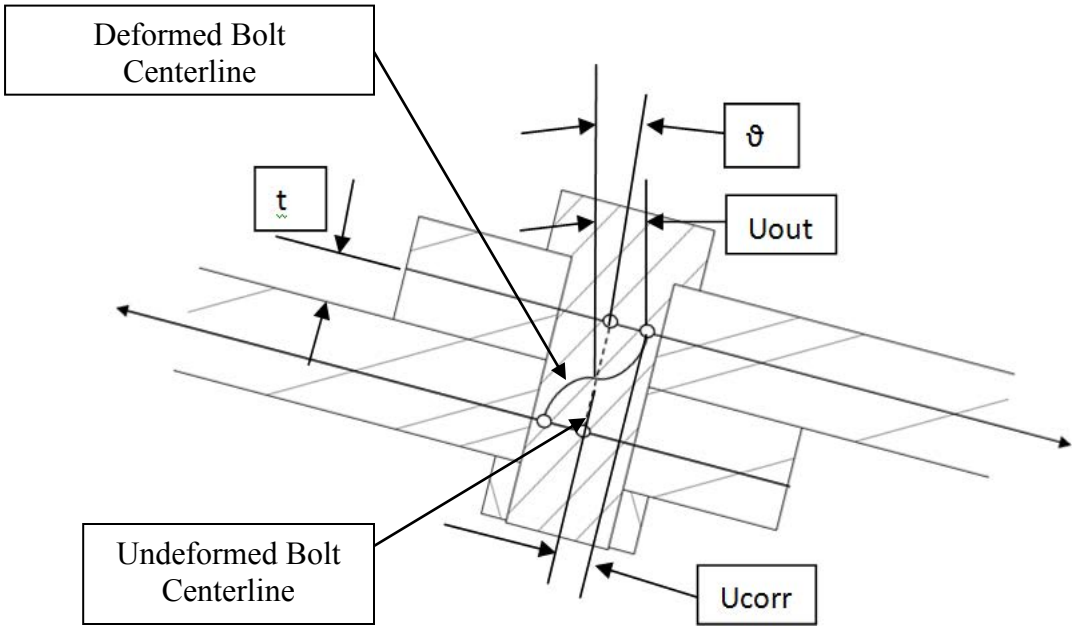

Figure 4.9: Corrected transverse deflection (Uoutput vs. Ucorrected).

4.2 Results and Analysis

To illustrate the differences between the various approaches, of the 256 combinations, the most useful data set for presentation in this text is one that shows the largest deflections, yielding the maximum differences between those approaches. The data set involves the highest deflection, which means that it has the highest applied load and the highest stiffness ratio. That data set is the one that models the aluminum plates versus steel fasteners that are pulled with the maximum load used in the data set, or 2,000 lbs. The data was evaluated across the various thicknesses, and a deflection versus "slenderness ratio" was plotted. The slenderness ratio is defined as the length of the fastener length versus the diameter of the bolt. Plotting across various slenderness ratios show the range where transverse deflection due to bending and the deflection due to transverse shear have their effects. To extend the data set to obtain a more complete picture, additional data points were included in both baselines for this presentation. Plate thicknesses of 0.125 L/D_1 and 2 L/D_1 are added to the study on the short end as well as 0.5 L/ D_1 and 0.75 L/ D_1 to illustrate the extremes.

Two programs were created: one in Maple 16, to determine the symbolic version of the modified stiffness matrix, the formulation of which is discussed in Chapter 3 and the value of which, in its entirety, is shown in Appendix G; and the other in MathCad 15, to determine the numerical values of the deflections of a singular beam element. Both programs used to calculate the various behaviors are shown in their entirety in Appendix G. For the traditional analyses, FEMAP was used for the preprocessor and NEi NASTRAN was used for both the linear plate/beam/plate calculations and the nonlinear solid calculations. The transverse deflection versus slenderness ratios are illustrated in Figures 4.10 and 4.11.

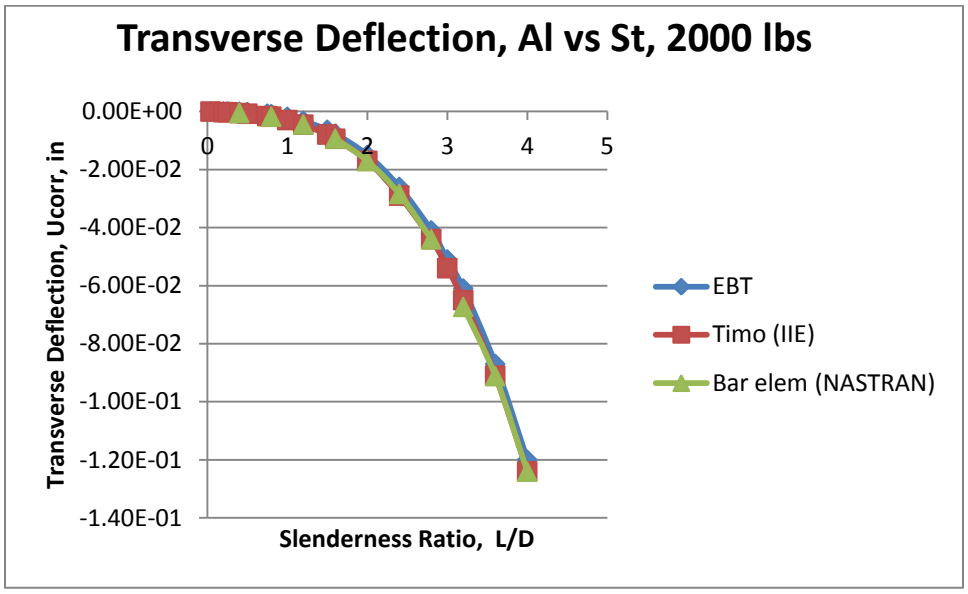

Figure 4.10: Transverse deflection vs. slenderness ratio.

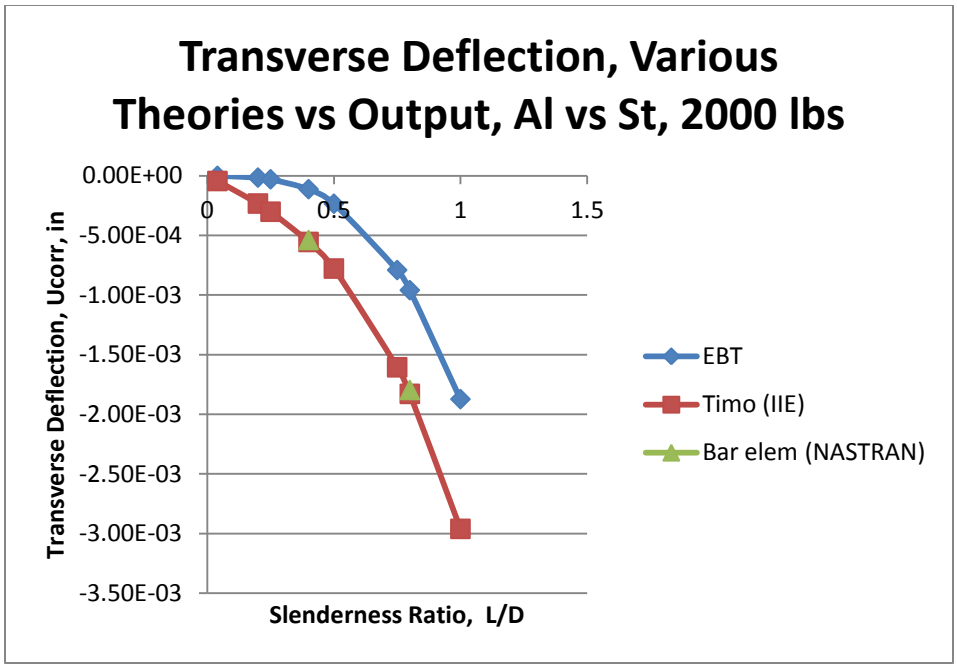

Figure 4.11: Transverse deflection vs. slenderness ratio.

Close inspection of the deflection responses illustrate the effect that the Timoshenko beam theory has on the Euler-Bernoulli theory. From a slenderness ratio of less than 1, the EBT is stiffer than the TBT, as expected. When the length of the beam gets longer, the TBT effect gradually disappears, and both theories match closely. Also, differences can be seen between the TBT using CIE-2 (IIE) finite element coding. Additionally, NASTRAN output follows TBT coding precisely.

When deflections of the solid models are considered, the response follows a different path. Figure 4.12 shows that for very short beams (L/D < 0.5), the solid model roughly follows the same trend as the Timoshenko bar element, thus indicating the dominance of transverse shear stiffness. However, as the fastener becomes longer, bending becomes dominant. This is where both the TBT and EBT depart from the response of the solid models. After the slenderness ratio surpasses the L/D > 0.5, the solid model responds by leveling out the transverse deflection with

the longer fastener. Extending this response well past most reasonable fastener lengths (L/D = 4) is illustrated in Figure 4.13.

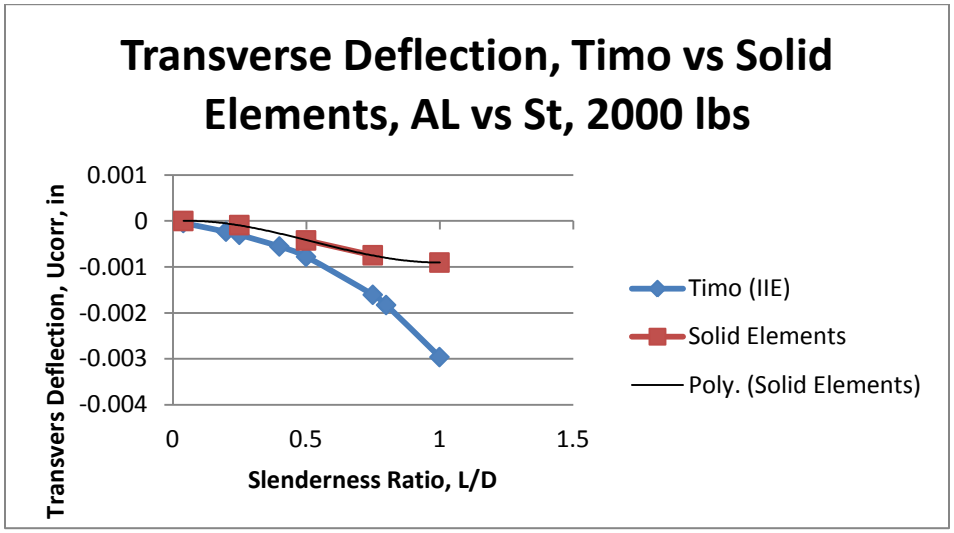

Figure 4.12: Deflection vs. slenderness ratio, Timoshenko (IIE) vs. solid elements.

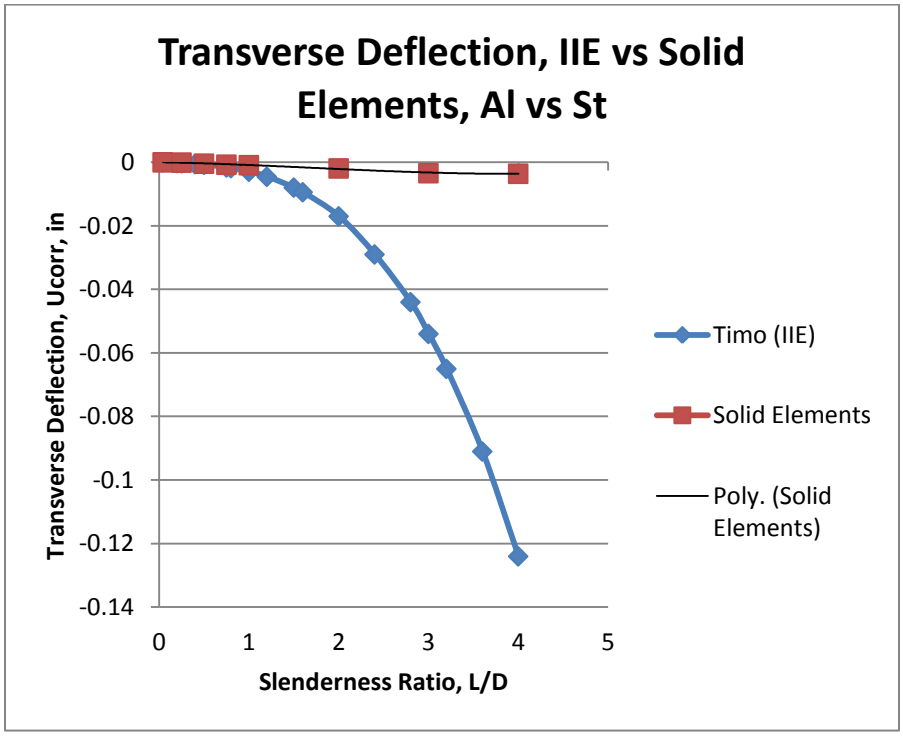

Figure 4.13: Deflection vs. slenderness ratio, Timoshenko (IIE) vs. solid elements.

Figure 4.14 incorporates into the comparison the novel finite element with stiffnesses based on the contact stiffnesses that is assumed for all load cases, and also divides that grouping into half of the stiffness. As can be seen, the new finite element matches very closely to the scale required to view the curve representing Timoshenko's theory. When the Timoshenko beam element is removed from Figure 4.14, what results is illustrated in Figure 4.15.

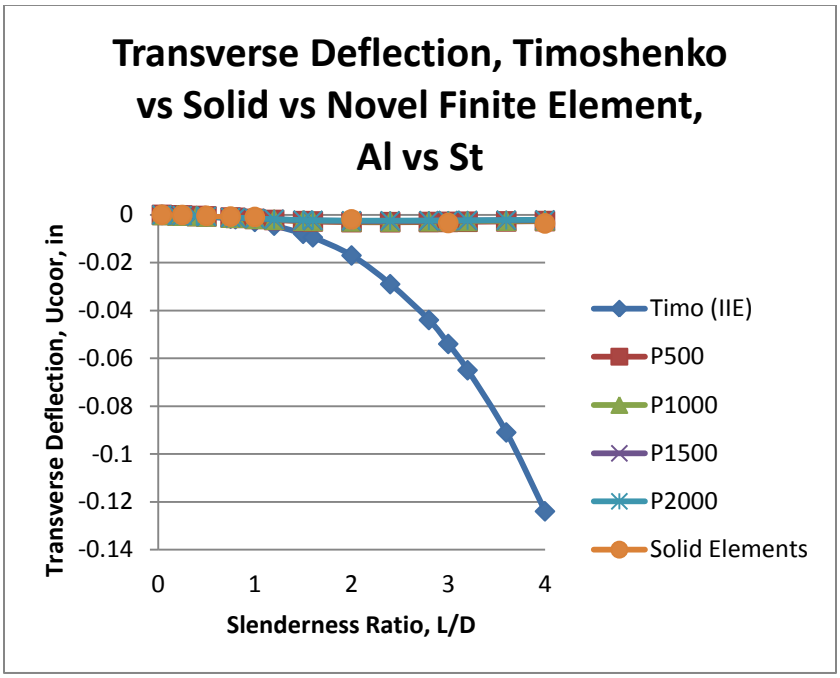

Figure 4.14: Timoshenko (IIE) vs. solid elements vs. novel finite element.

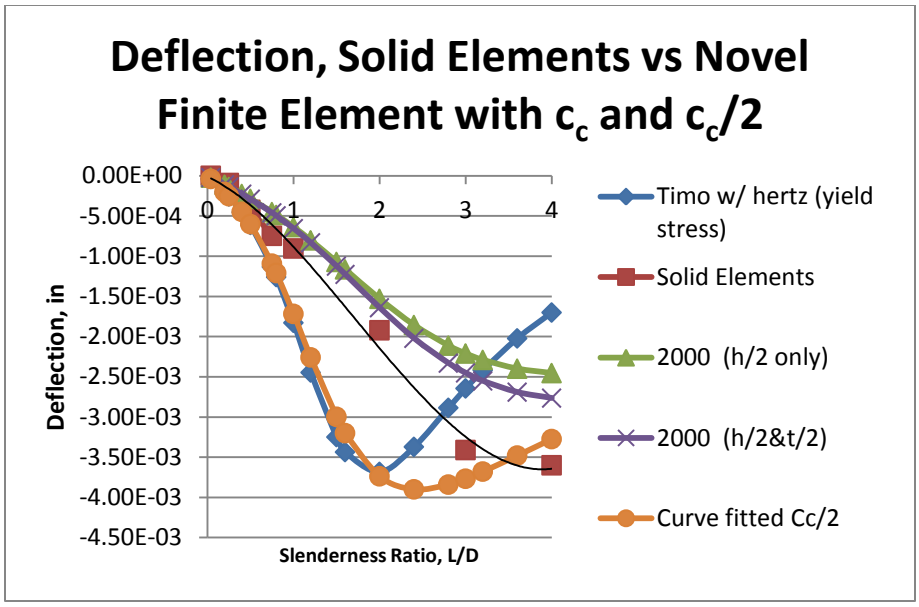

Figure 4.15: Solid elements vs. novel finite element with various c_c values.

Here, some adjustments are made on the parameters of the length of the fastener elements and the length against which stiffness is applied. The values of h and t represents the values of the length of the fastener and the thickness of the plates, respectively, where the full length represents the sum of the thicknesses of the plates, and h/2 represents the distance from the mid-planes of the plates. The value of t represents the amount of plate thickness that Hertzian contact is assumed to occur. Using the full value of t assumes that Hertzian contact is evenly distributed. Since loading along the shaft of the fastener is not uniform in a secondary bending scheme, half of this value represented by a t/2 term is warranted and is shown in the Figure 4.15.

It is clear that the novel finite element shows stiffness closest to the solid model by integrating a beam element that is equal to half of the sum of the plate thicknesses, h = (t1 + t2)/2. Also using half of the c_c value follows the solid model closer than using the full amount. This conclusion seems reasonable given that the plates are not evenly loaded across the thicknesses in a lap joint. This allows for consistency in a future application of a clevis joint, where the middle node would have the summation of two halved contact stiffnesses into a full measure. In relation

to the traditional finite elements, the amount of load assumed in establishing the contact stiffness is largely insensitive, and a given value, based on a logical premise as in this case, could be used.

Compared to traditional beam elements, the novel element behaves more like an actual fastener, as shown by the solid finite elements. Compared to the scale of deflection seen by traditional beam elements, when the fastener gets considerably longer, using different values for the length of the novel fastener element or numerical values applied to the contact stiffness does not show much difference. It makes sense that the values used for the length of the fastener finite element should be half of the sum of the thicknesses of the plates. For the treatment of the contact stiffnesses between the plates and the fasteners in a lap joint, considering half of the contact stiffnesses is consistent.

CHAPTER 5.

TEST CASE STUDY 2

5.1 Three-Bolt Test Case Layout

As with the first case study, this case study illustrates the response of the new element and overlays that output over the output generated from the two baseline modeling techniques. Once again, a variety of parameters are chosen and adjusted throughout the study.

The second case study is laid out using the same assumptions that are used in the joint formulation discussed in Chapter 3. The lap joint consists of two identical plate elements that are fastened with three fasteners spaced four bolt diameters wide. This case study differs from the first case study only in that it adds two more fasteners in tandem with the single fastener. Additional length, to account for the additional eight bolt diameters, is added to retain the standard fastener spacing. Once again, the fastener head has a diameter that is 1.5 times the shaft diameter. The head/nut height is at least half the shaft diameter. Again, as stated in Chapter 3, the location of the fastener is at least two shaft diameters from any edge. The overall length of each of the plate members is at least 28 fastener diameters (Figures 5.1 and 5.2).

Like the first case study, to provide a useful database to draw from for the second case study, four parameters are varied to four values, which results in 256 different combinations (4^4). The varied parameters are the external tensile loading, fastener preload, plate thickness, and fastener material/plate material ratio. Table 5.1 illustrates the size of this database. Considering the two baselines, the plate/beam/plate elements baseline and solid element baseline, 512 data sets are analyzed in this case study.

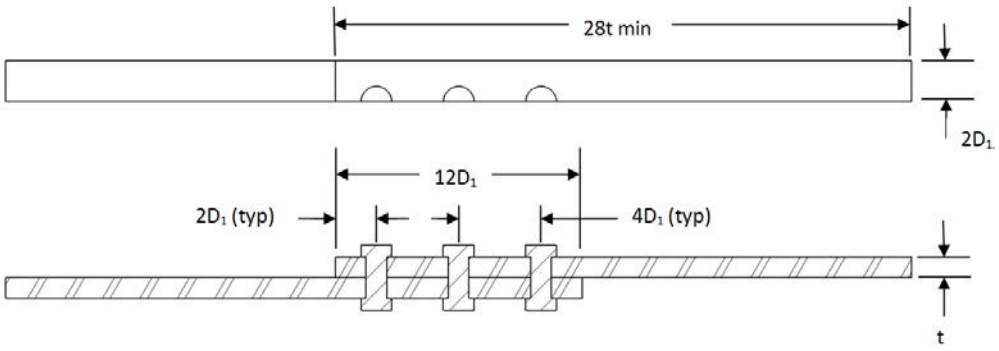

Figure 5.1: Case Study 2 layout.

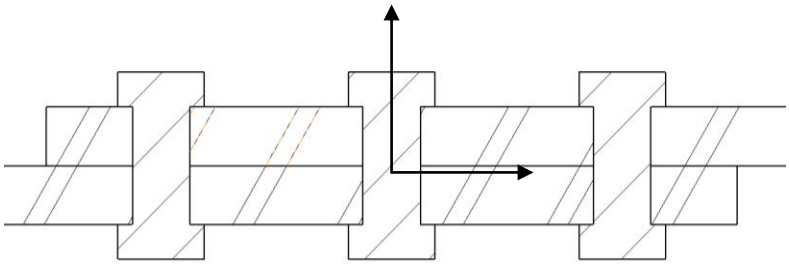

Figure 5.2: Cross section of Case Study 2 layout.

TABLE 5.1: CASE STUDY 2 PARAMETERS

	Parameter							
	Plate Load	Pre Load	Plate Thickness	Fastener Material	Plate Material	Elastic Modulus Fastener (10^6psi)	Elastic Modulus Plate (10^3psi)	Ef/Ep ratio
Parameter	500 lbs	500 lbs	1/4D	Steel	Aluminum	29	10.7	2.71
	1000lbs	1000 lbs	1/2D	Steel	Titanium	29	16	1.81
	1500 lbs	1500 lbs	3/4D	Titanium	Aluminum	16	10.7	1.49
	2000 lbs	2000 lbs	1D	Steel	Steel	29	29	1

In both baselines of the finite element models, the middle of the fasteners are constrained in the middle node of the middle bolt, and the ends of the plates are free to slide longitudinally only. Figure 5.3 illustrates how the models are constrained. The rationale for doing this is to isolate the deflection of the middle fastener and make trends more readily apparent.

In this case study, modeling of the plate and solid models is similar to the single-bolt problem. The only difference in modeling between both case studies is that the fastener area is copied forward and aft in the model to generate the two additional fasteners for this case study.

That drives the overall plate member length from a minimum of 20 times the plate thickness to a minimum of 28 times the plate thickness. For the plate model, the three-bolt problem has 60 elements (91 nodes, 546 DOF). For the solid models, the two larger thicknesses have 26,116 elements (32,229 nodes, 96,687 DOF). The two thinner thicknesses in the solid model have 16,921 elements (21,797 nodes, 65,391 DOF). As shown in Figures 5.4 to 5.6, half of the problem is modeled.

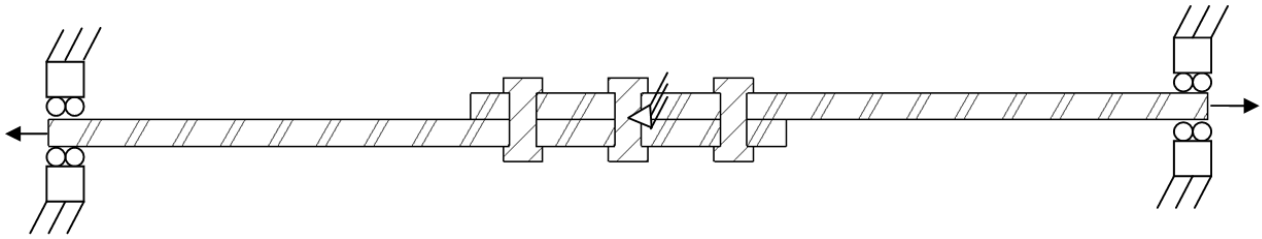

Figure 5.3: Three-bolt finite element model constraints.

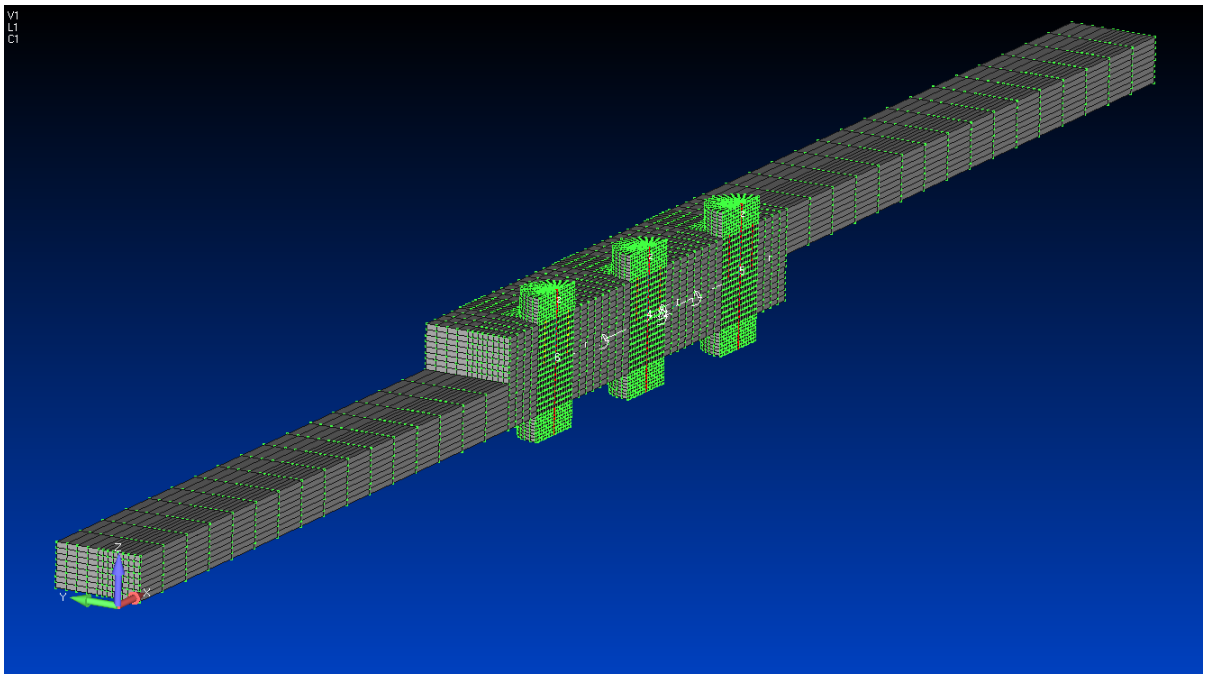

Figure 5.4: Three-bolt finite element plate model.

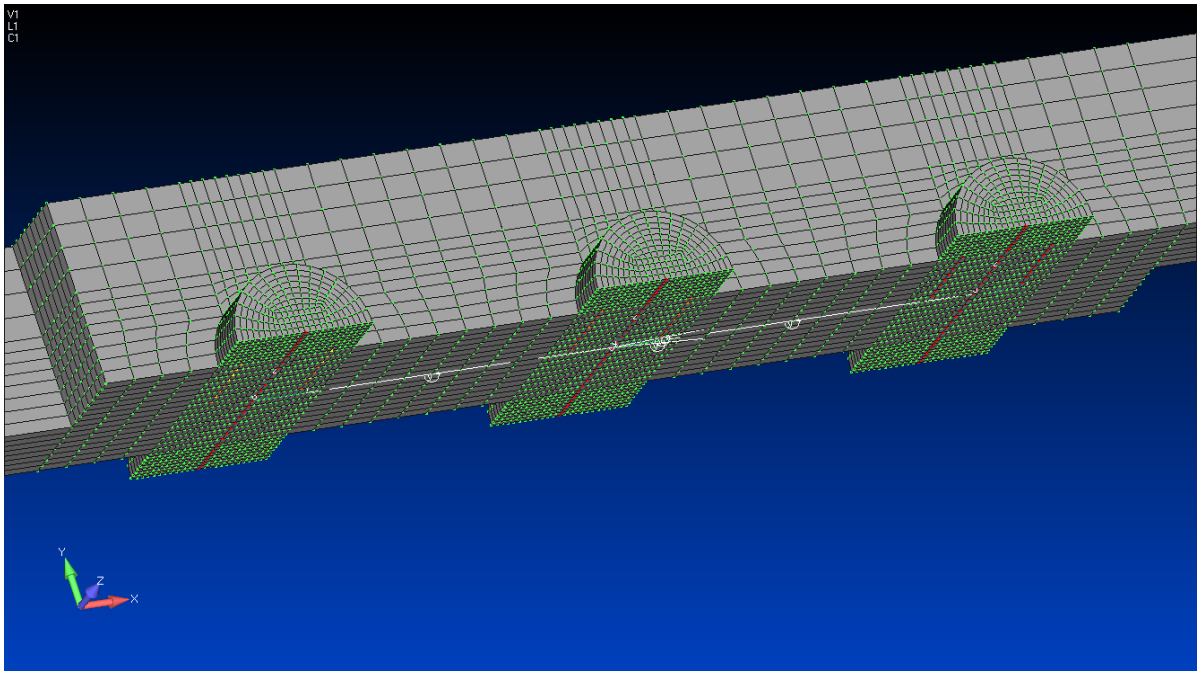

Figure 5.5: Three-bolt solid model problem.

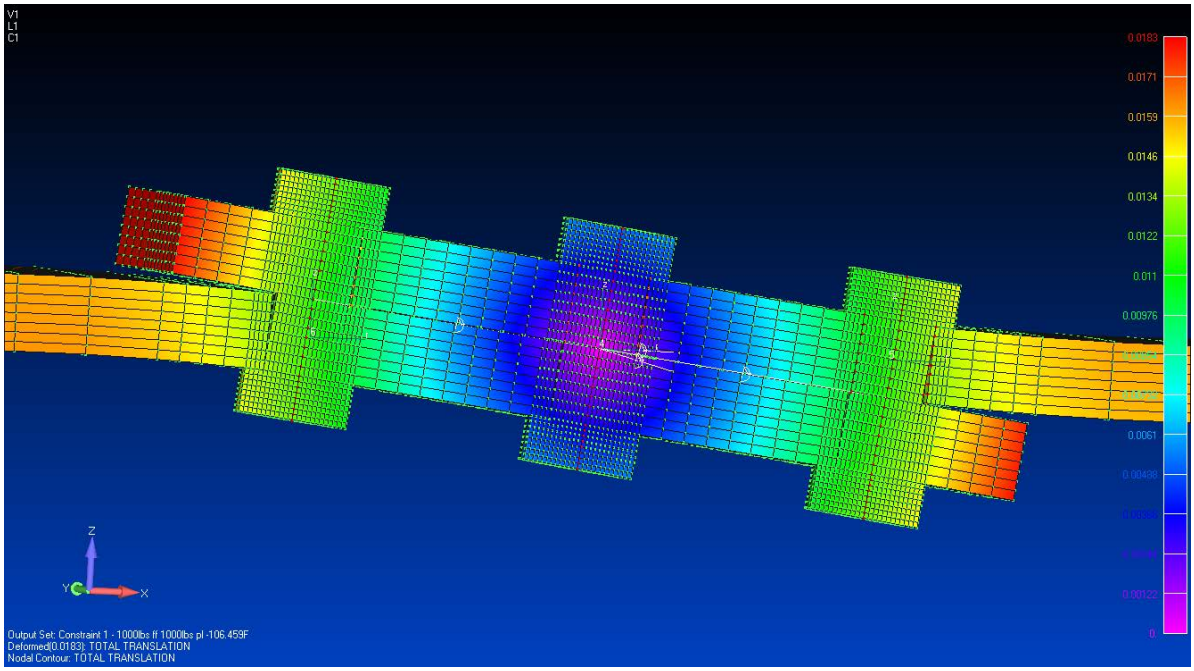

Figure 5.6: Three-bolt solid model deflection.

5.2 Results and Analysis

For the three-fastener model testing the novel element, a program was created in MathCad 15 to determine the numerical values of the fastener loads of the three novel fastener elements previously created for Test Case 1. The program, shown in its entirety in Appendix G, incorporated a coupled element using plane elasticity and classical plate theory (using Bathe and Dvorkin's [1986] mixed interpolation of tensorial components [MITC]4 formulation). The mesh density in the MathCad program is identical to traditional modeling used for the plate/beam/plate modeling using FEMAP/NEi NASTRAN. For traditional analyses, FEMAP is used for the preprocessor, and NEi NASTRAN is used for both the linear plate/beam/plate calculations and the nonlinear solid calculations.

Because deflection is of paramount concern in the single-fastener in the first case study, in this second case study, with a three-fastener model and fasteners arranged in tandem, the fastener loads are of interest. For this case study, the problem was analyzed using traditional beam elements, pulling the nodal values for force. In traditional solid models, nodal loads of all bolts that exist on the interface plane between the two joined plates are summed for each bolt. For solid models, zero friction is used between the contact surfaces of the joined members to ensure that the load transfer from plate to plate occurred solely through the fasteners in shear. Table 5.2 shows transfer loads seen by traditional commercial codes for this particular problem. Table 5.3 shows the summation of internal nodal forces that are exhibited by solid models. Table 5.4 shows loads experienced using the fastener flexibility incorporated into the neutral line model. Table 5.5 shows loads of the novel beam elements utilizing contact stiffness.

TABLE 5.2: FASTENER LOAD REACTIONS, PLATE/BEAM/PLATE

Bolt Loads (PLATE ELEMENTS NASTRAN SOLUTION)						
Plate Thick	Materials		Far Field Load	Max Plate def T3	Bolt 1/3 shear	Bolt 2 shear
	Plate	Bolt				
0.25	Al	St	500	0.00617	193.57	112.87
0.25	Al	St	1000	0.01230	387.13	225.73
0.25	Al	St	1500	0.01850	580.70	338.60
0.25	Al	St	2000	0.02470	774.27	451.46
0.1875	Al	St	500	0.01080	200.30	99.39
0.1875	Al	St	1000	0.02160	400.61	198.78
0.1875	Al	St	1500	0.03240	600.91	298.17
0.1875	Al	St	2000	0.04320	801.22	397.56
0.125	Al	St	500	0.02400	206.39	87.21
0.125	Al	St	1000	0.04810	412.79	174.42
0.125	Al	St	1500	0.07210	619.18	261.63
0.125	Al	St	2000	0.09610	825.58	348.85
0.0625	Al	St	500	0.09540	210.72	78.56
0.0625	Al	St	1000	0.19100	421.44	157.12
0.0625	Al	St	1500	0.28600	632.16	235.69
0.0625	Al	St	2000	0.38100	842.88	314.25

TABLE 5.3: FASTENER LOAD REACTIONS, SOLID MODELS

Solids														
Solid models with averaged first and third bolt loads (NASTRAN SOLUTION)												Average Loads across all preloads		Bolt 1/Bolt 2 Ratio
				Bolt1/3	Bolt2	Bolt1/3	Bolt2	Bolt1/3	Bolt2	Bolt1/3	Bolt2	Bolt1/3	Bolt2	
Thickness	Plate	Bolt	Load	preload	500	preload	1000	preload	1500	preload	2000			
0.25	Al	St	500	192.43	115.14	194.54	110.92	194.37	111.25	195.91	108.17	194.31	111.37	1.74
0.25	Al	St	1000	383.95	232.10	384.28	231.44	379.46	241.09	381.66	236.67	382.34	235.32	1.62
0.25	Al	St	1500	578.48	343.04	579.55	340.89	572.27	355.46	573.12	353.75	575.86	348.29	1.65
0.25	Al	St	2000	775.34	449.31	778.27	443.45	775.78	448.43	836.69	326.63	791.52	416.95	1.90
0.1875	Al	St	500	198.01	103.98	196.11	107.78	195.87	108.26	190.97	118.06	195.24	109.52	1.78
0.1875	Al	St	1000	394.23	211.54	396.62	206.77	389.34	221.33	376.07	247.86	389.06	221.87	1.75
0.1875	Al	St	1500	575.73	348.54	584.71	330.58	590.25	319.49	592.01	315.99	585.68	328.65	1.78
0.1875	Al	St	2000	794.40	411.20	795.52	408.95	785.55	428.91	753.76	492.47	782.31	435.38	1.80
0.125	Al	St	500	204.25	91.51	203.91	92.18	198.82	102.37	200.16	99.68	201.78	96.43	2.09
0.125	Al	St	1000	379.44	241.13	403.63	192.74	398.87	202.27	406.16	187.69	397.02	205.95	1.93
0.125	Al	St	1500	622.20	255.59	625.80	248.41	591.28	317.43	599.21	301.58	609.62	280.75	2.17
0.125	Al	St	2000	833.49	333.03	844.83	310.35	830.78	338.45	853.26	293.47	840.59	318.82	2.64
0.0625	Al	St	500	201.24	97.52	207.63	84.75	199.38	101.24	188.40	123.20	199.16	101.68	1.96
0.0625	Al	St	1000	387.10	225.79	408.79	182.42	402.67	194.66	411.52	176.96	402.52	194.96	2.06
0.0625	Al	St	1500	537.46	425.08	667.78	164.43	609.86	280.28	605.36	289.28	605.12	289.77	2.09
0.0625	Al	St	2000	891.49	217.02	777.61	444.77	816.44	367.11	795.15	409.70	820.18	359.65	2.28

TABLE 5.4: LOAD REACTIONS, NEUTRAL LINE MODEL WITH HUTH

Calculated Forces (using Neutral Line Model with Huth Flexibility)						
Plate Thick	Materials		Bolt 1/3 shear	Bolt 2 shear	Bolt 1/Bolt 2 Ratio	Far Field Load
	Plate	Bolt				
0.25	Al	St	173.34	153.32	1.13	500
0.25	Al	St	346.69	306.63	1.13	1000
0.25	Al	St	520.03	459.63	1.13	1500
0.25	Al	St	693.37	613.26	1.13	2000
0.1875	Al	St	174.62	150.76	1.16	500
0.1875	Al	St	349.24	301.52	1.16	1000
0.1875	Al	St	523.86	452.29	1.16	1500
0.1875	Al	St	698.48	603.05	1.16	2000
0.125	Al	St	176.79	146.43	1.21	500
0.125	Al	St	353.58	292.85	1.21	1000
0.125	Al	St	530.36	439.27	1.21	1500
0.125	Al	St	707.15	585.70	1.21	2000
0.0625	Al	St	181.66	136.67	1.33	500
0.0625	Al	St	363.33	273.35	1.33	1000
0.0625	Al	St	544.99	410.02	1.33	1500
0.0625	Al	St	726.65	546.70	1.33	2000

TABLE 5.5: LOAD REACTIONS, PLATE WITH NOVEL ELEMENT

				PLATE ELEMENTS (NEW SOLUTION)					
Plate Thick	Materials		Far Field Load	Pre Load	Max Plate def T3	Bolt 1/3 shear	Bolt 2 shear	Bolt Sums	Bolt 1/Bolt 2 Ratio
	Plate	Bolt							
0.25	Al	St	500		0.00384	187.10	125.80	500.00	1.49
0.25	Al	St	1000		0.00767	374.20	251.61	1000.00	1.49
0.25	Al	St	1500		0.01200	561.29	377.40	1499.98	1.49
0.25	Al	St	2000		0.01500	748.39	503.21	2000.00	1.49
0.1875	Al	St	500		0.00693	189.65	120.71	500.00	1.57
0.1875	Al	St	1000		0.01400	379.29	241.42	1000.00	1.57
0.1875	Al	St	1500		0.02100	568.94	362.13	1500.00	1.57
0.1875	Al	St	2000		0.02800	758.58	482.84	2000.00	1.57
0.125	Al	St	500		0.01600	191.92	116.17	500.00	1.65
0.125	Al	St	1000		0.03200	383.83	232.34	1000.00	1.65
0.125	Al	St	1500		0.04800	575.75	348.51	1500.00	1.65
0.125	Al	St	2000		0.06300	767.66	464.68	2000.00	1.65
0.0625	Al	St	500		0.06500	193.60	112.81	500.00	1.72
0.0625	Al	St	1000		0.12900	387.19	225.62	1000.00	1.72
0.0625	Al	St	1500		0.19400	580.79	338.43	1500.00	1.72
0.0625	Al	St	2000		0.25900	774.38	451.24	2000.00	1.72

Again, as with the single-fastener case, there does not seem to be any direct relationship between bolt preload and load transfer with this element. The data implies that there is no direct

connection between the fastener preloads and the transferred load in a friction-free environment. For the beam element models including the novel element, tensile loading and transverse loading are uncoupled. Another observation is that there is generally little difference between the two different methods using commercial code. For example, for the 0.25-inch thick aluminum plates with steel fasteners and a 500 lb far-field tension load, the plate/beam/plate element method results in a bolt transfer load of 193.57 lbs and 125.80 lbs for the end fastener and the middle fastener, respectively, whereas for the methods using solids, the loads average 194.31 lbs and 111.37 lbs, respectively. For the novel method, loads for the front and middle fasteners are 187.10 lbs and 125.80 lbs, respectively. This trend is largely consistent across the study. Additionally, as the joined members get thinner, the data of the solid models becomes more inconsistent. The likely cause of this is due to a smaller number of elements used across the length of the fasteners and joined members. Table 5.6 shows load ratios between the leading and middle fasteners.

TABLE 5.6: LOAD REACTIONS, FIRST/MIDDLE LOAD RATIO, ALUMINUM VS STEEL

Plate Thick	Materials		Far Field Load	Bolt 1/Bolt 2 Ratio	Bolt 1/Bolt 2 Ratio	Bolt 1/Bolt 2 Ratio
	Plate	Bolt		Plates	Solids	Novel
0.25	Al	St	500	1.7150	1.7447	1.4872
0.25	Al	St	1000	1.7150	1.6247	1.4872
0.25	Al	St	1500	1.7150	1.6534	1.4873
0.25	Al	St	2000	1.7150	1.8983	1.4872
0.1875	Al	St	500	2.0153	1.7826	1.5711
0.1875	Al	St	1000	2.0153	1.7535	1.5711
0.1875	Al	St	1500	2.0153	1.7821	1.5711
0.1875	Al	St	2000	2.0153	1.7968	1.5711
0.125	Al	St	500	2.3665	2.0925	1.6520
0.125	Al	St	1000	2.3666	1.9277	1.6520
0.125	Al	St	1500	2.3666	2.1714	1.6520
0.125	Al	St	2000	2.3666	2.6365	1.6520
0.0625	Al	St	500	2.6822	1.9588	1.7161
0.0625	Al	St	1000	2.6823	2.0647	1.7161
0.0625	Al	St	1500	2.6822	2.0883	1.7161
0.0625	Al	St	2000	2.6822	2.2805	1.7161

Interestingly, the novel beam element begins to approach the load ratios that are seen in the Huth fastener using the neutral line model, rather than loads that are seen using traditional methods. Consistently, the Huth fastener flexibility predicts smaller front-fastener loads than the traditional element methods and the novel element as well. Differences between the methods are difficult to discern when the applied load is small. These differences become larger with an increase in applied load. Figures 5.7 to 5.11 illustrate loads of the leading edge/front fastener versus the amount of applied far-field load for each of the four plate member thicknesses. Again, this is for an aluminum/steel plate/fastener combination. Differences in thicknesses can be more easily seen in Figure 5.11. There is less difference in load ratios across thicknesses between the plates and solids using traditional modeling methods. The novel element model lies between traditional modeling methods and the neutral line model with Huth flexibility. Also, the load ratio is independent of the far-field load when modeled using the plate/beam/plate model as well as the neutral line model, and the novel finite element follows this course. There are some differences when modeling solids, and the singular curve representing the average deflection of the different thicknesses is represented in Figure 5.11. The different averages for each thickness across the four different far-field loads are applied in this case study.

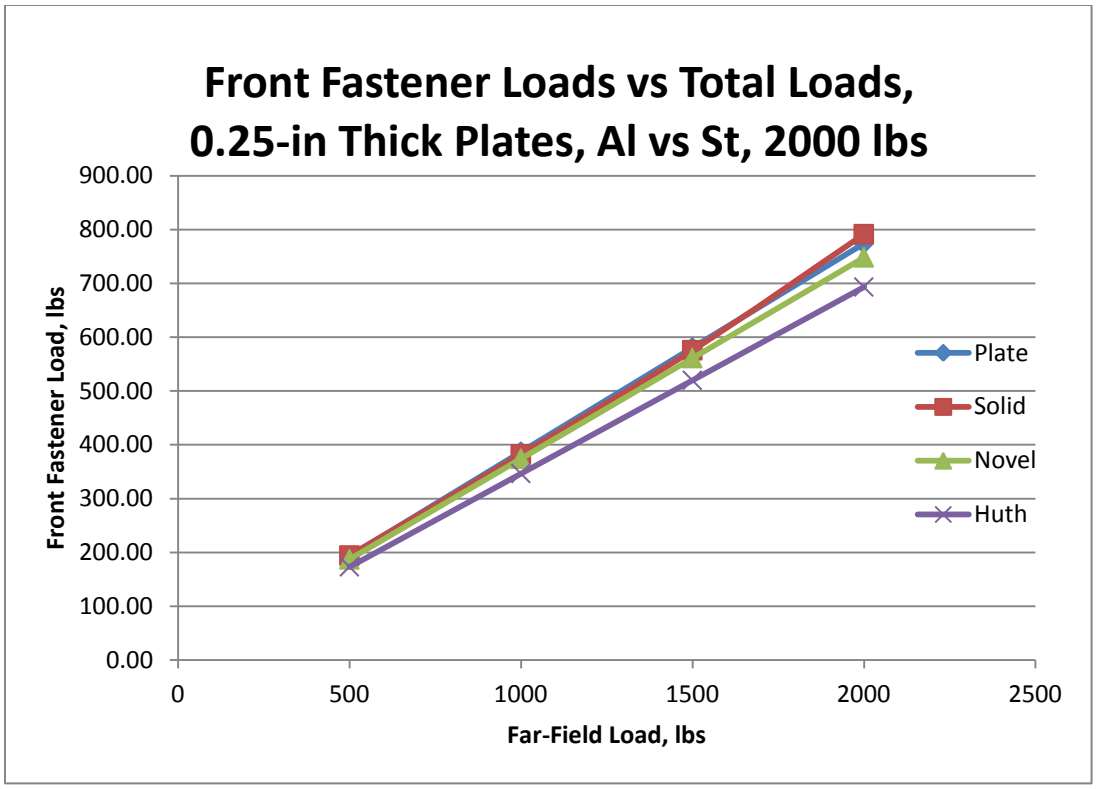

Figure 5.7: Front fastener loads vs. total loads, 0.25-inch thick plates, Al vs. St.

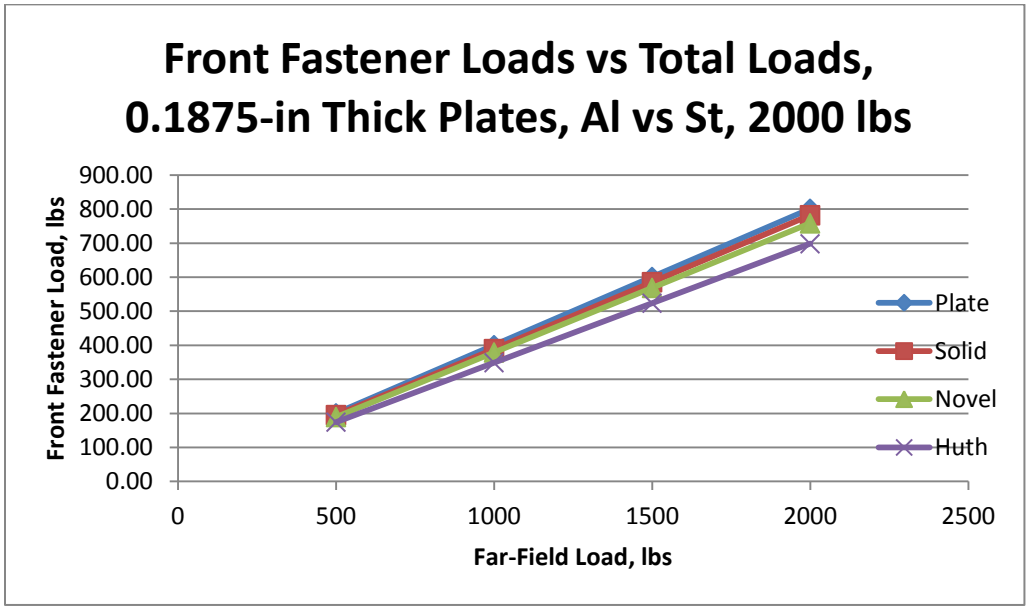

Figure 5.8: Front fastener loads vs. total loads, 0.1875-inch thick plates, Al vs. St.

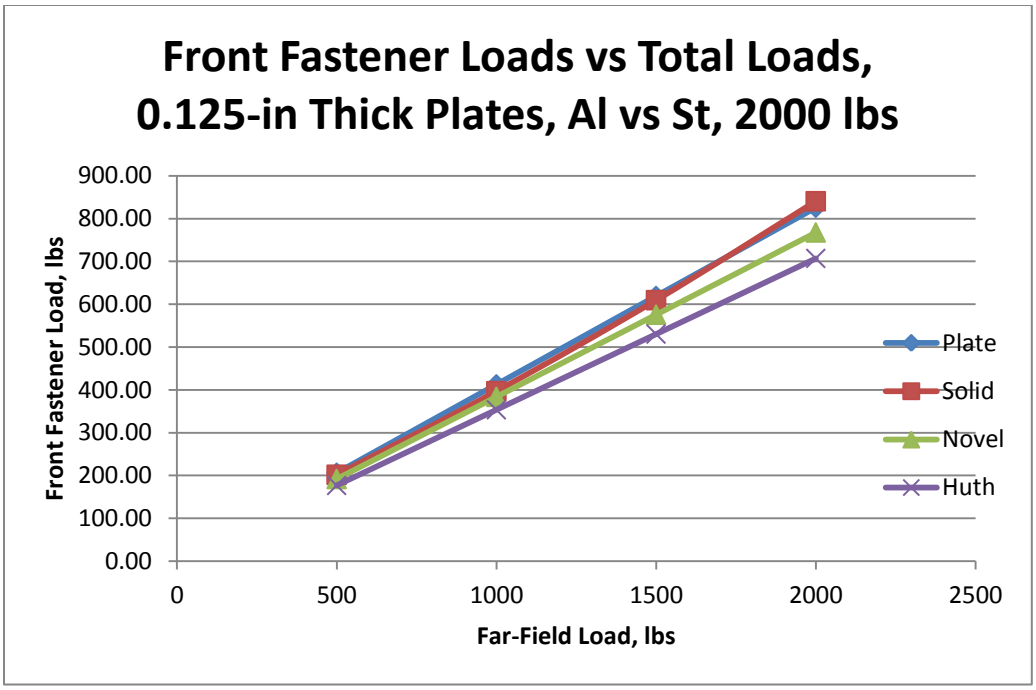

Figure 5.9: Front fastener loads vs. total loads, 0.125-in thick plates, Al vs. St.

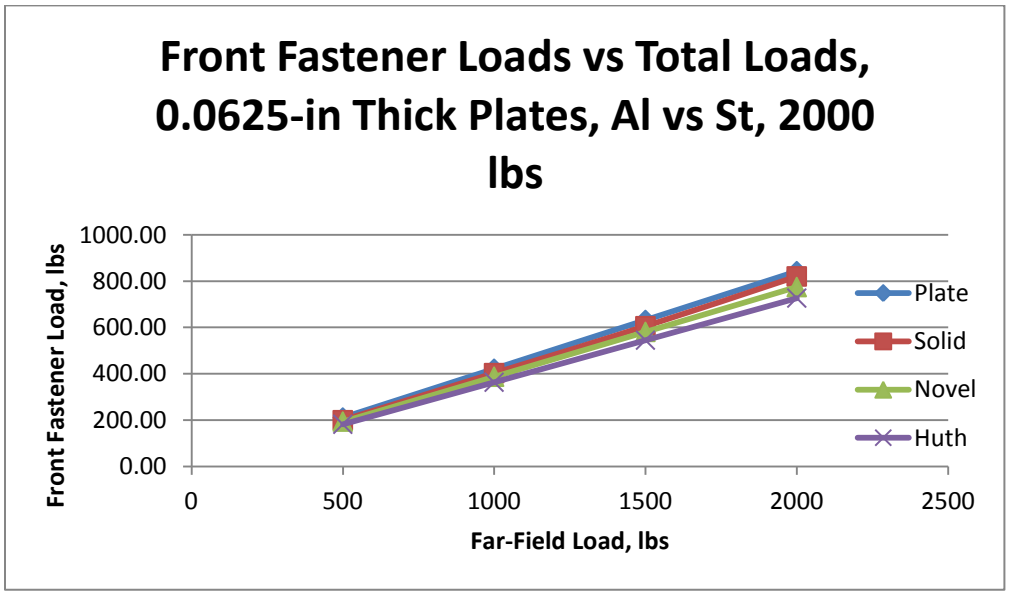

Figure 5.10: Front fastener loads vs. total loads, 0.0625-inch thick plates, Al vs. St.

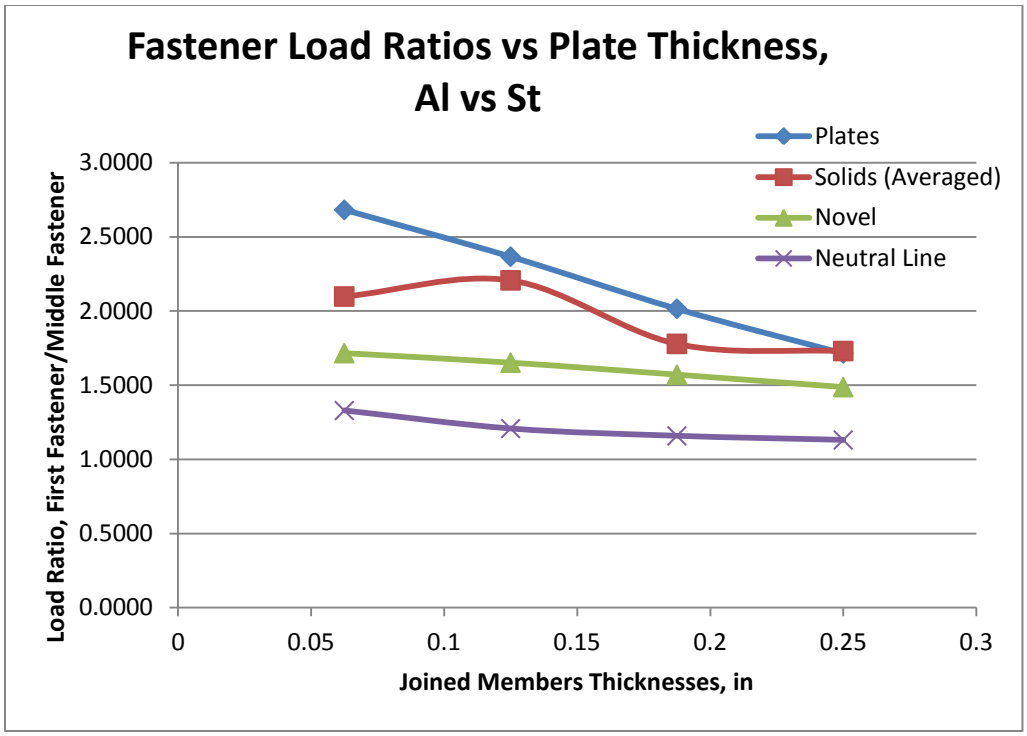

Figure 5.11: Load ratios vs. plate thickness, Al vs. St.

CHAPTER 6.

TEST CASE STUDIES 3 AND 4

6.1 Three-Bolt Test Case Layout

As with earlier case studies, these case studies illustrates the response of the new element and overlays that output over the output generated from the two baseline modeling techniques. Also, a variety of parameters were chosen and adjusted throughout the study.

Similar to the second case study, the third and fourth case studies consist of three-bolt models in which the shear load distributions are of sole interest. The difference between these two case study models and the second case study model is that while the constraints are similar, the problem is no longer symmetric. Case Study 3 illustrates the differences in thicknesses between the joined plates, but the joined plates still have the same plate materials. Case Study 4 utilizes the same thicknesses between the upper and lower plates, but the plates utilize different materials. The assumptions for the joint formulation in Case Studies 3 and 4 are the same as for Case Studies 1 and 2. The lap joints consist of two plate elements fastened with three fasteners spaced four bolt diameters wide. These case studies differ from the first case study only in that they adds two more fasteners in tandem with the single fastener. As with the previous two case studies, the fastener head has a diameter that is 1.5 times the shaft diameter. The head/nut height is at least half the shaft diameter. Again, as stated in Chapter 3, the location of the fastener is at least two shaft diameters from any edge. The overall length of each of the plate members is at least 28 fastener diameters (Figure 6.1). For all models in both case studies, 0.25-inch diameter steel bolts are used exclusively. Case Studies 3 and 4 parameters are shown in Tables 6.1 and 6.2, respectively.

TABLE 6.1: CASE STUDY 3 PARAMETERS

	Parameter				
	Plate Load	Plate 1 Thickness	Plate 2 Thickness	Fastener Material	Plate 1 and 2 Material
Parameter	500 lbs	1D	1/4D	Steel	Aluminum
	1000lbs		1/2D		
	1500 lbs		3/4D		
	2000 lbs		1D		

TABLE 6.2: CASE STUDY 4 PARAMETERS

	Parameter				
	Plate Load	Plate 1 Material	Plate 2 Material	Fastener Material	Plate Thicknesses (Both)
Parameter	500 lbs	Al	Al	Steel	1D
	1000lbs	Al	St		
	1500 lbs	Ti	St		
	2000 lbs	Al	Ti		

For Case Studies 3 and 4, the number of different parameters used are attenuated, and the configurations chosen are meant to display the largest differences between the parameters, primarily for illustrative purposes. Without this attenuation, additional parameters of different plate thicknesses and different plate materials can increase the number of different combinations from 4^4 (from the previous case studies) to 4^6 for plates and solids or 4,096 combinations (8,192 combinations total between plates and solids baselines).

The modeling in Case Study 2 and the two studies discussed in this chapter are different only in the constraints. Since there is no symmetry between the top and bottom plates in Case Studies 3 and 4, the constraint existing in the second case study located in the middle bolts is released, and one end is fixed in all degrees of freedom (Figure 6.1).

The plate element modeling baselines here are identical to those in Case Studies 1 and 2, and the modeling program used for the solid modeling is Elfini, which is an embedded module that exists in CATIA V5. The Elfini FEM program models exclusively with either four-node or

ten-node tetrahedrons. All models of the solid baseline in Case Studies 3 and 4 utilize 0.0625-inch ten-node tetrahedrons. The modeling for the plate element variants remained in Femap, with NEi NASTRAN or NX NASTRAN as the calculating engines.

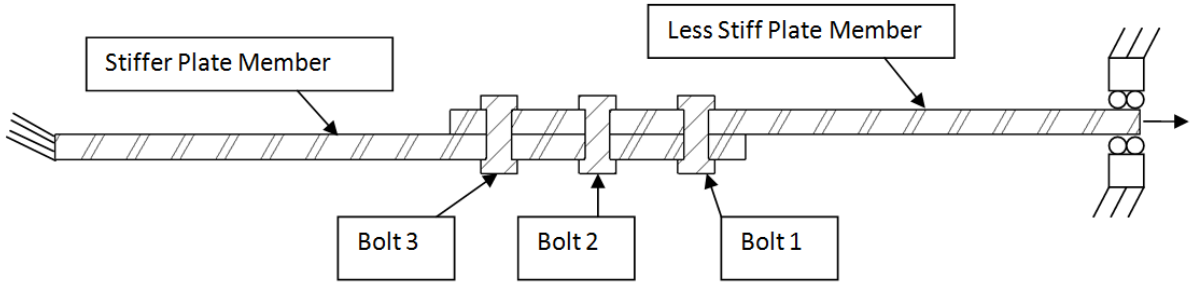

Figure 6.1: Case Studies 3 and 4 layout.

6.2 Results and Analysis

The difference in shear loads between the bolts in Case Studies 3 and 4 and Case Study 2 is that the loads in leading and trailing bolts are no longer equal. The output in Case Study 2 is sufficiently descriptive as a load ratio between bolt 1 and bolt 2. In Case Studies 3 and 4, the shear loading in bolt 1 and bolt 3 are no longer equal, and a simple bolt loading ratio is no longer sufficient. Case Studies 3 and 4 load results are shown in Tables 6.3 to 6.6.

The most apparent trend shown in the baselines, as well as in the novel element, is that the highest shear loads result on the side that has the smallest stiffness. This is an expected trend and indicates that the major contributor for this lack of "load symmetry" is from the behavior of the joined plate elements rather than of the fastening elements themselves. For examples of the different models used in illustrating the range of load transfer through shear of the fasteners, see Figures 6.2 to 6.10.

TABLE 6.3: CASE STUDY 3 LOAD RESULTS PART 1

Different Plt Member Thknss 0.25 vs various Thknss (ALvsSt)									
Plate Thick	Materials			Plate Elements			Solids		
	Plates	Bolt	Load	Bolt1	Bolt2	Bolt3	Bolt1	Bolt2	Bolt3
0.25	Al	St	500	193.57	112.87	193.57	192.56	115.70	191.75
0.25	Al	St	1000	387.13	225.73	387.13	385.11	231.39	383.50
0.25	Al	St	1500	580.70	338.60	580.70	577.67	347.09	575.24
0.25	Al	St	2000	774.27	451.46	774.27	769.69	461.19	769.69
0.1875	Al	St	500	197.26	111.55	191.19	215.54	78.75	205.72
0.1875	Al	St	1000	394.51	223.10	382.38	431.07	157.49	411.44
0.1875	Al	St	1500	291.77	334.65	573.57	646.61	236.24	617.16
0.1875	Al	St	2000	789.03	446.21	764.76	862.14	314.98	822.88
0.125	Al	St	500	198.54	103.82	197.64	231.73	69.52	198.75
0.125	Al	St	1000	397.08	207.64	395.28	463.46	139.04	397.50
0.125	Al	St	1500	595.62	311.46	592.92	695.19	208.56	596.26
0.125	Al	St	2000	794.16	415.27	790.56	926.92	278.07	795.01
0.0625	Al	St	500	201.51	98.73	199.76	242.91	234.76	22.33
0.0625	Al	St	1000	403.01	197.47	399.52	485.82	469.51	44.67
0.0625	Al	St	1500	604.52	296.20	599.28	728.73	704.27	67.00
0.0625	Al	St	2000	806.03	394.93	799.04	924.32	298.44	777.24

TABLE 6.4: CASE STUDY 3 LOAD RESULTS PART 2

Different Plt Member Thknss 0.25 vs various Thknss (ALvsSt)									
Plate Thick	Materials			Novel			Huth		
	Plates	Bolt	Load	Bolt1	Bolt2	Bolt3	Bolt1	Bolt2	Bolt3
0.25	Al	St	500	191.59	116.82	191.59	173.81	152.37	173.81
0.25	Al	St	1000	383.18	233.65	383.18	347.63	304.75	347.63
0.25	Al	St	1500	574.76	350.47	574.76	521.44	457.12	521.44
0.25	Al	St	2000	766.35	467.29	766.35	695.25	609.49	695.25
0.1875	Al	St	500	185.15	131.91	182.94	177.52	156.55	165.93
0.1875	Al	St	1000	370.30	263.82	365.89	355.04	313.11	331.85
0.1875	Al	St	1500	555.44	395.72	548.83	532.56	469.66	497.78
0.1875	Al	St	2000	740.59	527.63	731.77	710.08	626.22	663.70
0.125	Al	St	500	190.47	127.54	181.99	186.97	155.53	157.50
0.125	Al	St	1000	380.94	255.08	363.98	373.93	311.07	315.00
0.125	Al	St	1500	571.41	382.62	545.97	560.90	466.60	472.50
0.125	Al	St	2000	761.88	510.17	727.96	747.87	622.13	630.00
0.0625	Al	St	500	199.75	115.97	184.15	187.38	157.96	143.62
0.0625	Al	St	1000	399.50	231.93	368.30	374.76	315.92	287.25
0.0625	Al	St	1500	599.25	347.90	552.45	562.13	473.87	430.87
0.0625	Al	St	2000	799.00	463.86	736.60	749.51	631.83	574.49

TABLE 6.5: CASE STUDY 4 LOAD RESULTS, PART 1

Different Plt Member Materials 0.25 vs 0.25 (Steel Bolt)									
Plate Thick	Materials with steel bolts			Plate Elements			Solids		
	Plate 1	Plate 2	Load	Bolt1	Bolt2	Bolt3	Bolt1	Bolt2	Bolt3
0.25	Al	St	500	206.52	126.03	167.46	212.35	110.23	177.42
0.25	Al	St	1000	413.03	252.05	334.92	424.70	220.45	354.85
0.25	Al	St	1500	619.55	378.08	502.37	637.05	330.68	532.27
0.25	Al	St	2000	826.06	504.11	669.83	849.40	440.91	709.70
0.25	Ti	St	500	196.22	129.98	173.80	227.56	89.56	182.88
0.25	Ti	St	1000	392.45	259.96	347.59	455.11	179.12	365.76
0.25	Ti	St	1500	588.67	389.95	521.39	682.67	268.68	548.64
0.25	Ti	St	2000	784.89	519.93	695.19	910.23	358.25	731.52
0.25	Al	Ti	500	191.68	131.74	176.58	215.54	84.08	200.38
0.25	Al	Ti	1000	383.36	263.49	353.15	431.07	168.16	400.77
0.25	Al	Ti	1500	575.41	395.23	529.73	646.61	252.24	601.15
0.25	Al	Ti	2000	766.73	526.97	706.30	862.14	336.32	801.54

TABLE 6.6: CASE STUDY 4 LOAD RESULTS, PART 2

Different Plt Member Materials 0.25 vs 0.25 (Steel Bolt)									
Plate Thick	Materials with steel bolts			Novel			Huth		
	Plate 1	Plate 2	Load	Bolt1	Bolt2	Bolt3	Bolt1	Bolt2	Bolt3
0.25	Al	St	500	211.66	136.82	151.52	202.18	154.20	143.62
0.25	Al	St	1000	423.32	273.63	303.04	404.35	308.40	287.24
0.25	Al	St	1500	634.98	410.45	454.56	606.53	462.60	430.87
0.25	Al	St	2000	846.64	547.26	606.08	808.71	616.81	574.49
0.25	Ti	St	500	197.20	138.86	163.94	180.45	158.48	161.07
0.25	Ti	St	1000	394.41	277.71	327.88	360.89	316.97	322.14
0.25	Ti	St	1500	591.61	416.57	491.82	541.34	475.45	483.21
0.25	Ti	St	2000	788.81	555.42	655.76	721.78	633.93	644.28
0.25	Al	Ti	500	194.81	135.84	169.34	178.47	157.63	163.90
0.25	Al	Ti	1000	389.63	271.69	338.69	356.93	315.26	327.81
0.25	Al	Ti	1500	584.44	407.53	508.03	535.40	472.89	491.71
0.25	Al	Ti	2000	779.26	543.37	677.37	713.87	630.52	655.61

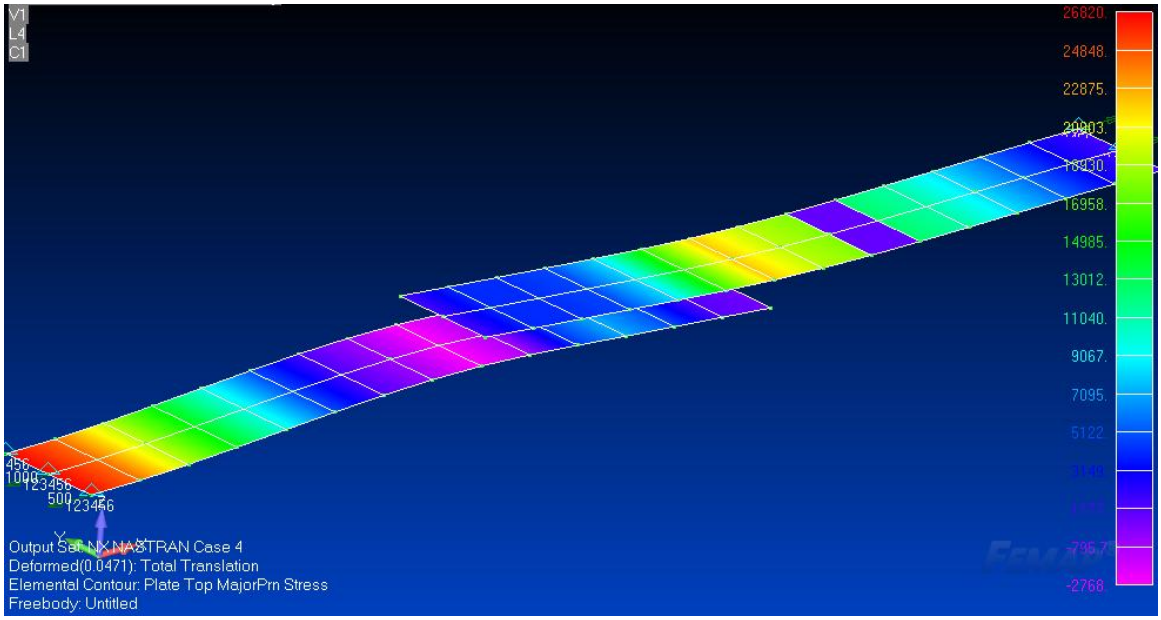

Figure 6.2: Three-bolt plate FE model, 0.1875-in x 0.25-in Al plates.

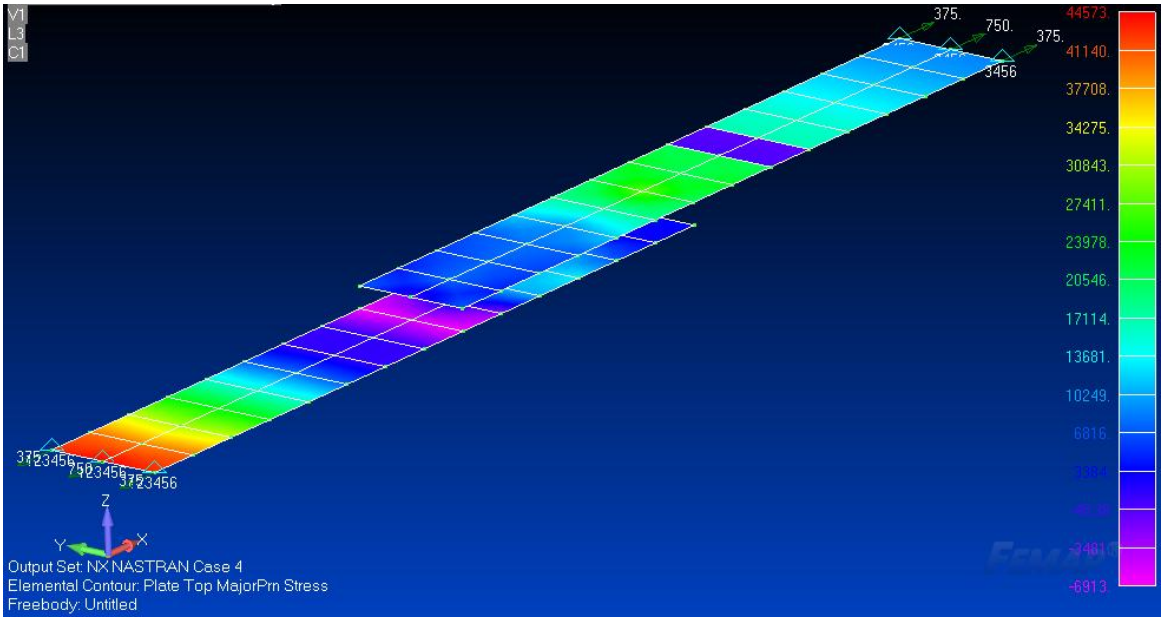

Figure 6.3: Three-bolt plate FE model, 0.125-in x 0.25-in Al plates.

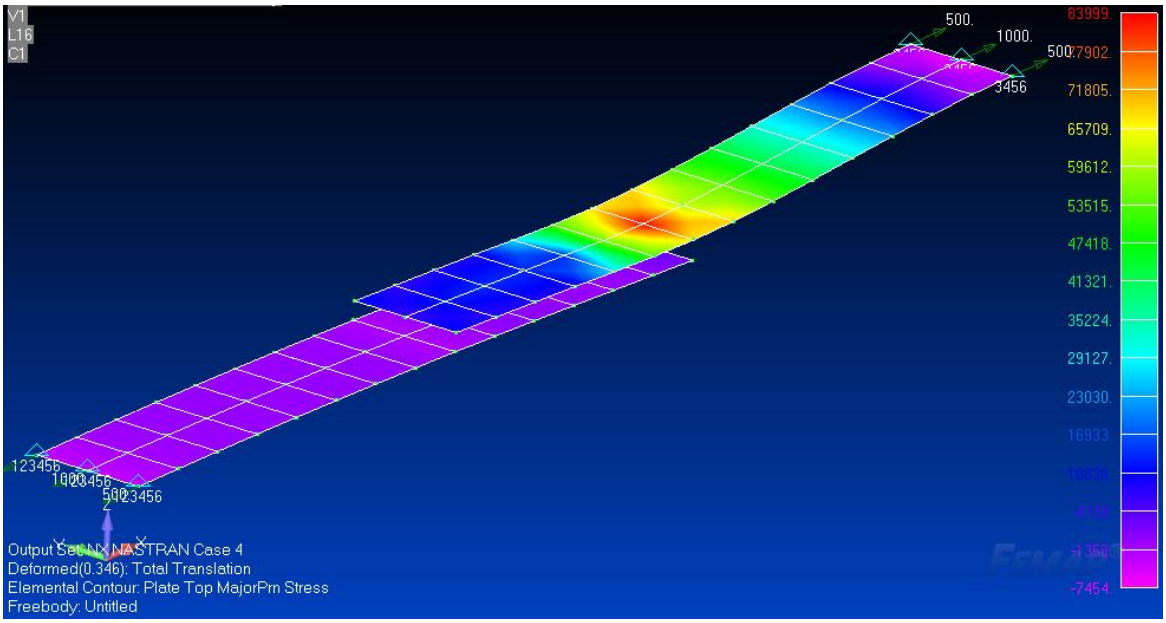

Figure 6.4: Three-bolt plate FE model, 0.0625-in x 0.25-in Al plates.

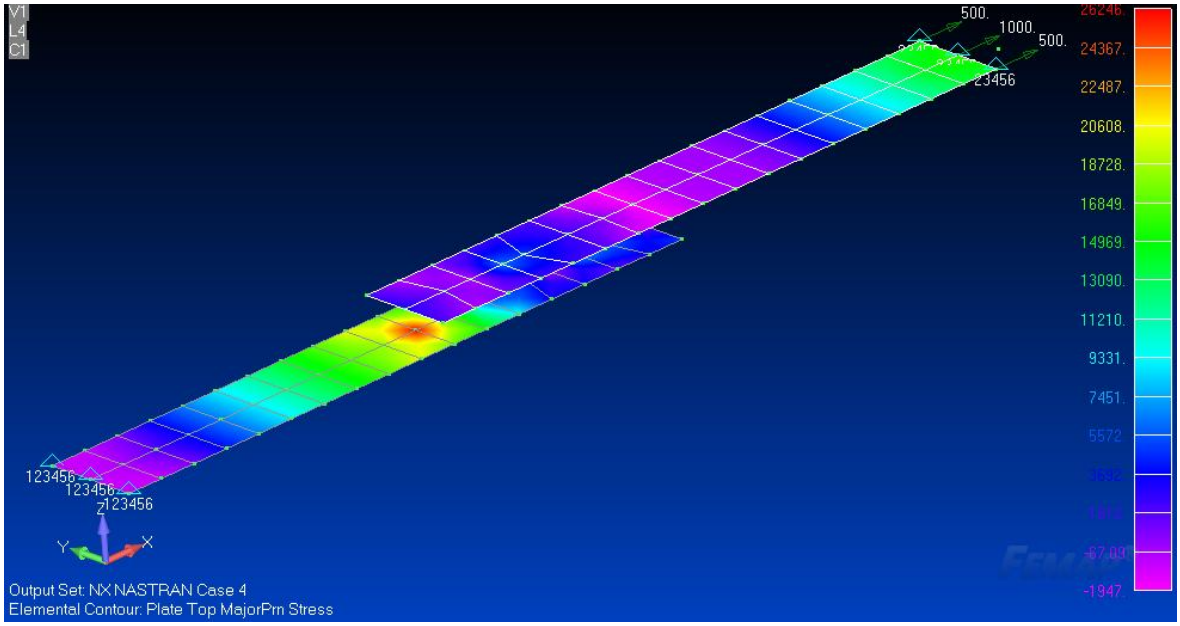

Figure 6.5: Three-bolt plate FE model, 0.25-in x 0.25-in Al/St plates.

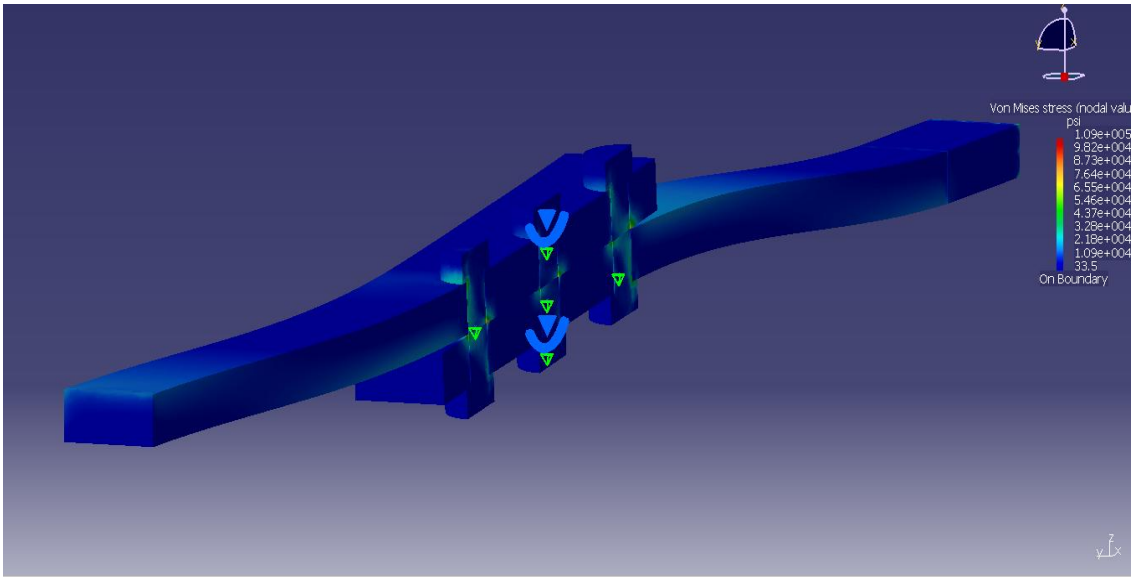

Figure 6.6: Three-bolt solid FE model, 0.25-in x 0.25-in Al/St plates.

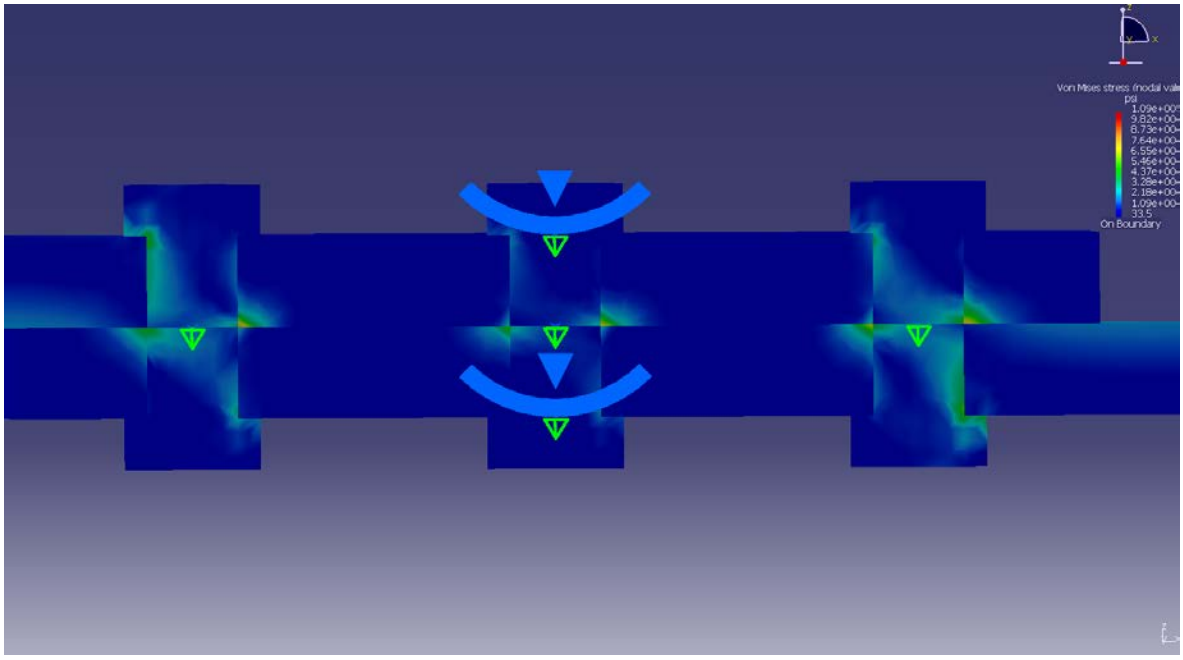

Figure 6.7: Three-bolt solid model, side view.

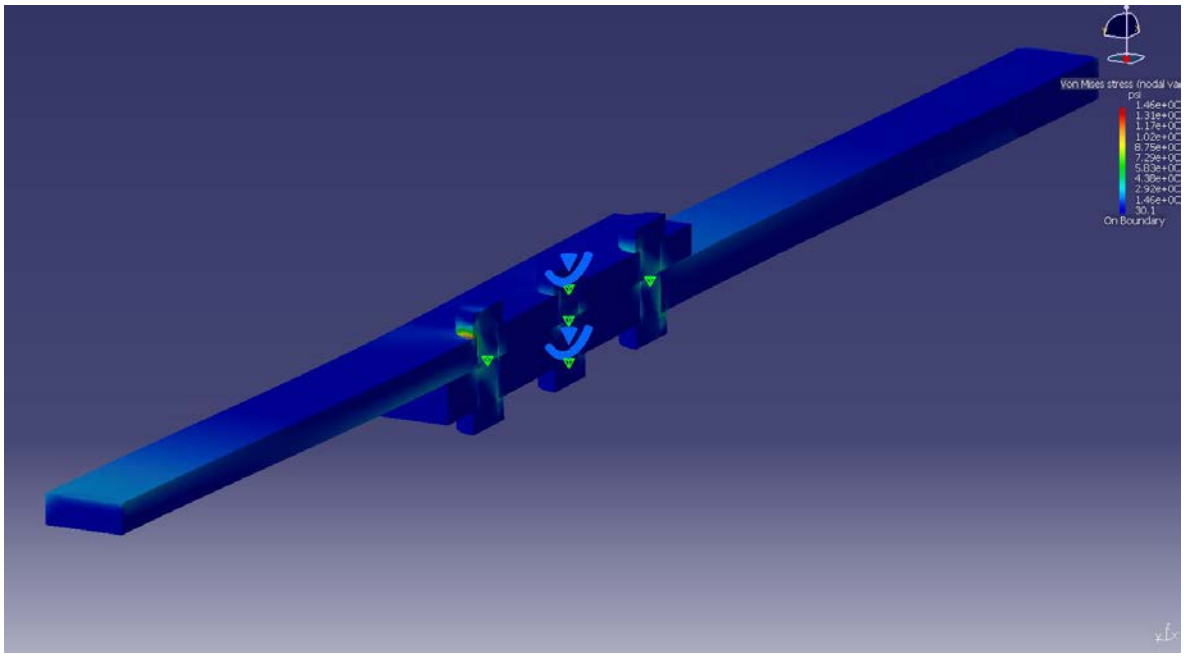

Figure 6.8: Three-bolt solid FE model, 0.1875-in x 0.25-in Al plates.

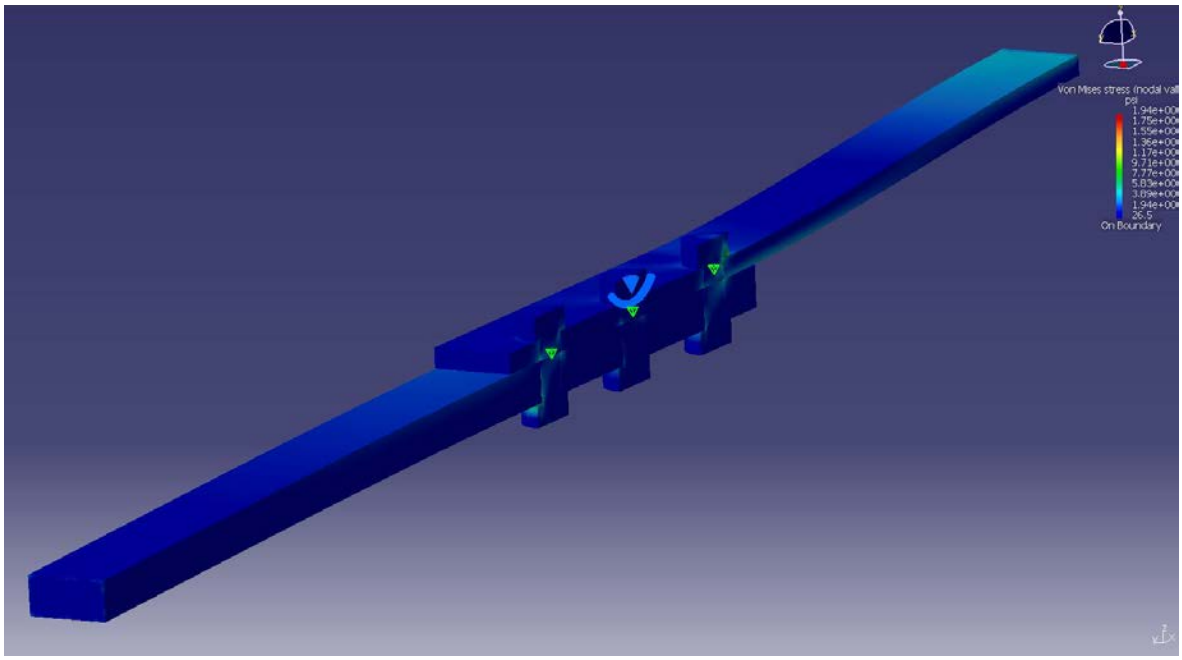

Figure 6.9: Three-bolt solid FE model, 0.125-in x 0.25-in Al plates.

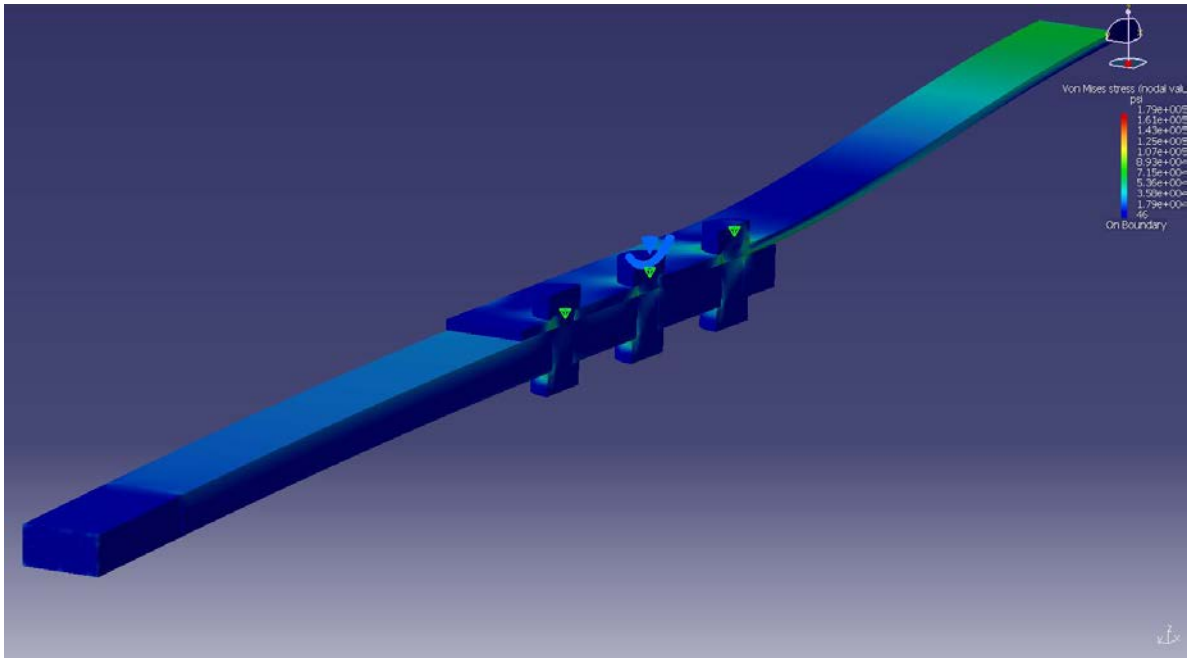

Figure 6.10: Three-bolt solid FE model, 0.0625-in x 0.25-in Al plates.

The loads that are seen in the three fasteners are symmetric, as shown in the second case study, meaning that the load of the leading fastener and the trailing fastener are the same. As an illustration, the loading between a plate of finite stiffness and a rigid one, shows that the leading fastener has the highest load, and the trailing fastener has the lowest load. Case Studies 3 and 4 reside between these two scenarios and show that the primary driver in load transfer is the stiffnesses of the plate materials and not necessarily the flexibility of the fasteners themselves. This trend is shown in Tables 6.7 and 6.8 and in Figures 6.11 and 6.12.

In the data shown here, all scenarios are loaded at 2,000 lbs and the plates are fastened with three 0.25-inch-diameter bolts. For the first columns of Tables 6.7 and 6.8, a 0.25-inch-thick aluminum plate is modeled, but the bolts are rigidly fastened. The columns in the two succeeding tables, Tables 6.8 and 6.9, show 0.25-inch-thick aluminum plates for both plate members. The third column in the tables start with both plates that are 0.25-inch thick, but one plate is modeled with aluminum, while the other plate is modeled with the stiffer steel. The

fourth and final columns have plates that are made of the same aluminum, but one of the plates is 0.25-inch thick, and the other plate is 0.0625-inch thick. Tables 6.7 and 6.8 illustrate the difference in loads when rigid body elements are incorporated. This is because rigid body elements effectively replace finite stiffness between joined plate material, which drives up load of the leading and trailing fasteners.

TABLE 6.7: CASE STUDIES 3 AND 4 SHEAR (WITHOUT RBE) (PLATE MODELS)

Bolt	rigid on one plate	same stiffness	diff mats	diff thck
1	927.5	762.25	825.5	806.03
2	620.66	475.51	503.5	394.93
3	443.84	762.25	671	799.04

TABLE 6.8: CASE STUDIES 3 AND 4 SHEAR (W ITH RBE) (PLATE MODELS)

Bolt	rigid on one plate	same stiffness	diff mats	diff thck
1	939.54	780.2	848.82	853.85
2	638.55	439.42	482.56	320.49
3	421.91	780.38	668.63	825.66

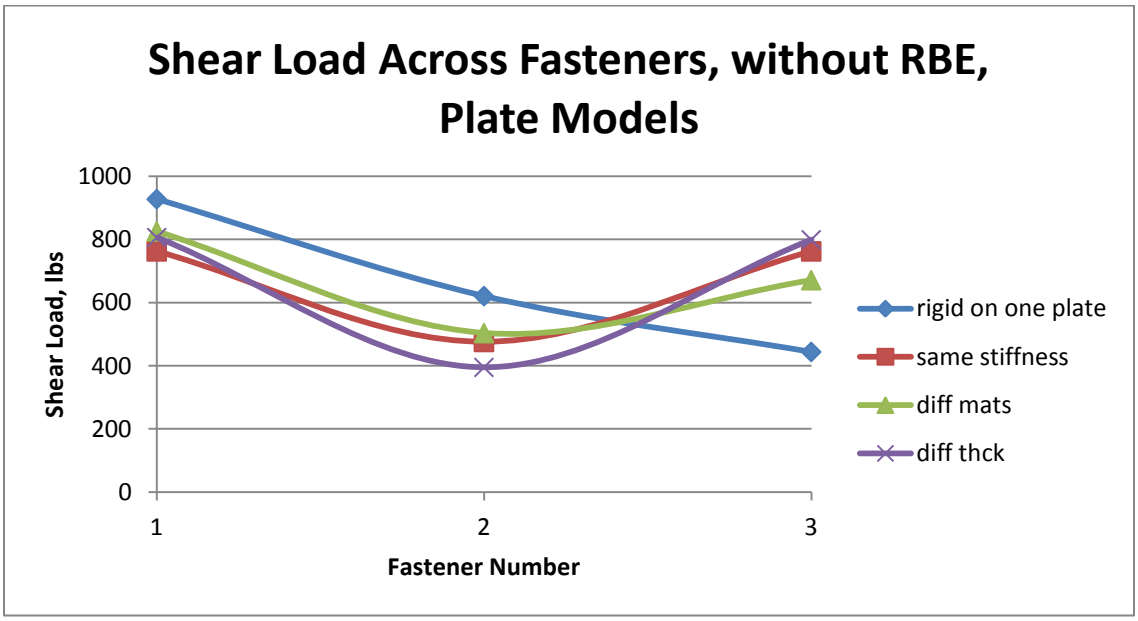

Figure 6.11: Shear load across fasteners without RBE.

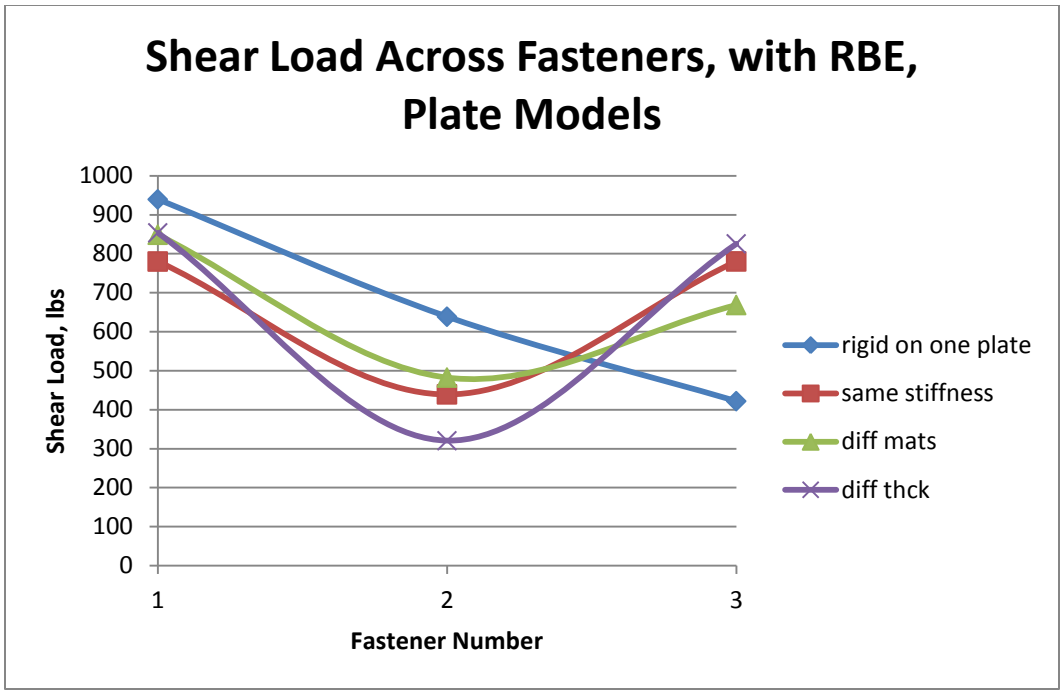

Figure 6.12: Shear load across fasteners with RBE.

Table 6.9 shows the shear results for Case Studies 3 and 4 with RBE. Figures 6.13 and 6.14 show the trends of load transfer between fasteners using the different modeling techniques. Despite the loading of the solid modeling output being considerably different from the rest of the models, the novel element follows the same trends between the traditional plate element modeling and the neutral line method utilizing Huth flexibility.

TABLE 6.9: CASE STUDY 2 COMPARED TO CASE STUDIES 3 AND 4 SHEAR (WITH RBE) (PLATE MODELS)

			Case Studies		
Al vs St		**1**	**2**	**3**	**4**
	Bolt	**rigid on one plate**	**same stiffness**	**diff mats**	**diff thck**
Plates	**1**	927.5	762.25	826.06	806.03
	2	620.66	475.51	504.11	394.93
	3	443.84	762.25	669.83	799.04
			Case Studies		
		1	**2**	**3**	**4**
	Bolt	**rigid on one plate**	**same stiffness**	**diff mats**	**diff thck**
Solids	**1**	900.380117	769.69	849.40	924.32
	2	602.5120468	461.19	440.91	298.44
	3	497.1078363	769.69	709.70	777.24
			Case Studies		
		1	**2**	**3**	**4**
	Bolt	**rigid on one plate**	**same stiffness**	**diff mats**	**diff thck**
Novel	**1**	851.318	766.35	846.70	973.01
	2	678.02	467.29	547.25	462.99
	3	470.02	766.35	606.05	563.98
			Case Studies		
		1	**2**	**3**	**4**
	Bolt	**rigid on one plate**	**same stiffness**	**diff mats**	**diff thck**
Huth	**1**	NA	695.25	808.71	749.51
	2	NA	609.49	616.81	631.83
	3	NA	695.25	574.49	618.66

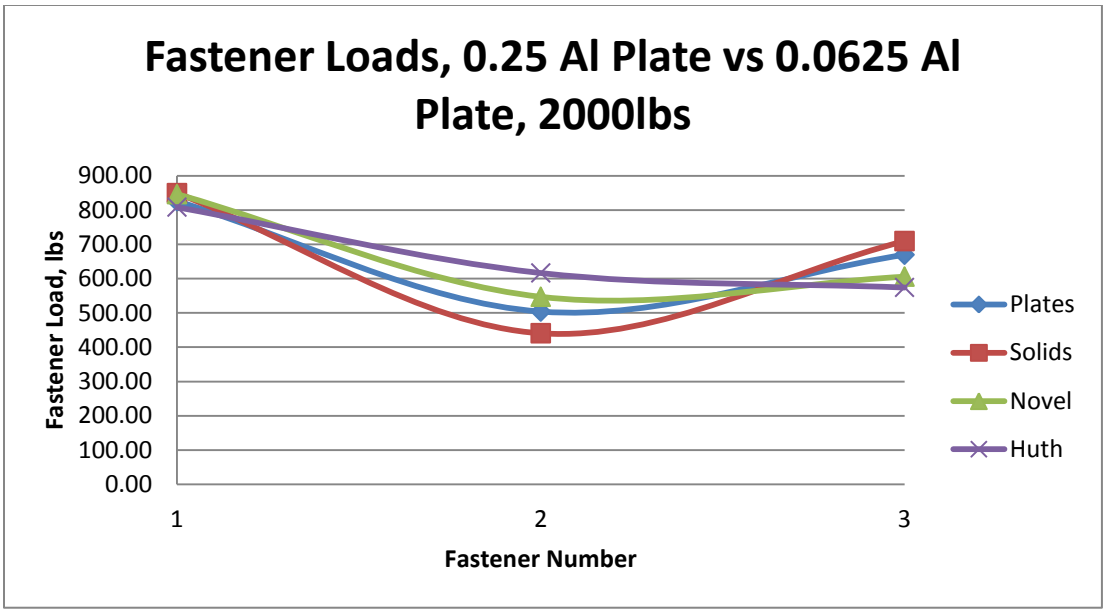

Figure 6.13: Shear loads for Case Study 3.

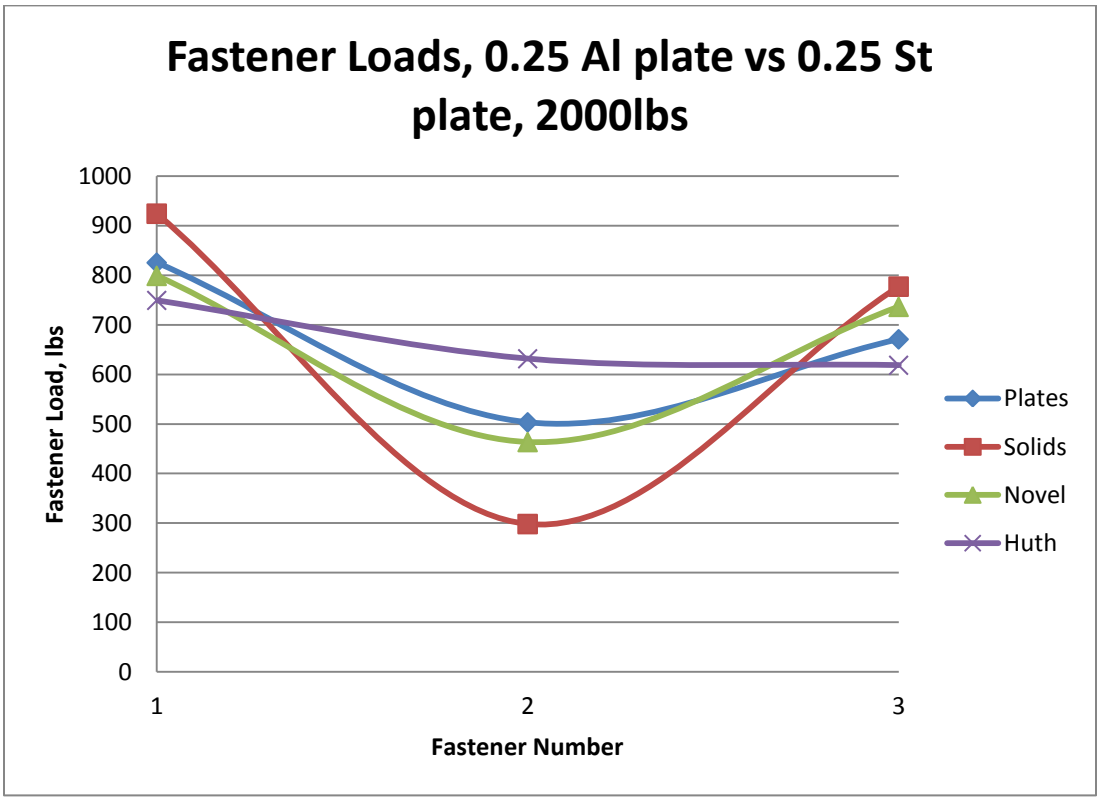

Figure 6.14: Shear loads for Case Study 4.

CHAPTER 7.

CONCLUSIONS, RECOMMENDATIONS, AND FURTHER STUDY

7.1 Conclusions

The scope of this research is to develop a simple, two-node linear finite element specifically tailored to model a fastener of a lap joint in tension and experiencing secondary bending. In the development, the novel finite element incorporates a contact stiffness into a consistent interpolation element utilizing a linearized version of Hertzian contact theory of two parallel cylinders.

Augmenting the traditional beam finite element codes with contact stiffness and assuming linearity of contact mechanics is feasible, and for fasteners that have a slenderness ratio of 0.5 or higher, this is desirable. For slenderness ratios that are high, the simple Timoshenko beam theory element overestimates the amount of deflection that actually occurs with the fastener. Adding in the contact stiffness using a linearized form of the Hertzian contact fits the deflection, which is evident in the solid finite element models that use a full nonlinear calculation. In order to linearize the Hertzian contact, which is actually a non-linear theory that models a non-linear phenomenon, the derived stiffness assumes only that the load applied is what would be required to achieve one-third of the far-field stress given a typical fastener spacing of four fastener diameters and two fastener diameters for edge distances. It was determined in Case Study 1 that there is little difference in contact stiffness, despite the value of the load used to derive it.

From the results of Case Study 2, the load transfer of the traditional finite elements shows little difference between the two baseline methods showcased; however, this novel finite element captures load transfer more closely resembling load transfers that are seen using the neutral line

model with Huth fastener stiffness. Case Studies 3 and 4 introduce the possibility that joined members do not have the same stiffnesses and allow for members to have different thicknesses and/or materials. The trends shown discount the accuracy of the solid finite element modeling, and while there are differences in actual loads between the traditional plate modeling methods, the neutral line model and the plate methods using the novel element all follow the same trends.

The new formulation follows a displacement that matches what is expected in the solid model finite element method, and the simple beam elements will result in less conservative loads. This novel finite element utilizes half of the linear stiffness derived from the Hertzian contact for each plate because the distributed load across the fastener is not constant across the plate member. This result offers another benefit. This finite element could be used to join multiple plates together, and only the end nodes would have half of the plate stiffness, while the inner plates would have the full measure of the plate stiffnesses applied to the fastener. For clevis joints and other joints involving more than two plates, it is possible to stack this novel element from end to end to generate the overall fastener, with no additional formulation.

7.2 Recommendations

For short fasteners, the traditional methods of beam and plate elements are sufficient in determining the deflection. The added complexity introduced in the novel finite element's stiffness matrix is especially advantageous for joints with thick plates.

The advantage of utilizing this novel finite element, regardless of the thickness of joined elements, is that the stiffness matrix now takes on the properties of the joined plate members and uses it for its element properties, not just the properties of the fastener itself. Traditional beam elements do not do this. The significance of this is that the stiffness matrix is no longer dependent on the actual distance between the two nodes that define its ends but, rather, the sum

of the thicknesses assigned to the plates it joins. This means that it does not matter what the distance between the joined members actually is in space, since it always assumes that the fastener's length is the sum of the thicknesses of the plates it joins, and since it is a joint, those plate members are assumed to be in contact anyway. This essentially makes the claim that the element assumes what a joint is and not a single element defining a shaft. This fact potentially frees up the time-consuming process of pulling mid-planes from solid model geometry and allows one to choose the outer faces of the solid models for generating the plate elements. This advantage was not originally foreseen in this research, but the time that it potentially saves in conditioning modeling for an FEM analysis cannot be underestimated. Designing other finite elements that are formulated in such a manner could present time savings in the preprocessing of a finite element analysis.

7.3 Areas for Further Research

What is learned from nearly any research project is that the research could continue ad infinitum. There is almost always something new that could be learned on a given topic, and this topic is no different.

The first thing that could be done to advance this course of study would be to introduce friction into the joint and transfer load in some way from one joined member to another that circumvents the novel beam element. In plate elements connected by beam elements, there is no actual interface between the plate elements that allows for load to transfer in that route. One possible method to address this would be to make loads that pass through the fastener and loads that pass through the plates add to the force that actually goes through the beam finite element, making the actual loads a "recovered parameter," not necessarily a directly determined value. The ratio of plate transfer loads to fastener loads could be determined by assuming the stiffness

of the coned annulus assumed by Shigley and Mischke (1988) and Wileman et al. (1991) for joint stiffness (see Figure 2.3) of the plate when it undergoes load transfer. How else to accomplish this load transfer is presently not clear.

In addition, this novel element has uncoupled tensile loading and transverse loading of the fastener, which is similar to traditional beam elements. This research found that fasteners are made to trade off additional pre-load to allow more transverse load to pass the joint altogether and transfer via the plates. This fact could mean coupling the tensile loading equations and the bending equations together in the finite element modeling.

The scope of this research is to develop a singular element with two nodes. Modification to the plate elements is beyond the scope of this research, but it is clear to the author that modification of the plate elements, or modeling rigid body elements as spiders on the end of these novel elements, and then connecting them to circular boundaries of mating holes in the plates, is warranted, if it is desired to see the stress distribution around the hole. However, rigid body elements do not typically provide an accurate picture of that contact stress of the hole, and rigid elements tend to increase the shear loads of leading and trailing bolts.

The addition of existing elements is beyond the central scope of this research, as was seen in the various methods used in combining elements together in Chapter 2 and also seen in Appendix F. What the singular element would look like in connecting hole to hole is not presently clear. Fortunately, many fastener standards post maximum shear loads and not necessarily the maximum stresses as the limiting factor for the joint.

Also with the restriction that the novel element contains only two nodes, there was no addition of stiffness to the fastener due to the existence of the fastener head or nut. The novel element assumed that the contact between the fastener element and the head was rigid.

Using Hertzian contact theory for cylinders in parallel has a limitation that the hole and the shaft diameter cannot be the same. Using Huth fastener stiffness is a solution that has been used to model Hi-Lok^{TM} fasteners. However, using this for fastener stiffness has no direct relationship for fastener diameters. One distinct advantage to adding the term that is incorporated into the shear equations of the Timoshenko beam element is that Hertzian contact fastener stiffness could be readily replaced by other contact models, such as the empirical models discussed in the literature research, including Huth flexibility, or other theoretical contact models.

This research is primarily interested in the shear of fasteners in lap joints in secondary bending. Research could continue by working on the primary bending of the fastener. It is interesting to note that in primary bending, there is considerably more interaction between the plate members. Incorporating this into the novel fastener element would be extremely challenging.

Although this research is limited to static loading, dynamic loading and vibration seems like a normal progressive step in the study. One possible hurdle in using this element in vibration or dynamics is the departure from the assumption used in formulation of the Hertzian contact theory that the two bodies involved in the contact are in static equilibrium. One may be compelled to show the effect of departing from this assumption to accommodate the different types of loading.

BIBLIOGRAPHY

BIBLIOGRAPHY

Akoz, A.Y., and Kadioglu, F. (1996) "The Mixed Finite Element Solution of Circular Beam on Elastic Foundation," *Computers and Structures*, Vol. 60, No. 4, pp. 643–651.

Alkatan, F., Stephan, P., Daidie, A., and Guillot, J. (2007) "Equivalent Axial Stiffness of Various Components in Bolted Joints Subjected to Axial Loading," *Finite Elements in Analysis and Design*, Vol. 43, pp. 589–598.

Allen, D., and Haisler, W. (1985) *Introduction to Aerospace Structural Analysis*. John Wiley and Sons, Inc.

Astley, R. J. (1992) *Finite Elements in Solids and Structures*, *an Introduction*. Chapman and Hall, London.

Atkin, R. J., and Fox, N. (1980) *An Introduction to the Theory of Elasticity*.Dover Publications, New York.

Averill, R., and Reddy, J. N. (1989) "Behaviour of Plate Elements Based on the First-Order Shear Deformation Theory," *Engineering Computations*, Vol. 7, Iss. 1, pp. 57–74.

Barber, J. R. (1983) "The Solution of Elasticity Problems for the Half-Space by the Method of Green and Collins," *Journal Applied Scientific Research*, Vol. 40, pp. 135–157.

Barrios, W. (1978) "Stresses and Displacements Due to Load Transfer by Fasteners in Structural Assemblies," *Engineering Fracture Mechanics*, Vol. 10, pp. 115–176.

Bathe, K. J., and Dvorkin, E. (1985) "A Four-Node Plate Bending Element Based on Mindlin/Reissner Plate Theory and a Mixed Interpolation," *International Journal for Numerical Methods in Engineering*, Vol. 21, pp. 367–383.

Bathe, K. J., and Dvorkin, E. (1986) "A Formulation of General Shell Elements—The Use of Mixed Interpolation of Tensorial Components," *International Journal for Numerical Methods in Engineering*, Vol. 22, pp. 697–722.

Batoz, J. L., Zheng, C., and Hammadi, F. (2001) "Formulation and Evaluation of New Triangular, Quadrilateral, Pentagonal, and Hexagonal Discrete Kirchoff Plate/Shell Elements," *International Journal for Numerical Methods in Engineering*, Vol. 52, pp. 615–630.

Bickley, W. G. (1928) "The Distribution of Stress Round a Circular Hole in a Plate," *Philosophical Transactions of the Royal Society*, Vol. 227, No. 647-658, pp. 383–415.

Bower, A. (2010) *Applied Mechanics of Solids*. CRC Press, Boca Raton, FL.

Brewer, Brett A. (2012) "Simplified Modeling Methods for Mechanically Fastened Connections in Flight Structures." Thesis. Department of Structural Engineering, University of California, San Diego.

Chaktari, J., Daidie, A., Chaib, Z. and Guillot, J. (2008) "Numerical Model for Two-Bolted Joints Subjected to Compressive Loading," *Finite Elements in Analysis and Design*, Vol. 44, Iss. 4, pp. 162–173.

Chamis, C., and Murthy, P. (1991) "Simplified Procedures for Designing Composite Bolted Joints," *Journal of Reinforced Plastics and Composites*, Vol. 10, No. 1, pp. 29–41.

Chang, F. K., Scott, R., and Springer, G. (1982) "Strength of Mechanically Fastened Composite Joints," *Journal of Composite Structures*, Vol. 16, pp. 470–494.

Chao, P. C., and Pagano, N. J. (1992) *Elasticity*, *Tensor*, *Dyadic*, *and Engineering Approaches*. Dover Publications, New York.

Ciavarella, M., Baldini, A. Barber, J., and Strozzi, A. (2006) "Reduced Dependence on Loading Parameters in Almost Conforming Contacts" *Internal Journal of Mechanical Sciences*, Vol. 48, Iss. 9, pp. 917–925.

Cope, D., and Lacy, T. (2004) "Modeling Mechanical Fasteners in Single-Shear Lap Joints," *Journal of Aircraft*, Vol. 41, pp. 1491–1497.

Crews, J., and Naik, RA. (1987) "Bearing-Bypass Loading on Bolted Composite Joints." NASA Technical Memorandum.

Dabke, P., Prabhakar, V., and Sheppard, S. (1994) "Using Features to Support Finite Element Idealizations." Center for Design Research, Stanford University.

de Rijck, R. (2005) *Stress Analysis of Fatigue Cracks in Mechanically Fastened Joints*. Ph.D. Dissertation. Delft University Press, The Netherlands.

de Rijck, J. J. M., and Fawaz, S. (2000) "A Simplified Approach for Stress Analysis of Mechanically Fastened Joints." SAFE Engineering, Inc.

De Jong, Th. (1977) "Stresses Around a Pin-Loaded Hole in an Elastically Orthotropic or Isotropic Plate," *Journal of Composite Materials*, Vol. 11, No. 3, pp. 313–331.

Ekh, Johan. (2006) "Multi-Fastener Single-Lap Joints in Composite Structures." Doctoral Thesis. Department of Aeronautical and Vehicle Engineering, Royal Institute of Technology, Stockholm, Sweden.

Ekh J., and Schon, J, (2005) "Effect of Secondary Bending on Strength Prediction of Composite, Single Shear Lap Joints," *Composites Science and Technology*, Vol. 65, Iss. 6, pp. 953–965.

Ekh J., and Schon, J., (2008a) "Load Transfer in Multirow, Single Shear, Composite-to-Aluminum Lap Joints," *Composites Science and Technology*, Vol. 66, Iss. 7-8, pp. 875–885.

Ekh J., and Schon, J., (2008b) "Finite Element Modeling and Optimization of Load Transfer in Multi-Fastener Joints Using Structural Elements," *Composite Structures*, Vol. 82, Iss. 2, pp 245–256

Ekh J., Schon, J, and Melin, L. (2005) "Secondary Bending in Multi Fastener, Composite-to-Aluminum Single Shear Lap Joints," *Composites Part B: Engineering*, Vol. 36, Iss. 3, pp. 195–208.

Felippa, Carlos, PhD, (1998) "Introduction to Finite Element Methods," University Course Materials, ASEN 5007, University of Colorado.

Gokhale, N. S., Deshpande, S. S., Bedekar, S.V., and Thite, A.N. (2008) *Practical Finite Element Analysis*. Finite to Infinite, Ltd., Pune, India.

Gong, K. (2000) "Bending Theories for Beams and Plates with Single Generalized Displacement," *Applied Mathematics and Mechanics*, Vol. 21, pp. 1091–1098.

Grant, F., Rouch, P., Louf, F., and Champaney, L. (2011) "Definition and Updating of Simplified Models of Joint Stiffness," *International Journal of Solids and Structures*, Vol. 48, pp. 775–784.

Green R., and McCauley, C. J., Editors. (1996) *Machinery's Handbook*. 25th ed. Industrial Press, Inc.

Greenhill, L. M., Bickford, W., and Nelson, H. (1985) "A Conical Beam Finite Element for Rotor Dynamics Analysis," *Journal of Vibration*, *Acoustics*, *Stress*, *and Reliability in Design*, Vol. 107, pp. 421–430.

Gruttmann, F., and Wagner, W. (2001) "Shear Correction Factors in Timoshenko's Beam Theory for Arbitrary Shaped Cross-Sections," *Computational Mechanics*, Vol. 27, No. 3, pp. 199–207.

Haidar, N., Obeed, S., and Jawad, M. (2011) "Mathematical Representation of Bolted-Joint Stiffness: A New Suggested Model," *Journal of Mechanical Science and Technology*, Vol. 25, pp. 2827–2834.

Henson, G., and Hornish, B. A. (2010) "An Evaluation of Common Analysis Methods for Bolted Joints in Launch Vehicles." *AIAA Structures*, *Structural Dynamics and Materials Conference*, Orlando, FL, April 12–15.

Hertz, H., (1882) "Über die berührung fester elastischer Körper (About the non-slip elastic body)." In *Gesammelte Werke (Collected Works)*, Vol. 1, Springer, Leipzig, Germany.

Hsu, Allan. (2011) "Realistic Simulation of Thick Composite Bolted Joints: A Novel NASTRAN Method." SAMPE 2011 Fall Technical Conference, Fort Worth, TX, October 17–20.

Hughes, T. J. R. (2000) *The Finite Element Method*, *Linear Static and Dynamic Finite Element Analysis*. Dover Publications, New York.

Huth, H. (1986) "Influence of Fastener Flexibility on the Prediction of Load Transfer and Fatigue Life for Multiple-Row Joints." In *Fatigue in Mechanically Fastened Joints*, J. M. Potter, ed., pp. 221–250. A symposium sponsored by ASTM Committee E-9 on Fatigue, Charleston, SC, March 18–19, 1985. Library of Congress Cataloging-in-Publication Data, ASTM Special Technical Publication 927.

Hyer, M. W. (1987) "The Effects of Pin Elasticity, Clearance and Friction on the Stresses in a Pin-Loaded Orthotropic Plate," *Journal of Composite Materials*, Vol. 21, pp. 190–206.

Hyer, M. W., and Klang, E. C. (1985) "Stresses Around Holes in Pin-Loaded Orthotropic Plates," *Journal of Aircraft*, Vol. 22, pp. 1099–1101.
Iancu, F., Ding, X, Cloud, G. L., and Raju, B. (2004) "Three-Dimensional Investigation of Thick Single-Lap Bolted Joints," *Journal of Experimental Mechanics*, Vol. 4, pp. 351–358.

Ireman, Thomas. (1999) "Design of Composite Structures Containing Bolt Holes and Open Holes." Department of Aeronautics, Kungliga Tekniska Hogskolan, Stockholm, Sweden.

Ito, Y., Toyoda, J. and Nagata, S., (1977) "Interface Pressure Distribution in a Bolt-Flange Assembly." ASME Paper No. 77-WA/DE-11.

Keshavanarayana, S., Smith, B., Gomez, C., Caido, F., Shiao, M., and Nuss, M. (2010) "Fatigue-Based Severity Factors for Shear-Loaded Fastener Joints," *Journal of Aircraft*, Vol. 7, No. 1, pp. 181–191.

Kim, J., Yoon, Joo-C., and Kang, B. (2007) "Finite element Analysis and Modeling of Structure with Bolted Joints," *Applied Mathematical Modeling*, Vol. 31, pp. 895–911.

Kouhia, R. (2000) "On Stabilized Finite Element Methods for the Reissner-Mindlin Plate Model," *International Journal for Numerical Methods in Engineering*, Vol. 00, pp. 1–13.

Kradinov, V., Barut, A., and Madenci, E. (2000) "Bolted Double Lap Composite Joints Under Mechanical and Thermal Loading." Final Report of NASA Agreement No. NAG-1-2052.

Kradinov, V., Madenci, E., and Ambur, D. R. (2004) "Combined In-Plane and Through-the-Thickness Analysis for Failure Prediction of Bolted Composite Joints." 45rd AIAA/ASME/ ASCE/AHS/ASC Structures, Structural Dynamics, and Materials Conference, Palm Springs, California, April. Paper No. 2004-1703.

Kratochivil, J, and Becker, W. (2010) "Structural Analysis of Composite Bolted Joints Using the Complex Potential Method," *Composite Structures*, Vol. 92, pp. 2512–2516.

Landau, L., and Lifshitz, E. (1959) *Theory of Elasticity*. Pergamon, London.

Lee, M.-Z. (2010a) "Structural Properties of Bolted Joints." *Machine Design* website, February 17. http://machinedesign.com/archive/structural-properties-bolted-joints.

Lee, M.-Z. (2010b) "How External Loads Affect Bolted Joints." *Machine Design* website, April 20. http://machinedesign.com/archive/how-external-loads-affect-bolted-joints.

Lee, M.-Z. (2010c) "A Simpler Way to Predict Bolt Preload." *Machine Design* website, April 19. http://machinedesign.com/news/simpler-way-predict-bolt-preload.

Lee, M.-Z. (2010d) "Modeling the Effects of Bolt Preload." *Machine Design* website, September 9. http://machinedesign.com/fasteners/modeling-effects-bolt-preload.

Lee, M.-Z. (2010e). "How Internal Loads Affect Bolt Preload." *Machine Design* website, November 5. http://machinedesign.com/fasteners/how-internal-loads-affect-bolt-preload.

Lekhnitski, S. G. (1981) *Theory of Elasticity of an Anisotropic Body*, Mir Publishers, Moscow, Russia.

Logan, D. (2011) *A First Course in the Finite Element Method*. 5th ed. Cengage Learning.

Love, A. (1982) *A Treatise on the Mathematical Theory of Elasticity*, Cambridge University Press.

Lubkin, J. (1962) "Contact Problems." In *Handbook of Engineering Mechanics*, ed.W. Flugge. McGraw-Hill, New York.

MacNeal, R. (1982) "Derivation of Element Stiffness Matrices by Assumed Strain Distributions," *Nuclear Engineering and Design*, Vol. 70, pp. 3–12.

MacNeal, R. (1976) “A Simple Quadrilateral Shell Element,” *Computers and Structures*, Vol. 8, pp. 175–183.

Madenci, E., Shkarayev, S., and Sergeev, B. (1998) “Analysis of Composite Laminates with Multiple Fasteners,” *International Journal of Solids Structures*, Vol. 35, No. 15, pp. 1793–1811.

McCarthy, C. T., and McCarthy, M. A. (2005) “Three-Dimensional Finite Element Analysis of Single-Bolt, Single-Lap, Composite Bolted Joints: Part II—Effects of Bolt-Hole Clearance,” *Composite Structures*, Vol. 71, No. 2, pp. 159–175.
McCarthy, M., McCarthy, C., Lawlor, V., and Stanley, W. (2005) “Three-Dimensional Finite Element Analysis of Single-Bolt, Single-Lap, Composite Bolted Joints: Part I-Model Development and Validation,” *Composite Structures*, Vol. 71, pp. 140–158.

MIL-HDBK-60. (1990) Military Handbook: Threaded Fasteners—Tightening to Proper Tension.

Mundo, D., Hadjit, R., Donders, S. Brughmans, M., Mas, P., and Desmet, W. (2009) “Simplified Modeling of Joints and Beam-Like Structures for BIW Optimization in a Phase of the Vehicle Design Process,” *Finite Elements in Analysis and Design*, Vol. 45, pp. 456–462.

Murty, A.V.K, (1984) “Toward a Consistent Beam Theory,” *AIAA Journal*, Vol. 22, No. 6, pp. 811–816.

Musto, J., and Konkle, N.. (2006) “Computation of Member Stiffness in the Design of Bolted Joints,” *Journal of Mechanical Design*, Vol. 128, pp. 1357–1360.

Oden, J.T. (2006) *Finite Elements of Nonlinear Continua*. Dover Publications, New York.

Ojalvo, I. U., and Pilon, D. (1987) “Assumptions and Accuracies Associated with the MSC/NASTRAN Rod, Bar and Quad4 Elements.” MSC World User’s Conference, Los Angeles, CA, March 1987.

Osgood, C. C., (1979) “Saving Weights on Bolted Joints,” *Machine Design*, Vol. 51, pp. 128–133.

Oterkus, E., Barut, A., and Madenci, E. (2007) “Analysis of Bolted-Bonded Composite Lap Joints.” AIAA Conference, Honolulu, HI, April 2007. AIAA 2007-2187.

Oterkus, E., Madenci, E., and Ambur, D. (2006) “Validated Analysis Method for Bolted Composite Lap Joints.” AIAA Conference, Newport, RI, May 2006. AIAA 2006-2270.

Park, H. J., Lee, B., and Im, S. (1999) “Contact Analysis of Mechanically Fastened Joints in Composite Laminates Based on Layerwise Theory,” *Computer Modeling and Simulation in Engineering*, Vol. 4, pp. 19–28.

Paroissien, E., Sartor, M., Huet, J., and Lachaud, F. (2006) "Hybrid (Bolted/Bonded) Joints Applied to Aeronautic Parts: Analytical Two-Dimensional Model of a Single-Lap Joint." AIAA Structures Conference, Newport, RI, May, 2006. AIAA 2006-2268.

Paroissien, E., Sartor, M., Huet, J., and Lachaud, F. (2007) "Analytical Two-Dimensional Model of a Hybrid (Bolted/Bonded) Single-Lap Joint," *Journal of Aircraft*, Vol. 44, No. 2, pp. 573–579.
Pedersen, N. L., and Pedersen, P. (2008a) "On Prestress Stiffness Analysis of Bolt-Plate Contact Assemblies," *Archive of Applied Mechanics*, Vol. 78, Iss. 2, pp. 75–88.

Pedersen, N. L., and Pedersen, P. (2008b) "Stiffness Analysis and Improvement of Bolt-Plate Contact Assemblies," *Archive of Applied Mechanics*, Vol. 78, Iss. 2, pp. 47–66.

Pedersen N. L., and Pedersen, P. (2009) "Bolt-Plate Contact Assemblies with Prestress and External Loads: Solved with Super Element Technique," *Computers and Structures*, pp. 1374–1383.

Peterson, R. E. (1974) *Stress Concentration Factors*. John Wiley & Sons, New York.

Pickhaver, J. (2006) "Numerical Modeling of Building Response to Tunneling." Ph.D. Thesis. Balliol College, Oxford University.

Pietrobon-Costa, F. (2008) "On Timoshenko's Beams Coefficient of Sensibility to Shear Effect," *Trends in Applied and Computation Mathematics*, Vol. 9, No. 3, pp. 447–457.

Prathap, G., and Bhashyam, G. (1982) "Reduced Integration and the Shear-Flexible Beam Element," *International Journal for Numerical Methods in Engineering*, Vol. 18, pp. 195–210.

Pratt, B. (2008) "An Assessment of Least Squares Finite Element Models with Applications to Problems in Heat Transfer and Solid Mechanics." Thesis. Texas A&M University.

Prescott, J. (1924) *Applied Elasticity*. Longmans Green, London.

Puttock, M. J., and Thwaite, E. G. (1969) "Elastic Compression of Spheres and Cylinders at Point and Line Contact." National Standards Laboratory Technical Paper No. 25. Commonwealth Scientific and Industrial Research Organization, Australia, Melbourne.

Reddy, J. N. (1997) "On Locking—Free Shear Deformable Beam Finite Elements," *Computer Methods in Applied Mechanics and Engineering*, Vol. 149, pp. 113–132.

Pratt, B. (2008) "An Assessment of Least Squares Finite Element Models with Applications to Problems in Heat Transfer and Solid Mechanics." Thesis. Texas A&M University.

Reddy, J. N. (2007) *Theory and Analysis of Elastic Plates and Shells*. 2nd edition. CRC Press, Boca Raton, FL.

Reddy, J. N. (2008) *An Introduction to Continuum Mechanics with Applications*. Cambridge, University Press.
Reid, J., and Hiser, N. (2005) "Detailed Modeling of Bolted Joints with Slippage," *Finite Elements in Analysis and Design*, Vol. 41, pp. 547–562.

Reismann, H., and Pawlik, P. (1980) *Elasticity*, *Theory and Applications*. John Wiley & Sons, New York.

Renton, J. (2002) *Elastic Beams and Frames*. 2nd Edition. Horwood Publishing, Chichester, England.

Riley, W., and Zachary, L. (1989) *Introduction to Mechanics of Materials*. Wiley, New York.

Rötscher, F. (1927) *Die Maschienenelemente*. Springer, Berlin.

Rosenfeld, S. J. (1947) "Analytical and Experimental Investigation of Bolted Joints." National Advisory Committee for Aeronautics. Technical Note 1458.

Rosinger, H. E. and Ritchie, I. G. (1977) "On Timoshenko's Correction for Shear in Vibrating Isotropic Beams," *Applied Physics*, Vol. 10, pp. 1461–1466.

Ross, C. (1977) "Studies on the Failure of Metal Mechanical Joints Subjected to Dynamic Loads." Air Force Office of Scientific Research, Report Number AFOSR-TR-78-0078.

Rutman, A., and Bales-Kogan, J. (2006) "Multi-Spring Representation of Fasteners for MSC/Nastran Modeling." Boeing Commercial Airplane Group.

Rutman, A., Boshers, C., Pearce, L., and Parady, J. (2007) "Fastener Modeling for Joining Parts Modeled by Shell and Solid Elements." 2007 Americas Virtual Product Development Conference, October 11–12, Detroit, MI.

Rutman, A., Vilsoreanu, A., and Parady Jr., J. (2000) "Fastners [sic] Modeling for MSC.Nastran Finite Element Analysis." 2000 World Aviation Conference, San Diego, CA, October 10–12. AIAA 2000-01-5585.

Schijve, J. (2009) "Fatigue Damage in Aircraft Structures, Not Wanted, But Tolerated?," *International Journal of Fatigue*, Vol. 31, pp. 1111–1123.

Shtaerman, I. (1949) “Kontaktnaya zadacha teorii uprugosti” (Contact Problem of Theory of Elasticity). Gostekhizdat, Moscow.

Shashishihar, A. (2005) “Finite Element and Analytical Models for Load Transfer Calculations in Mechanically Fastened Aluminum/Composite Hybrid Joints.” Master’s Thesis. Wichita State University.

Shigley, J., and Mischke, C. (1988) *Mechanical Engineering Design*. 5th edition. McGraw Hill, New York.

Shivaswamy, S. (2010) *Finite Element Analysis and Programming*, *An Introduction*. Narosa Publishing House, New Delhi.

Soltis, L., and Wilkenson, T. (1987) “Bolted-Connection Design.” United States Department of Agriculture, Forest Service. General Technical Report FPL-GTR-54.

Swift, T., (1971) “Development of the Fail-Safe Design Features of the DC-10.” *Damage Tolerance in Aircraft Structures*. ASTM STP 486.

Taiebat, H. (2001) “Three-Dimensional Non-Conforming Elements.” Department of Civil Engineering, Centre for Geotechnical Research, University of Sydney. Research Report No. R808.

Tate, M. B., and Rosenfeld, S. J. (1946) “Preliminary Investigation of the Loads Carried by Individual Bolts in Bolted Joints.” NACA TN 1051.

Tessler, A. (1989) “A Higher-Order Plate Theory with Ideal Finite Element Suitability.” U.S. Army Materials Technology Laboratory. Report MTL TR 89-85.

Tessler, A. (1991) “A Computationally Attractive Beam Theory Accounting for Transverse Shear and Normal Deformations.” U.S. Army Materials Technology Laboratory. Report MTL TR 91-4.

Theocaris, P. S. (1956) “The Stress Distribution in a Strip Loaded in Tension by Means of a Central Pin,” *Journal of Applied Mechanics*, Vol. 23, No. 1, pp. 85–90.

Timoshenko, S. P. (1921) “On the Correction Factor for Shear of the Differential Equation for Transverse Vibrations of Bars of Uniform Cross-Section,” *Philosophical Magazine*. Vol. 41, pp. 744–746.

Timoshenko, S. P., and Goodier, J. N. (1970) *Theory of Elasticity*. 3rd edition. McGraw Hill, New York.

Wileman, J., Choudhury, M., and Green, M. (1991) "Computation of Member Stiffness in Bolted Connections," *Journal of Mechanical Design*, Vol. 113, pp. 432–437.

Young, W. ed. (2011) *Roark's Formulas for Stress and Strain*. 8th edition. McGraw-Hill, New York.

Yunus, Mohd Azmi. (2011) "Finite Element Modelling and Updating of Structure of Sheet Metal with Bolted and Welded Joints." Doctoral Thesis. University of Liverpool.

Zeinkiewicz, O. C. , and Morgan, K. (1983) *Finite Elements and Approximation*. 5th edition. McGraw Hill, New York.

Zeinkiewicz, O. C., and Taylor, R. L. (2000) *Finite Element Method*. 5th edition. McGraw Hill, New York.

Zhang, O., and Poirier, J. (2004) "New Analytical Model of Bolted Joints," *Journal of Mechanical Design*, Vol. 126, pp. 721–728.

APPENDICES

APPENDIX A

AN ALTERNATIVE DERIVATION

The starting point in the development is the introduction of the consistent interpolation element (CIE-1) of the Timoshenko beam theory. The element utilizes two sets of Lagrangian shape functions—one set to capture the transverse deflection using three nodes (quadratic) and the other to capture the rotation and shear term (denoted by S) using two nodes. The simplest 1D beam element can be defined across two nodes. In order to utilize quadratic shape functions, the finite element must have an additional node located between the two end nodes. For purposes of this application, the center node is located along the shaft of the element where the joined plates contact each other at the plate interface. If both joined plates have the same thickness, then the central node is located at the midpoint of the element.

As mentioned previously, typical commercial finite elements utilize the reduced integration element (RIE) for beam elements. The choice in using the simpler CIE-1, is that it has the advantage of uniquely having a singular node that can be chosen to locate the interface of the plate elements. The RIE element, however, has first-order shape functions for displacement and first-order shape functions for rotation. In the case of CIE-2 (IIE), the shape functions are third order in displacement and second order in rotation. For CIE-2, this means that there are three additional nodes, one that is usually located at the center but governs rotation only. This fact does not help here since foundational stiffness, c_f, is affected by displacement only, and the other two nodes govern displacement, neither of which would be placed at the interface of the joined plate elements being modeled.

Equations (A.1) to (A.5) illustrate the terms of the stiffness matrix for the general formulation of the Timoshenko beam element. Commercial codes do not include contact

stiffnesses, c_c, shown in the first stiffness term, K^{11}. This indicates that the element is insensitive to the effect of the plate elements on the fastener that is being modeled when using typical commercial FEM codes. The contact stiffnesses for the contact between the first plate and the fastener and between the second plate and the fastener, are c_{c1} and c_{c2}, respectively.

$$\begin{bmatrix} [K^{11}] & [K^{12}] \\ [K^{21}] & [K^{22}] \end{bmatrix} \begin{Bmatrix} \{W\} \\ \{S\} \end{Bmatrix} = \begin{Bmatrix} \{Q^1\} \\ \{Q^2\} \end{Bmatrix} \tag{A.1}$$

$$K_{ij}^{11} = \int_0^h GAKs \frac{d\Psi i}{dx} \frac{d\Psi j}{dx} dx + \int_0^{ah} Cc_1 \Psi i \Psi j \, dx + \int_{ah}^h Cc_2 \, \Psi i \Psi j dx \tag{A.2}$$

$$K_{ij}^{12} = K_{ij}^{21} = \int_0^h GAKs \frac{d\Psi i}{dx} \Psi j dx \tag{A.3}$$

$$K_{ij}^{22} = \int_0^h EI \frac{d\Psi i}{dx} \frac{d\Psi j}{dx} + GAK_s \Psi i \Psi j dx \tag{A.4}$$

$$F_i^1 = \int_0^h q\Psi \, dx \tag{A.5}$$

The equations used for the shape functions are quadratic for displacement and linear for rotation using the CIE-1 element, and since a general finite element that may join different plate elements together is being developed, thus placing the central node as the plate interface, this element is uniquely tailored to implement different foundational stiffnesses across a singular element. Since the foundational stiffness is not necessarily continuous along the element, it is necessary to handle the integration of the K^{11} term with some care.

Shape Functions

Quadratic shape functions used for deflection are

$$\Psi_1(\mathrm{x})^{(1)} = \left(1 - \frac{\mathrm{x}}{\mathrm{h}}\right)\left(1 - \frac{\mathrm{x}}{\alpha \mathrm{h}}\right) \tag{A.6}$$

$$\Psi_2(\mathrm{x})^{(1)} = \left(\frac{1}{(\alpha - \alpha^2)} \frac{\mathrm{x}}{\mathrm{h}}\right)\left(1 - \frac{\mathrm{x}}{\mathrm{h}}\right) \tag{A.7}$$

$$\Psi_3(\mathrm{x})^{(1)} = -\left(\frac{\alpha}{(1-\alpha)} \frac{\mathrm{x}}{\mathrm{h}}\right)\left(1 - \frac{\mathrm{x}}{\alpha \mathrm{h}}\right) \tag{A.8}$$

Linear shape functions used for rotation are

$$\Psi_1(x)^{(2)} = \left(1 - \frac{x}{h}\right) \tag{A.8}$$

$$\Psi_1(x)^{(2)} = \frac{x}{h} \tag{A.9}$$

Stiffness Formulation

In order to properly handle the discontinuity in the foundational stiffnesses, a piecewise integration for the K11 term must be utilized. That term becomes

$$K_{ij}^{11} = \int_0^h GAK_s \frac{d\Psi_i(x)^{(1)}}{dx} \frac{d\Psi_j(x)^{(1)}}{dx} dx + \int_0^{\alpha h} c_{f1} \Psi_i(x)^{(1)} \Psi_j(x)^{(1)} dx$$

$$+ \int_{\alpha h}^h c_{f2} \Psi_i(x)^{(1)} \Psi_j(x)^{(1)} dx \tag{A.10}$$

With a three-node element covering w_1, w_c, and w_2, the K^{11} term is described by a 3 x 3 matrix.

When the values of the matrix have a single, constant foundational stiffness and equal plate thicknesses, the K^{11} term becomes

$$K^{11} = \frac{GAKs}{3h} \begin{bmatrix} 7 & -8 & 1 \\ -8 & 16 & -8 \\ 1 & -8 & 7 \end{bmatrix} + \frac{c_f h}{30} \begin{bmatrix} 4 & 2 & -1 \\ 2 & 16 & 2 \\ -1 & 2 & 4 \end{bmatrix} \tag{A.11}$$

Assuming that the joined plate members have the same thickness ($t_1 + t_2$, resulting in $\alpha = 0.50$), the value for that stiffness is

$$K^{11} = \frac{GAKs}{3h} \begin{bmatrix} 7 & -8 & 1 \\ -8 & 16 & -8 \\ 1 & -8 & 7 \end{bmatrix} + \frac{c_{c1} h}{240} \begin{bmatrix} 31 & 23 & -4 \\ 23 & 64 & -7 \\ -4 & -7 & 1 \end{bmatrix} + \frac{c_{c2} h}{240} \begin{bmatrix} 1 & -7 & -4 \\ -7 & 64 & 23 \\ -4 & 23 & 31 \end{bmatrix} \tag{A.12}$$

Since K^{12}, K^{21}, and K^{22} do not involve c_{f1} and c_{f2}, no modification of those terms is required. What must be done next is to convert this matrix from a 5 x 5 stiffness matrix to a 4 x 4 matrix, where the w_c term will be eliminated. We take the second equation of the system of equations in terms of the central node that determines w_c and substitute it into the four remaining equations, as is shown by Reddy (2006) for the formulation of CIE-1.

APPENDIX B

AVERAGING OF STIFFNESS TERMS

Utilizing a similar process in determining the behavior of a fastener with a factor that models deformation of the fastener using foundational stiffness poses an additional challenge when using that procedure for modeling contact stiffness. Close examination of the stiffness matrix does not provide a balanced finite element. The reason for this is that traditional foundational stiffness takes the following forms:

$$\mathrm{K} = \begin{bmatrix} A & -B_1 & -A & -B_2 \\ -B_1 & C & B_3 & D \\ -A & B_3 & A & B_4 \\ -B_2 & D & B_4 & C \end{bmatrix} \quad \text{(Reddy Formulation) (B.1)}$$

$$\mathrm{K} = \begin{bmatrix} A & B_1 & -A & B_2 \\ B_1 & C & -B_3 & D \\ -A & -B_3 & A & -B_4 \\ B_2 & D & -B_4 & C \end{bmatrix} \quad \text{(Bathe and Dvorkin [1985] Formulation) (B.2)}$$

The physical interpretation of this formulation is explained by the rationalization that the force transmitted to the foundation is equivalent to the difference in the forces between the nodes. This, however, is not realistic for the fastener application. To correct this difference between the nodes and simultaneously adding contact stiffness, the different values represented by B_1, to B_4, those values are replaced with an average value of the four "B_n" terms:

$$B_{ave} = \frac{B_1 + B_2 + B_3 + B_4}{4} \quad \text{(B.3)}$$

$$K_{contact} = \begin{bmatrix} A & B_{ave} & -A & B_{ave} \\ B_{ave} & C & -B_{ave} & D \\ -A & -B_{ave} & A & -B_{ave} \\ B_{ave} & D & -B_{ave} & C \end{bmatrix} \quad \text{(B.4)}$$

APPENDIX C

METHODS USED FOR PRELOAD IN SOLID ELEMENTS

The first, and possibly most common, method used to simulate fastener preload in solid finite element modeling is to utilize a given temperature difference between the elements in the shaft of the fasteners and surrounding elements, and using coefficients of thermal expansion. Using a cooler temperature in the shaft causes a contraction that effectively simulates preload. Cooling the fastener, however, does cause a contraction, not only along the shaft of the fastener, which is desired, but also radially around the shaft, which is not necessarily wanted. Doing this causes additional shrinkage radially, which exceeds the shrinkage due to Poisson's effect from the axial preloading alone. The formulation begins with Hooke's law and thermal expansion utilizing the shaft diameter:

$$\epsilon = \alpha \cdot \Delta T \tag{C.1}$$

$$\sigma = E \cdot \epsilon \tag{C.2}$$

$$\sigma = \frac{P}{A} = \frac{4P}{\pi d^2} = E \cdot \alpha \cdot \Delta T \tag{C.3}$$

$$\Delta T = \frac{4P}{E \cdot \alpha \cdot \pi d^2} \tag{C.4}$$

The case studies use steel and titanium fasteners, and preload occurs at 250, 500, 750, and 1,000 lbs. The temperature differences that are used for the solid models are shown in Table C.1

TABLE C.1: PRELOAD AND TEMPERATURE DIFFERENCE RELATIONSHIP

Preload (lbs)	Fastener Material	Young's Modulus (psi)	Coefficient of Expansion, (in/inF)	Temperature difference (F)
250	Steel	29x10^6	6.6x10^-6	26.608
500				53.217
750				79.826
1000				106.459
250	Titanium	16x10^6	4.8x10^-6	66.314
500				132.629
750				198.943
1000				265.258

A second method, not used in this study, utilizes the fact that establishing contact surfaces between the fastener and plates can force a change in deflection. This method models the fastener intentionally in unloaded interference with the connected members. The interference is resolved into a preload prior to the analysis by ensuring that the solids intended to be in contact are enforced into a compatible configuration. A variation of this method is described by Shashishihar (2005). It describes a method in which a row of elements, the length of which is equivalent to the strain predicted in the preload, is eliminated or "collapsed" to provide the strain, and a pre-tensioned node transmits load across the cross section. This method utilizes flexibility provided by the finite element modeling code in Abacus.

APPENDIX D

HERTZIAN CONTACT OF PARALLEL CYLINDERS

Hertzian contact is the basis for most contact problems encountered in engineering. Primary applications involve normal contact between two elastic solids that are smooth and can be described locally with orthogonal radii of the curvature. The size of the actual contact area must be small compared to the dimensions of each body and to the radii of curvature. Hertz theory does not account for tangential forces that can develop where the surfaces slide or carry traction.

When dealing with the contact of curved surfaces, two parameters emerge. The first is defined as the contact modulus, C_e:

$$C_e = \frac{1-\nu_1^2}{E_1} + \frac{1-\nu_2^2}{E_2} \tag{D.1}$$

where E_n and ν_n are Young's modulus and Poisson's ratio, respectively, for the different materials in contact. The second parameter is known as the relative radius, K_D:

$$K_D = \frac{D_1 D_2}{D_1 + D_2} \tag{D.2}$$

where D_n represents the diameters of the cylinders in contact. The formula as shown is tailored for two cylinders in contact. When a shaft and hole are in contact, the sign of the diameter for the smaller diameter (the shaft) is assigned to D_2 and the formula is

$$K_D = \frac{D_1 D_2}{D_1 - D_2} \tag{D.3}$$

Utilizing the formulation for cylinders in contact presented in *Roark's Formulas for Stress and Strain*, the deflection that occurs on a line between the centers of the two cylinders are given by

$$\delta = \left(\frac{2F}{\pi t}\right)\frac{1-\nu^2}{E}\left(\frac{2}{3} + ln\left(\frac{2D_1}{b_1}\right) + \ln\ ln\left(\frac{2D_2}{b_2}\right)\right) \tag{D.4}$$

where

$$b_i = 1.60\left(\frac{FK_D C_e}{t_i}\right)^{1/2} \tag{D.5}$$

which is the full width of the contact between the two cylinders. The assumption that is made in Roark's formula is that the plate and fastener are made of the same material. More generally,

$$\delta = \left(\frac{F}{\pi t}\right) C_e \left(\frac{2}{3} + ln\left(\frac{4D_1 D_2}{b_1 b_2}\right)\right) \tag{D.6}$$

Using the definition of stiffness, $c_c = F/\delta$, its value can be rewritten as

$$c_c = \frac{\pi t}{C_e\left(\frac{2}{3} + ln\left(\frac{4D_1 D_2}{b_1 b_2}\right)\right)} \tag{D.7}$$

APPENDIX E

NEUTRAL LINE MODEL

This appendix provides a brief description of the neutral line model, as excerpted from de Rijck (2005), where a complete description is available. The purpose of using this in the multi-fastener case studies is to provide an accepted means of deriving the load transfer from one plate to another through the mechanical fasteners in a lap joint.

The elementary neutral line model is one-dimensional, such that the displacement of the neutral axis (of the plate members) determines the behavior of the joint as a single structural element. The option of adding load transfer to the model is what is desired, and the same formulation is used. That is the focus of this explanation.

Due to high stresses around the fastener holes, fastener flexibility affects the load transfer and secondary bending. Assuming three fasteners, as considered in Case Study 2, the load transmitted by the three rows—T_1, T_2, and T_3—considering there is symmetry in the model, is $P = 2T_1 + T_2$. The loads in the various parts of the joint are indicated in the Figure E.1. In the elementary neutral line model, the middle row does not contribute to load transfer, but by introducing fastener flexibility, T_2 is no longer 0. An internal moment is introduced at the fastener rows—M_1, M_2, and M_3. The loads in the upper and lower sheets are different due to the load transfer associated with different tensile elongations of the upper and lower sheets. In the neutral line mode, the upper and lower sheets between the first and third row, in the overlap region, and are assumed to act as an integral beam subjected to secondary bending. However, the resultant force of the load transfer in the previous figure does not act at the neutral line of the overlap region. In order to account for this effect, an internal moment is introduced. The summation of moments results in

$$-M_1 + T_1 \cdot \frac{t}{2} - T_1 \cdot \frac{3t}{2} = 0 \tag{E.1}$$

$$M_1 + T_1 \cdot t = 0 \tag{E.2}$$

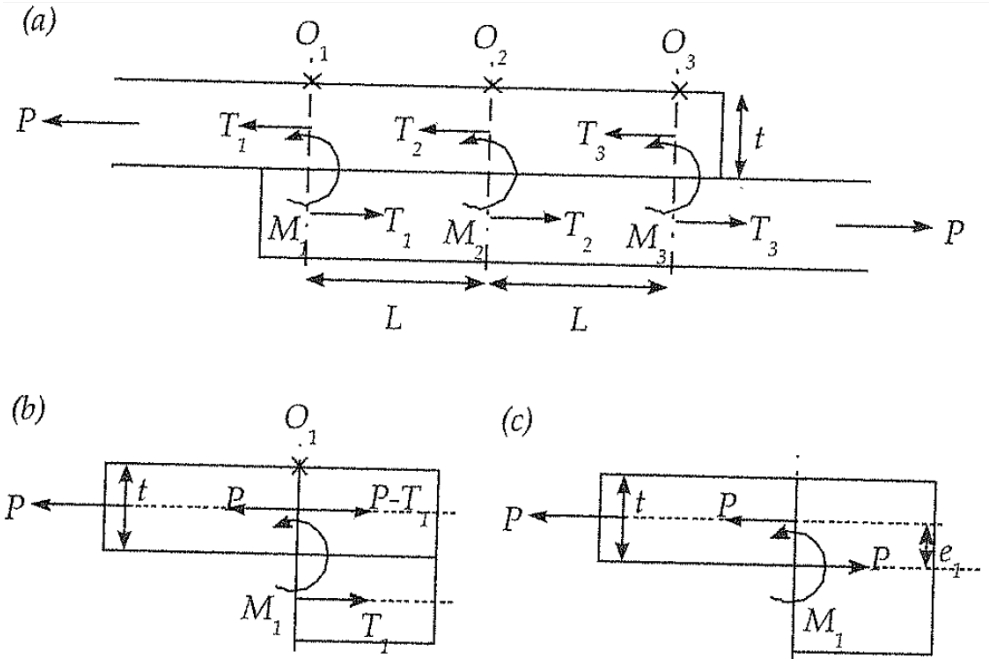

Figure E.1: Load transfer of three fastener rows.

The moments generated by the load transfer also take part of the moment introduced by the eccentricity. Since this moment is already a non-linear influence in the neutral line model, the influence should be removed from the internal moments. So what is actually needed is a change in moment.

$$\Delta M_1 = -M_1 + Pe_1 \tag{E.3}$$

$$\Delta M_2 = -M_2 \tag{E.4}$$

$$\Delta M_3 = -M_3 + Pe_3 \tag{E.5}$$

The calculation of T1 and T2 is based on the different elongations of the upper and lower sheets, which occur as a result of fastener flexibility. Due to some plastic deformation around the fastener holes, some rotation of the fasteners occurs. This phenomenon is described

by a linear function between the applied load, P, transmitted by a row of fasteners, and displacement, δ, occurring in the joint due to plastic deformation around the fastener holes.

$$f = \frac{\delta}{P} \tag{E.6}$$

For the lap joint, the displacement of the lower sheet at a row relative to the upper sheet, while P is the load associated with the relevant internal moment (T_1 or T_2). The symbol f is empirically obtained. For the first and second row,

$$\delta_1 = f \cdot T_1 \tag{E.7}$$

$$\delta_2 = f \cdot T_2 \tag{E.8}$$

The fastener flexibility displacements and the tensile elongations of the upper and lower sheets must be compatible (see Figure E.2).

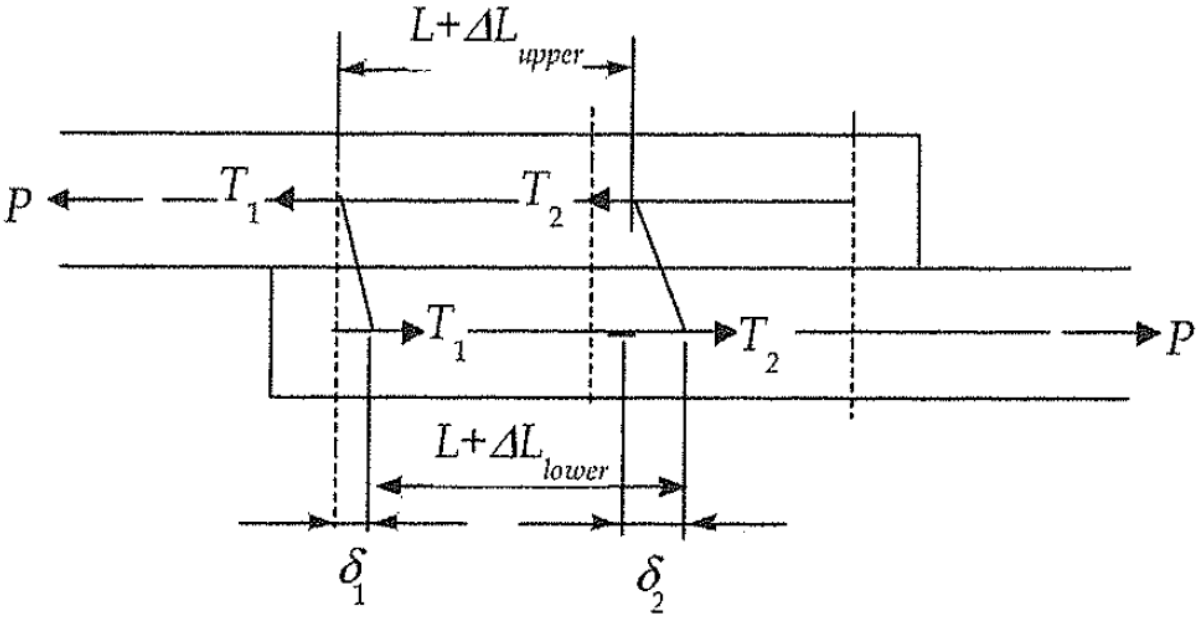

Figure E.2: Displacement between two fastener rows.

Following the stress/strain relation:

$$\Delta L_{upper} = \frac{L}{AE} \cdot (P - T_1) \tag{E.9}$$

$$\Delta L_{lower} = \frac{L}{AE} \cdot (T_1) \tag{E.10}$$

The value of the fastener loads can then be calculated as

$$T_1 = \left(\frac{\frac{L}{AE}+f}{2\frac{L}{AE}+3f}\right)P \tag{E.11}$$

$$T_2 = \left(\frac{f}{2\frac{L}{AE}+3f}\right)P \tag{E.12}$$

The fastener flexibility, f, is derived empirically, and the Huth formulation is shown here for a lap joint with single shear fasteners:

$$f_{Huth} = \left(\frac{t_1+t_2}{2d}\right)^{2/3} 3\left(\frac{1}{t_1E_1}+\frac{1}{t_2E_2}+\frac{1}{2t_1E_f}+\frac{1}{2t_2E_f}\right) \tag{E.13}$$

Other formulations of the fastener flexibility from Boeing, Grumman, Swift, Tate and Rosenfeld, and Morris are as follows:

$$f_{Boeing} = \frac{2^{\left(\frac{t_1}{d}\right)^{0.85}}}{t_1}\left(\frac{1}{E_1}+\frac{3}{8E_f}\right)+\frac{2^{\left(\frac{t_2}{d}\right)^{0.85}}}{t_2}\left(\frac{1}{E_2}+\frac{3}{8E_f}\right) \tag{E.14}$$

$$f_{Grumman} = \frac{(t_1+t_2)^2}{E_f d^3}+3.7\left(\frac{1}{t_1E_1}+\frac{1}{t_2E_2}\right) \tag{E.15}$$

$$f_{Swift} = \frac{5}{dE_f}+0.8\left(\frac{1}{t_1E_1}+\frac{1}{t_2E_2}\right) \tag{E.16}$$

$$f_{Tate\ and\ Rosenfeld} = \left(\frac{1}{t_1E_1}+\frac{1}{t_2E_2}+\frac{1}{t_1E_f}+\frac{1}{t_2E_f}\right)+\frac{32}{9\pi E_f d^2}(t_1+t_2)(1+\nu_f)+\frac{8}{5\pi E_f d^4}({t_1}^3+5{t_1}^2t_2+5t_1{t_2}^2+{t_2}^3) \tag{E.17}$$

$$f_{Morris} = (Refer\ to\ deRijck[2005]) \tag{E.18}$$

where:

$t_{1,2}$ = sheet thicknesses

$E_{1,2}$ = modulus of elasticity of sheets

E_f = modulus of elasticity of fastener

d = fastener diameter

APPENDIX F

MODELS WITH AND WITHOUT RIGID BODY ELEMENTS

Chapter 2 provides a brief summary of popular modeling techniques of lap joints. One is the bar/plate element model (Figure F.1) and another is the bar/plate element model with rigid body elements (Figure F.2), providing connectivity between the bar and plate elements. This appendix illustrates the difference between the loads of the bar elements in the presence of rigid body elements that provide connectivity. For this comparison, the example used is the three-fastener model from Case Study 2, and specifically the aluminum plates joined by steel fasteners.

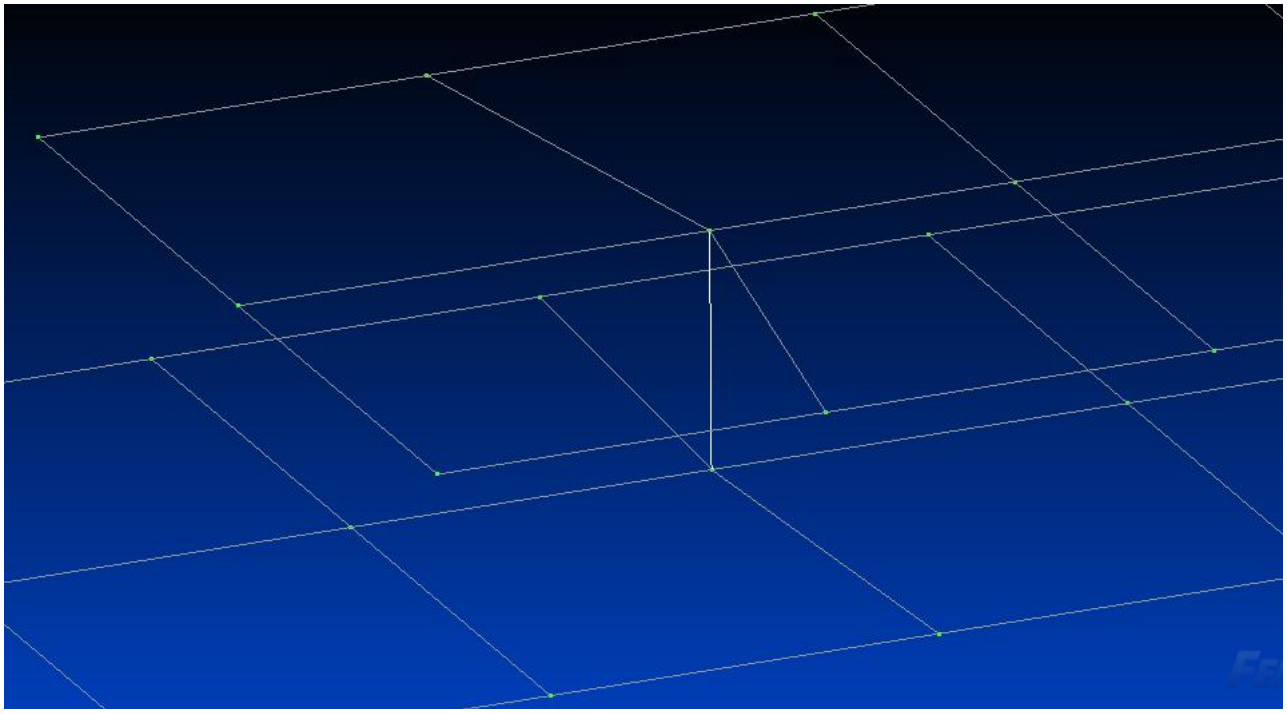

Figure F.1: Bar element in direct connection with plate elements.

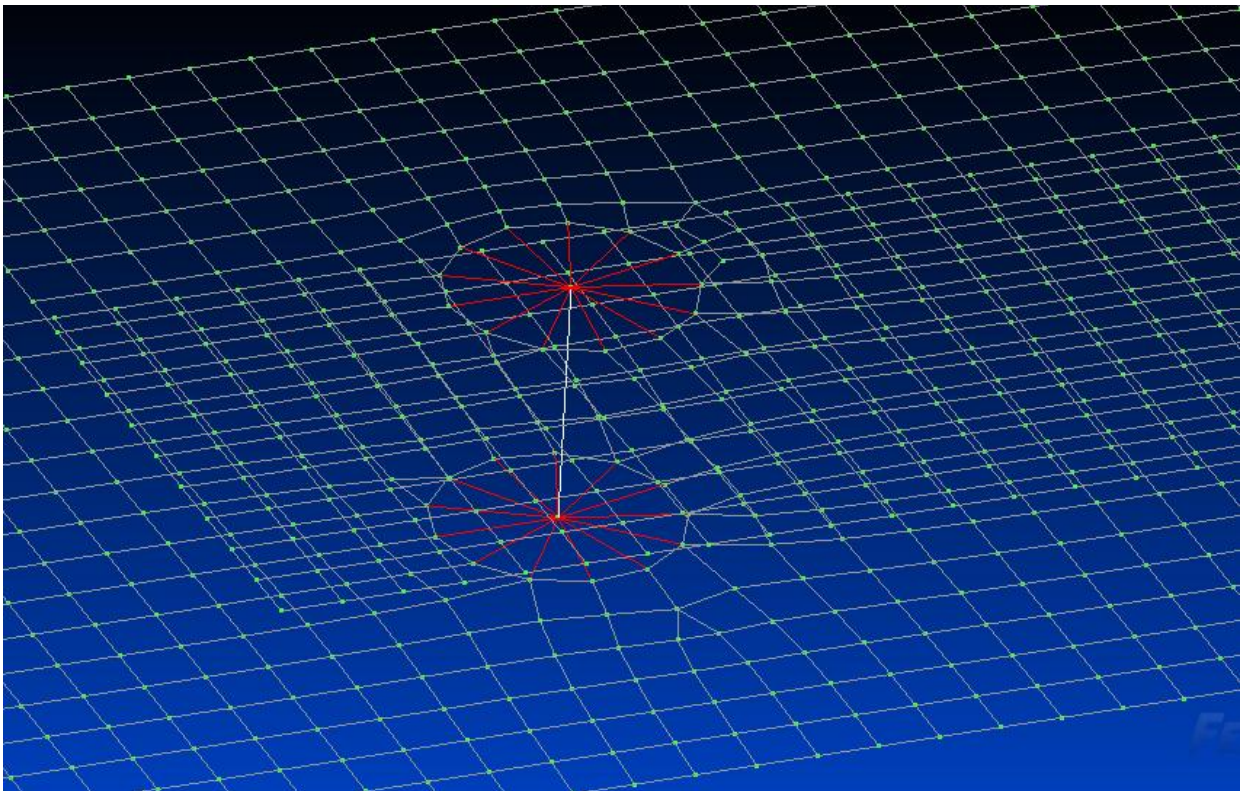

Figure F.2: Bar element and plate elements connected by rigid body elements.

Tables F.1 and F.2 show the load reactions without and with rigid body elements, respectively. Table F.3 shows the percent difference in fastener loads.

TABLE F.1: LOAD REACTIONS (WITHOUT RIGID BODY ELEMENTS)

Al vs St	Without RBE				
Load	Thickness	Bolt 1/3	Bolt 2	1/2 Ratio	Total
500	0.0625	205.48	89.043	2.307649	500.003
	0.125	201.47	97.064	2.075641	500.004
	0.1875	196.21	107.58	1.823852	500
	0.25	190.56	118.877	1.603001	499.997
Load	Thickness	Bolt 1/3	Bolt 2	1/2 Ratio	Total
1000	0.0625	410.96	178.086	2.307649	1000.006
	0.125	402.94	194.128	2.075641	1000.008
	0.1875	392.42	215.16	1.823852	1000
	0.25	381.12	237.754	1.603001	999.994
Load	Thickness	Bolt 1/3	Bolt 2	1/2 Ratio	Total
1500	0.0625	616.44	267.129	2.307649	1500.009
	0.125	604.41	291.192	2.075641	1500.012
	0.1875	588.63	322.74	1.823852	1500
	0.25	571.68	356.631	1.603001	1499.991
Load	Thickness	Bolt 1/3	Bolt 2	1/2 Ratio	Total
2000	0.0625	821.92	356.172	2.307649	2000.012
	0.125	805.88	388.256	2.075641	2000.016
	0.1875	784.84	430.32	1.823852	2000
	0.25	762.24	475.508	1.603001	1999.988

TABLE F.2: LOAD REACTIONS (WITH RIGID BODY ELEMENTS)

Al vs St	With RBE				
Load	Thickness	Bolt 1/3	Bolt 2	1/2 Ratio	Total
500	0.0625	216.24	67.483	3.204363	499.963
	0.125	210.97	78.035	2.70353	499.975
	0.1875	203.32	93.329	2.17853	499.969
	0.25	195.05	109.85	1.775603	499.95
Load	Thickness	Bolt 1/3	Bolt 2	1/2 Ratio	Total
1000	0.0625	432.48	134.966	3.204363	999.926
	0.125	421.94	156.07	2.70353	999.95
	0.1875	406.64	186.658	2.17853	999.938
	0.25	390.1	219.7	1.775603	999.9
Load	Thickness	Bolt 1/3	Bolt 2	1/2 Ratio	Total
1500	0.0625	648.72	202.449	3.204363	1499.889
	0.125	632.91	234.105	2.70353	1499.925
	0.1875	609.96	279.987	2.17853	1499.907
	0.25	585.15	329.55	1.775603	1499.85
Load	Thickness	Bolt 1/3	Bolt 2	1/2 Ratio	Total
2000	0.0625	864.96	269.932	3.204363	1999.852
	0.125	843.88	312.14	2.70353	1999.9
	0.1875	813.28	373.316	2.17853	1999.876
	0.25	780.2	439.4	1.775603	1999.8

TABLE F.3: PERCENT DIFFERENCE IN FASTENER LOADS

Plate	Bolt 1/3	Bolt 2
Thickness	% difference	
0.0625	-5.23652	24.21302
0.125	-4.71534	19.60459
0.1875	-3.62367	13.24689
0.25	-2.35621	7.593563

APPENDIX G

PROGRAMS AND SUPPORTING DATA FILES

This appendix contains two programs written in MathCAD 15. The first program involves single-fastener modeling, which predicts the deflection in a single fastener configuration as well as the traditional bar element configurations and is showcased in Case Study 1. The second program models the assembly of a three-fastener combination, as shown in Case Studies 2 to 4. The main output of interest is the load reactions that are seen in the individual fasteners. The formulation of the second program requires implementation of plate elements that incorporate plane elasticity and plate bending. Interestingly, the plane elasticity portion of the plate elements joins the bending portion of the fastener elements, while the axial loading of the fastener elements joins the bending portion of the plate elements. In both fastener elements and plate elements, loading in the orthogonal directions is uncoupled. The formulation for bending the plate elements used is based on the MITC4 elements developed by Bathe and Dvorkin (1985) and programmed in MathCAD by Shivaswamy (2010).

This appendix also contains various files and data spreadsheets used for compilation presented in the research. This data is saved in a separate zip file from this document for the purposes of compact data storage and is readily retrievable.